Productivity, Water Wells Functionality and Hydraulic Structures of Selected Volcanic Aquifers in Ethiopia

By

Hassen Shube Sheko

A Thesis submitted to the School of Earth Sciences

Presented in partial fulfilment of the requirements for the Degree of Doctor of Philosophy (Hydrogeology)

Addis Ababa University

Addis Ababa, Ethiopia

March 2024

Addis Ababa University
School of Graduate Studies

This is to certify that the thesis prepared by **Hassen Shube Sheko**, entitled: "**Productivity, water wells functionality and hydraulic structures of selected volcanic aquifers in Ethiopia**" and submitted in the Partial fulfilment of the Degree of Doctor of Philosophy in Earth Sciences (Hydrogeology) complies with the regulations of the university and meet the accepted standard with respect to originality and quality.

Signed by the Examining Committee

Prof. Seifu Kebede	_____	_____
Principal Supervisor	Signature	Date
Dr.Tilahun Azagegn	_____	_____
Co-Supervisor	Signature	Date
Prof.Tenalem Ayenew	_____	_____
Examiner (Internal)	Signature	Date
Dr.Michael Owor	_____	_____
Examiner (external)	Signature	Date
Dr.Bayissa Regassa	_____	_____
Chair, School of Earth Sciences	Signature	Date

ABSTRACT

The volcanic aquifers of Ethiopia play a vital role in providing groundwater used for domestic, industrial and agricultural water supply purposes in both urban and rural areas. However, in such volcanic aquifers, research indicated that declining water levels due to over exploitation decreased natural recharge and climatic variability and failures of water wells within a short life span after construction. Therefore, the objective of this dissertation is to investigate volcanic aquifers' variation in hydraulic structures, classification and productivity based on a large data set of hydraulic parameters systematically examined for the age (Eocene to Quaternary) and depth (18 - 882m). This work also addresses the use of geospatial technique to estimate large-scale groundwater flow velocity (V_{gw}) and ^{222}Rn isotope in estimating V_{gw}, ^{222}Rn recovery, water residence time and testing the applicability of ^{222}Rn technique in post-construction hand pump wells (HPWs) functionality monitoring. The results revealed that there is a good correlation between the ages of the emplacement of rock with hydraulic properties and there is no depth-wise variation in aquifer productivity. The oldest (Eocene) basalts show lower productivity as compared to the youngest (Quaternary) basalts. The insights gained from the analysis show that increasing the depth of drilling does not necessarily increase aquifer yields and can inform the global-scale groundwater flow modelling efforts. The groundwater flow velocity estimation (V_{gw}) estimated from shallow volcanic aquifers reveals the characteristics of volcanic aquifers productivity and flow dynamics. The values of V_{gw} estimated by the geospatial and ^{222}Rn methods show similar trends in all study sites where the high values were observed in highly fractured and weathered basaltic aquifers, while the lowest values were in the slightly weathered, less fractured basalt, trachyte and pyroclastic deposits. But, the V_{gw} estimated by the geospatial technique (0 and 195 m/day) is higher than V_{gw} obtained from ^{222}Rn isotope (0.37 and 69.1 cm/day) indicating the lower value in the ^{222}Rn technique is due to the effects of aquifer conditions and borehole efficiency effects. The HPWs have been classified into four functionality classes: fully functional (FF), Unreliable (UR), low yield (LY) and unreliable and low yield (UR&LY). FF HPWs show a high ^{222}Rn recovery revealing a quick through flow of groundwater into the wells, healthy functioning of boreholes without screen clogging effects and a high permeability of the aquifer material in the vicinity of the well. Whereas, UR&LY HPWs show the lowest ^{222}Rn recovery revealing a slow flow of water in the well owing to low permeability, declining water level, screen clogging, poor initial design and high water stagnation in the boreholes. The substantial difference in ^{222}Rn recovery between the four categories reveals the applicability of a naturally occurring ^{222}Rn isotope as a promising independent tool to monitor post-construction changes in the performance of HPWs without the need for dismantling the HPWs for inspection.

Key Words: ^{222}Rn technique; geospatial technique; productivity; water wells functionality; age and depth wise; aquifer properties; aquifer classes; volcanic aquifers; Ethiopian highlands

ACKNOWLEDGEMENTS

I gratefully acknowledge my supervisor Prof. Seifu Kebede for his strong and invaluable support in all aspects throughout this dissertation work has always been vigorous. His support in correcting research manuscripts has quietly improved the quality of my work and without his unwavering cooperation; this dissertation work cannot be to this level. My sincere thanks go to my co-supervisor Dr. Tilahun Azagegn for his continuous support in facilitating all activities including field logistics, comments and suggestions during this thesis work and his help was irreplaceable. I am grateful to Dr. Dessie Nedaw for his help in data validation, important comments and suggestions during dissertation work. I am indebted to the immense help of Dr. Beheilu Birhanu for his help and kind cooperation on field instrumentation technique. I would like to acknowledge Dr.Balemwal Atnafu former head of the School of Earth Sciences, Addis Ababa University for facilitating field logistics during fieldwork. My sincere thank goes to Dr.Bayissa Regassa head of the School of Earth Sciences and Dr. Mebatsion Shawel (postgraduate program coordinator) for their kind cooperation in facilitating all the necessary support.

I am grateful to Prof. Kristine Walraevens for inviting me to the Ghent University for a short research stay in Belgium through global minds research cooperation. I need to express my sincere thanks to Dr. Muhammed Haji, Dr. Shankar Karuppanan for their various comments and suggestions on manuscript works. I would like to thank Dr. Mohammed Woyesso for his immense help while using Matlab software for numerical modelling. I would like to thank Mr.Dagmawi Shiferaw of Addis Ababa University for his help in facilitating field equipment. I would like to thank Mr. Daniel the driver from Addis Ababa University for his invaluable cooperation and Mr. Tibebu Bekele from Mecha District Water Resources who assisted me during the fieldwork.

The Ministry of Water Resources, Ethiopian Construction Design and Supervision (Water Works Supervision and Enterprise), Addis Ababa Water and Sewerage Authority and Engineering Corporation of Oromia for their kind cooperation in providing important data during this dissertation work. I would also like to extend my sincere gratitude to my home university Adama Science and Technology University for allowing me to pursue my Ph.D. study. I could not forget the strong moral support of Abda Berisso, Kelifa Loka and Dr. Yadeta Chimdessa for your unwavering support. Last but not least, I would like to thank my family (my father Shube Sheko, my beloved wife Leyla Hajo Bunti and my children) who were a strong source of support and inspiration, your love and support recharged me during all the tiresome times.

Table of Contents

List of Tables

List of Figures

List of Symbols, Nomenclature or Abbreviations

CFB = Continental flood basalt

C_{gw} = Radon Concentration in Groundwater

C_{ww} = Radon Concentration in Water Wells

FF = Fully functional

HPWs = Hand pump wells

k_1 = Hydraulic conductivity of filter screen

k_2 = Hydraulic conductivity of filter pack

k_3 = Hydraulic conductivity of the aquifer

LB = Lower Basal Sequence

LY = Low yield

MER = Main Ethiopian Rift

NF = None-functional

QV = Quaternary Volcanics

r_1 = Radius of filter screen

r_2 = Radius of filter pack

r_3 = radius of the aquifer

RMV = Rift Margin Volcanics

t = Residence time in a well

UB = Upper Basal Sequence

UR = Unreliable

UR&LY = Unreliable and low yield

V_{gw} = Groundwater Flow Velocity

V_{ww} = Flow Velocity in Water Wells

YTVL = Yere Tullu Welel Volcano-tectonic Lineament

α = Horizontal Convergence factor

λ = Decay constant

$\mathscr{E}$ = Empirical value

List of Appendices

Chapter One

1.1. Background and Justification

The occurrence of global volcanic rocks is associated with the large igneous provinces of the Deccan Trap (Mahoney, 1988), Karoo (Cox, 2000), Siberia (Zolotukhin & Al'mukhamedov, 1988), Columbia River (Hooper, 1982), Parana-Etendeka (Piccirillo et al., 1988), East Africa (Mohr & Zanettin, 1988; Mohr, 1983) and North Atlantic (Dickin, 1988). The East African igneous province encompasses large igneous provinces of Ethiopia which comprises Ethiopian volcanic rocks that covered the Ethiopian plateaus, Rift valley regions and lowland areas of Ethiopia (Figure 1). The current study area covers the volcanic aquifers of northern, central and south western Ethiopian plateaus (Figure 2).

The geology of Ethiopian volcanic rocks encompasses major rock units aged from Eocene to Quaternary characterized by complex litho-stratigraphic units. The major geological structures and tectonic features in the Ethiopian volcanic regions are the Main Ethiopian Rift marginal faults and the E - W trending Yerer-Tullu Welel Volcano Tectonic Lineaments (YTVL) (Abebe et al., 1998; Agostini et al., 2011; Boccaletti et al., 1998; Corti et al., 2013, 2019; Gani et al., 2009).

Mirroring with the geology of volcanic rocks, the hydrogeology of volcanic rocks were classified into four major hydrostratigraphic classes: lower basal sequence, upper basal sequence, shield volcanoes and Quaternary volcanics (Kebede, 2013a). The hydrogeology of Ethiopian volcanic Aquifers are characterized by the complex hydro-stratigraphic settings and structural nature that controls groundwater occurrence and flow dynamics (Ayenew et al., 2008a; Azagegn et al., 2015; Furi et al., 2012; Kebede et al., 2005, 2008; Yitbarek et al., 2012). The fracture networks and weathering intensity in heterogeneous distributions of hydrostratigraphic layers (Aquifer classes), thick volcanic piles, overburden weathering profile and alluvial deposits have distinctive features on the volcanic aquifer productivity.

Lack of large hydrogeological data sets in the Ethiopian volcanic aquifers was the major challenge to set up the general frame work of volcanic aquifer classes and aquifer productivity. Based on the assumption that deep drilling provides high productivities,

numerous water well drillings have been conducted without prior knowledge of hydrostratigraphic settings, aquifer productivity and sustainable water wells performance evaluation. This has caused substantial unnecessary drilling investment. Likewise, numerous hand pump wells (HPWs) were drilled in shallow groundwater as the major sources of rural water supply in the volcanic aquifers of Ethiopian highlands. However, researches conducted by Hidden crises project on the shallow groundwater resilience to drought (MacAllister et al., 2020), groundwater residence time and water wells functionality classification based on physical factors (Banks et al., 2021; DJ. MacAllister, 2022; Owor et al., 2019) revealed that HPWs have faced challenges of declining yield and performance within a short period of time after construction.

Volcanic aquifers productivity is also associated to the characteristics of groundwater flow system. Thus, estimating groundwater flow velocity has a vital importance to determine the response of aquifer to changes, groundwater flow dynamics and contaminant pluming in groundwater flow path (Devlin, 2020). Groundwater flow velocity estimation has been conducted using various direct and indirect methods (Arriaga & Leap, 2006; Bakx et al., 2023; Cook et al., 2003; Essouayed et al., 2019a; Hall, 1993; Hamada, 2000; Kearl, 1997; Matsumoto et al., 2020; Schubert et al., 2011). Groundwater flow velocity estimation using ^{222}Rn isotope has been conducted in shallow unconsolidated aquifers (Cook et al., 2003; Hamada, 2000; Schubert et al., 2011; Thao et al., 2017). Groundwater flow velocity magnitude and direction was also estimated by geospatial technique (T. Abdullah et al., 2021; T. O. Abdullah et al., 2020; Al-Madhlom et al., 2020).

The Ethiopian volcanic aquifers covered larger spatial extent known by high population settlements, increased water supply for domestic drinking water, industrialization and urbanization. There is climate variability and rainfall scarcity that affected rain-fed agriculture to meet the increased demand for food security. The climate change and drought resilient groundwater-irrigated agriculture is one of the major alternatives to increase food production for increased population growth and millennium development goal. Furthermore, increased demand for groundwater can cause heavy stress on groundwater resources. Therefore, detail understanding of volcanic aquifer characterization, systematic aquifer classification, groundwater resources flow system,

establishing post construction HPWs functionality monitoring technique plays significant role in sustainable groundwater resources development and management in larger volcanic settings of Ethiopia.

This dissertation work classified the volcanic aquifer classes based on the existing pumping test data sets, age of lithostratigraphic units and aquifer depth to reveal volcanic aquifers productivity and develop general conceptual flow model of volcanic aquifer. Likewise, this dissertation conducted geospatial and ^{222}Rn technique to estimate groundwater flow velocity magnitude and to test the applicability of ^{222}Rn technique in water wells' functionality monitoring and sustainable performance of water wells. This method can supplement HPWs performance monitoring conducted by pumping test data analysis that needs substantial running costs and field logistics. Thus, a multiple approach combining the litho-stratigraphic, hydrogeological, aquifer hydraulic properties and water well performance were analysed to investigate the productivity of volcanic aquifer and the ^{222}Rn-derived groundwater flow velocity was determined and compared with transmissivity and specific capacity to test the applicability of ^{222}Rn technique during post-construction water well functionality monitoring of shallow volcanic aquifers. This work improves the general understanding of volcanic hydrogeology (productivity, variation in hydraulic structures and post-construction water well functionality monitoring) that has a vital importance in groundwater resources development and management in the Ethiopian highland volcanic aquifers.

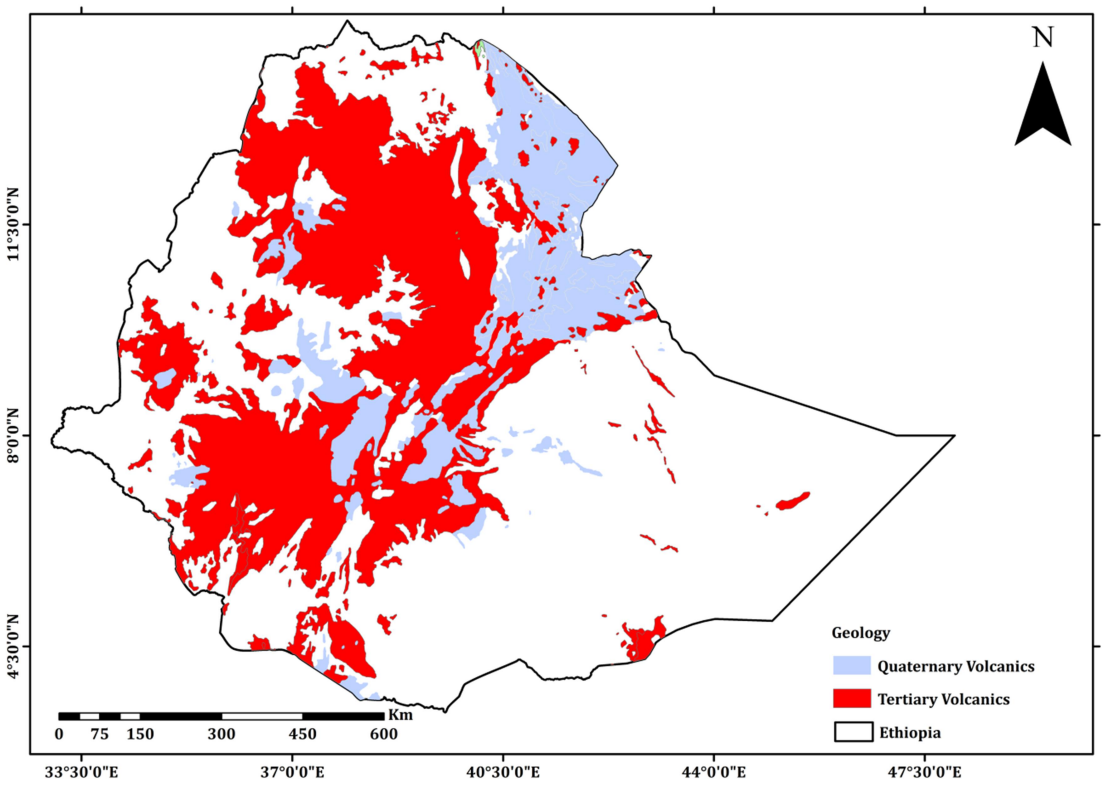

Figure 1.1: Geological Map of Ethiopian Volcanic Rocks (modified from USGS 2000)

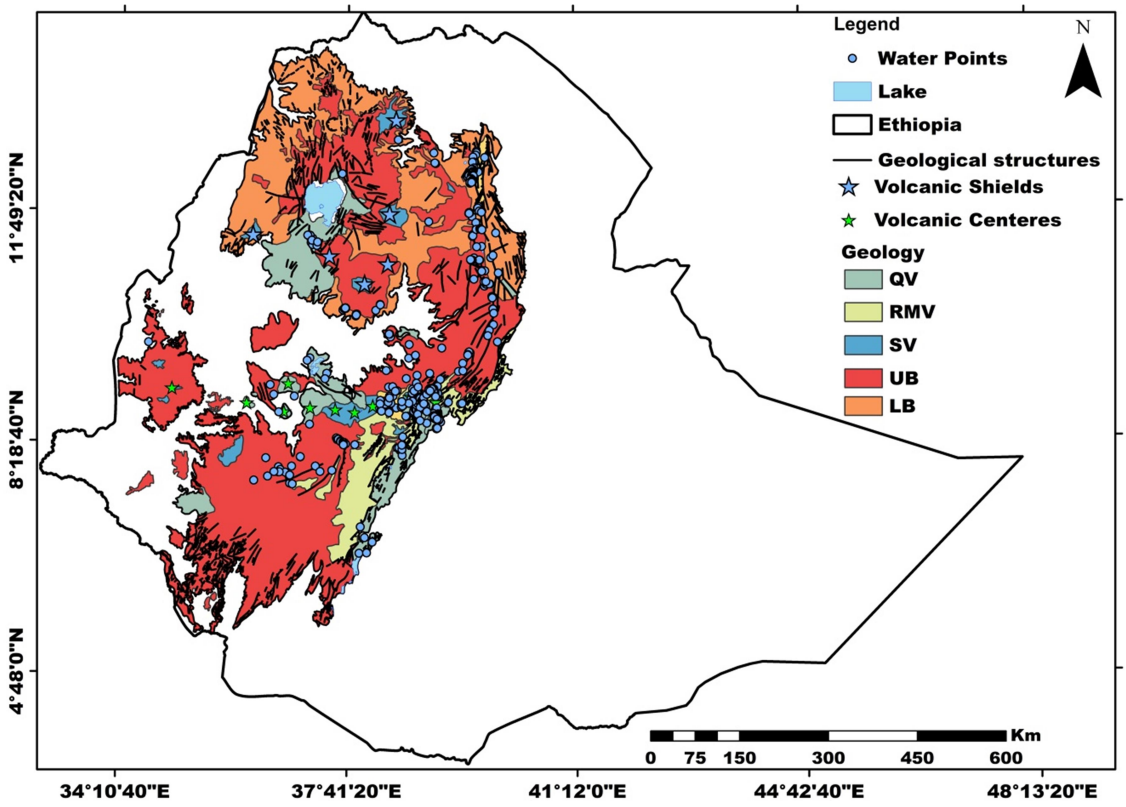

Figure 1.2: Location of study area, geology and water sampling points.

1.2. Literature Review

The Ethiopian volcanic rocks are part of continental flood basalts (CFB) of voluminous basaltic magma, laterally extensive lava flow of fissural eruption which occurs in the Deccan, Rajmahal, Madagascar, Karoo, Ferrar, Siberia, Emeishan, Columbia River, Parana-Etendeka, Yemen-Ethiopia, North and Central Atlantic, Snake River Plain, Oregon high lava plains (Kieffer et al., 2004a; Macdougall, 1988; Mahoney, 1988; P. Mohr & Zanettin, 1988b). The Ethiopian flood basalts were traditionally classified into four different stratigraphic units such as Ashangie, Aiba, Alaji and Tarmaber formations with the age ranging from Eocene to Miocene (Lebas & Mohr, 1970; P. Mohr & Zanettin, 1988b; Paul Mohr, 1983). However, recent studies classified the volcanic rocks into four stratigraphic units: the lower basal sequences (Ashangi), The upper basal sequence (Aiba, Alaji and Tarmaber), the broad-based shield volcanic capping the plateau and Quaternary scoriacious basalt (Kieffer et al., 2004a). The lower basal sequences (Ashangi) intercalated with the acidic volcanic ashes, rhyolites and ignimbrites characterized by rugged topography, thinly bedded,

brecciated, deeply weathered formation cut by dyke, irregular thickness in each flow sequence and laterally discontinuous. The upper basal basalt (Aiba, Alaji and Tarmaber) is characterized by massive basaltic flow, low degree of weathering and thick layering, jointing, cliff-forming topography that formed the plateaus. The broad-based shield volcanic unit capped the Ethiopian plateau and the Quaternary scoriacious basalt. The felsic lavas, pyroclastic rocks, rhyolite and trachyte were intercalated with flood basalt in the upper stratigraphy of the Ethiopian volcanic plateau (Ayalew et al., 1999).

The broad basaltic volcanism was classified in to three distinct phases based on their age of classification as the Eocene initial phase (45 to 34Ma) in the southern part of Ethiopia, the Oligocene trap phase (~33.9 to 27Ma) 1-2 km thick flood basalt that covered the North western Ethiopian Plateau and Yemen and the early Miocene resurgence phase (~26.9 to 22Ma) (Abbate et al., 2015; Kieffer et al., 2004a; P. A. Mohr, 1967; P. Mohr & Zanettin, 1988b; Pik et al., 1998). The south western Ethiopian Plateau is different from the north western Ethiopian plateau by the scarce flat lying thick piles of basalts (traps), large volcanic edifices (shield volcanoes) are not common, phonolithic lavas are abundant, the oldest ages are obtained from base of the flood volcanic fields, the Cenozoic volcanics directly rests on the crystalline basement (Abbate et al., 2015; Berhe et al., 1987; Davidson & Rex, 1980). The two volcanic provinces of the north western and south western Ethiopian plateaus are separated by the Yerer Tullu-Welel volcano tectonic lineament (YTVL) (Abebe et al., 1998). The basaltic plateau formed vertical cliffs, V-shaped valleys, vertical columnar basalts and hilly terrains of varying topography.

The volcanic aquifers of the Ethiopian plateau were classified into four major hydrostratigraphic units of lower basal sequence (Ashengi), the Upper Basal sequence (Aiba, Alaji and Tarmaber formation), the shield volcanoes and the quaternary basaltic volcanics (Ghibe, Lake Tana, Borena and Bale massifs) and alluvial deposits (Kebede, 2013a). Moreover, in the south western Ethiopian plateau the Jimma upper and lower volcanics and Mekonnen basalt were classified as part of the upper basal sequence.

The aquifer characteristics and productivity analysis were determined from the analysis of pumping test data and detail analysis of aquifer units. The pumping test data was analysed by constant discharge, recovery and step-drawdown tests. The duration of the constant

discharge rate pumping test in confined aquifers, leaky and unconfined aquifers are assumed as 24hrs, 20hrs and 72hrs respectively (Kruseman & De Ridder, 1983). The shorter duration of pumping is considered in the fractured aquifers about 10 to 15hrs. From the time-drawdown curve plot, the nature of fractures and matrix block in the aquifer, response to the early, medium and late time were analyzed whether there is the well-bore storage, skin effects and boundary (recharge and impermeable) conditions (Kruseman & De Ridder, 1983). Pumping test data analysis conducted by the transient flow of groundwater to the well was determined from the drawdown of the well (Theis, 1935). The Theis method is simplified by the Cooper and Jacob method (Cooper & Jacob, 1946). The step-drawdown test was conducted to estimate water well performance, select suitable pumping rates and estimate hydraulic characteristics of aquifers. The specific capacity is the ratio of well yield to the drawdown in the pumping well. It is a measure of the productivity of the aquifer and water well efficiency.

Volcanic aquifer flow dynamics, storage and groundwater flow velocity play a vital role in groundwater resources management. Groundwater flow velocity can be estimated by tracer tests that are performed by either introducing artificial tracer into the investigated groundwater system or the existing natural tracers' in groundwater chemistry. One of the natural tracers used for groundwater flow velocity estimation is radioactive radon (^{222}Rn) isotope. The ^{222}Rn is a natural by-product of the radioactive decay of uranium-series, an alpha-emitting noble gas, soluble in water and the gas is consequently incorporated into groundwater flows. The quantity of ^{222}Rn dissolved in groundwater depends on different factors such as the characteristics of the aquifer, water-rock interaction, water residence time within the aquifer and content of radium in the aquifer. The ^{222}Rn concentration in water decreases with a half-life of 3.824 days after the supply stops. When the groundwater enters in to the well, ^{222}Rn decay is no longer balanced by ^{222}Rn production. After the immediate loss from the contact of aquifer matrix, the source/decay reaches steady state equilibrium. The decreasing of initial equilibrium concentration of natural background concentration in an aquifer (C_{gw}) is because of the absence of radon production. The initial concentration in the groundwater and its relatively fast decrease in the water well are the central parameters to use ^{222}Rn as an environmental tracer.

The predictable ^{222}Rn deficit/recovery can therefore be used as a quantitative measure of its residence time in the well and thus for determining the groundwater flow velocity. The ^{222}Rn technique can be used as environmental tracer for estimating groundwater flow velocities in single-well tests. The velocity of groundwater is estimated from the ratio of ^{222}Rn concentration in groundwater before and after it flows into a well. The estimation of groundwater flow rate using the decay of ^{222}Rn, depth at which groundwater is influenced by surface water, velocity of groundwater in a well, the ^{222}Rn deficit by the ratio of concentration of ^{222}Rn in groundwater before and after it flowed in to the well (Cook et al., 1999; Hamada, 2000; Schubert et al., 2011).

The simplified mathematical approaches are used based on partial differential equations assuming that the net concentration inflow equals the net concentration of outflow plus decay assuming a perfectly mixed water column in the screened well section (Cook et al., 1999). The convergence of groundwater streamlines towards a well and its immediate surroundings is considered during groundwater flow velocity estimation (Schubert et al., 2011). Under steady-state flow condition, the residence time and ^{222}Rn deficit (C_{ww}/C_{gw}) depends on the radius(r) of the well and velocity of the water passing through the well (V_{ww}).

The advantages of using ^{222}Rn as an environmental tracer are because of its low cost, no need of injection of artificial tracers in to the aquifer, the immediate availability of results and the need for only a single monitoring well. However, several potential sources of errors such as poor sampling, inadequate hydraulic connection of the well because of a clogged screen and unstable well diameter is resulting in excessively long or short well water residence times (Schubert et al., 2011).

The geospatial technique is used based on the four essential input raster maps of groundwater elevation head, effective porosity, saturated thickness and transmissivity to estimate large scale groundwater flow velocity magnitude and direction (T. Abdullah et al., 2021; T. O. Abdullah et al., 2020; Al-Madhlom et al., 2020). The raster maps were prepared by considering the raster cell size for all four layers in a kriging interpolation. The raster maps were analysed in the spatial analyst toolbox under the groundwater Darcy velocity command window. This technique used the borehole history and aquifer hydraulic

parameters obtained from pumping test data analysis. This method has been employed in shallow unconsolidated aquifers and fissured-Karst aquifers.

Water wells functionality usually refers to whether a water point is working or not at the time of a spot check, while sustainability considers whether water services continue to function over time (Carter & Ross, 2016). The hand pump wells have different rate of functionality and life span as water supply structure where the yields of these wells were decreasing through the life span of the HPWs and some of them were abandoned after few years of services. These effects are associated with the failures related to the poor water well construction (engineering problems), community management problems, financing, spare parts, life cycle costs, hydrogeology, climate changes and flawed policies. Some studies show that low yield, poor water quality and mechanical failures are primary reasons, while poor water well siting, inappropriate design, low groundwater potential, inappropriate materials, poor construction, groundwater chemistry, lack of access to spare parts, lack of basic maintenance, operation and management is too difficult and lack of finance are the secondary reasons associated with failures of groundwater wells (Bonsor et al., 2015; Wilson et al., 2016). Based on the reliability of yield, the functionality of water points are classified into six classes: fully functional, poor reliability, low yield, poor reliability and low yield, not functioning and abandoned (Bonsor et al., 2018).

1.3. Statement of the problem

The Ethiopian volcanic aquifer comprises complex hydrostratigraphy and covers a wider spatial extent. Such broader volcanic aquifers are serving as a source of groundwater being exploited by numerous shallow and deep wells for domestic, industrial and irrigation purposes in Ethiopian highlands and the Main Ethiopian Rift system. However, aquifer productivity with respect to the aquifer depth and age of hydrostratigraphic emplacement and sustainability of water wells (functionality of water wells during post-water well construction) in Ethiopian volcanic aquifer is not well understood. Therefore, it is fundamental that understanding of the general framework of volcanic aquifer productivity with respect to aquifer depth and age of emplacement, groundwater flow velocity estimation and post-construction water well functionality monitoring have vital importance in groundwater resources exploration, development and management.

1.4. Research Questions/Hypothesis

In this study, the key research questions or the solutions to be hypothesized are:

- How the age of litho-stratigraphic emplacement and aquifer depth were related to the productivity of different volcanic aquifer classes?
- What are the trends of vertical and lateral aquifers' hydraulic properties, yields of water wells and effective drilling depth in Ethiopian volcanic aquifers?
- How to estimate groundwater flow velocity using ^{222}Rn isotope and geospatial techniques in shallow volcanic aquifers?
- How can the ^{222}Rn technique be applied to monitor HPWs functionality and performance during postwater well construction in shallow volcanic aquifers for sustainable groundwater resources management?
- What are the general conceptual hydrogeological frameworks of the Ethiopian highland volcanic aquifers?

1.5. Objectives

1.5.1. General Objective

The general objective of this research is to investigate the volcanic aquifers' productivity, water wells functionality and variation in hydraulic structures to establish the general hydrogeological framework of Ethiopian volcanic aquifers.

1.5.2. Specific Objectives

The specific objectives of this study include:

- To investigate the aquifer productivity using integrated aquifer properties from large data sets of pumping test data analysis (transmissivity, hydraulic conductivity, specific capacity and yield), depth to the aquifer, age of rock emplacement and hydrostratigraphic classification of volcanic aquifer classes.
- To estimate groundwater flow velocity using the ^{222}Rn technique in a single well from the ^{222}Rn-deficit/recovery obtained from the ratio of in-situ measurements of ^{222}Rn concentration in the water well and ^{222}Rn concentration from the aquifer in shallow hand pump wells.

- To estimate groundwater flow velocity from geospatial technique using four input raster maps of groundwater elevation head, effective porosity, saturated thickness and transmissivity obtained from hydraulic parameters and historical data of water wells analyzed in spatial data analyst tool (Darcy velocity) to compute groundwater flow velocity magnitude and direction.
- To examine the correlation between the ^{222}Rn derived groundwater flow velocity and ^{222}Rn recovery with hydraulic parameters obtained from pumping test data analysis in different HPWs functionality categories.
- To test the applicability of the ^{222}Rn technique in monitoring the functionality of post-water well construction in HPWs without dismantling pumps from hand pump wells.

1.6. Significance of the Study

The volcanic aquifers of Ethiopian highlands are distinctly known by their dense population settlement, urbanization, industry and agricultural activities. In such volcanic aquifers, due to rainfall scarcity and climate variability, water supplies for various purposes are mainly dependent on groundwater resources. The complex hydrostratigrpahic nature, large spatial extent and thick volume of volcanic eruption episodes with different ages of deposition and depths of volcanic aquifers are the concerning points to investigate the general framework of larger volcanic settings. Consequently, numerous water wells were drilled for various purposes without prior knowledge of aquifer productivity in different volcanic aquifer classes. Likewise, there are several problems associated with unnecessary and unsuccessful drilling depth, frequent water level declines and abandonments of water wells within a short life span after construction. Therefore, the systematic evaluation of all volcanic aquifer classes' productivity has paramount importance for planning water well drilling programs, sustainable groundwater resources management and groundwater flow modelling. Sustainable water resources management is also associated with the performance of water wells during post-construction.

Therefore, a comprehensive approach in integrating the hydraulic structures of volcanic aquifers in terms of depth to the aquifer and age of emplacement, multi-approaches of groundwater flow velocity estimation using ^{222}Rn technique and geospatial method, testing the applicability of ^{222}Rn method in hand pump wells performance monitoring during post-construction has a vital role in understanding the general framework of volcanic aquifers productivity and water wells functionality. This improves understanding of volcanic aquifer characteristics for proper groundwater resources management, flow dynamics, aquifer response to change and groundwater flow models. Testing the applicability of the ^{222}Rn technique to use as a tool in shallow HPWs functionality monitoring has also significant importance in rural water supply management.

1.7. Scope of the Study

The scope of this study is to investigate the productivity of volcanic aquifers of Ethiopian highlands based on large data sets of hydraulic structures (aquifer hydraulic properties, litho-stratigraphic settings, aquifer classification, model set up for general aquifer classes based on the age of emplacement and aquifer depth) to systematically set up the general conceptual framework of volcanic aquifer productivity, to estimate groundwater flow velocity magnitude and direction using geospatial technique (using four essential raster maps) and estimating groundwater flow velocity using ^{222}Rn technique, determining the water residence time in a well and ^{222}Rn recovery and testing the applicability of ^{222}Rn technique in shallow hand pump wells functionality monitoring.

1.8. Limitations of the Study

The limitation of this study is the lack of pumping test data in various regions like in shield volcanic units hinders characterizing the aquifer properties for the general overview of all volcanic aquifers of the study area. Lack of detailed geological, structural, geophysical, geophysical well logging and borehole log data to characterize the nature of each volcanic unit forming aquifer structures are rarely found and also challenging problems while classifying aquifer classes based on age of emplacement and depth to groundwater. In groundwater flow velocity estimation, to supplement and validate the two techniques (^{222}Rn and geospatial techniques) used in groundwater flow velocity estimation, single well

and multiple wells tracer techniques (dilution method) and direct velocity estimation tools were not conducted due to their expensive instrumentation and time-consuming nature.

1.9. Structure of the Dissertation

This dissertation is organized in the form of an article-based format into a series of interrelated chapters that address the research objectives. It is organized into six chapters that follow the sequences of tasks outlined. A brief review of the study background and justification, research problem statement, brief literature review, objectives of the research, significance of the research, scope and limitation of the research are presented respectively in chapter one. Chapter 2 presents the hydraulic structures of Ethiopian large igneous province. It addresses the volcanic aquifer classification based on the large data sets of aquifer hydraulic properties and hydrostratigraphic units. This work investigates the volcanic aquifer productivity based on the depth of the aquifer (shallow and deep wells) and the age of emplacement that determines which aquifer class is productive and how deep and shallow drilling can be successful in volcanic aquifers. Chapter 3 presents the groundwater flow velocity estimation using a geospatial technique. This chapter addresses how large-scale groundwater flow velocity be estimated using four essential raster maps (groundwater elevation head, aquifer thickness, effective porosity and transmissivity) as an input to determine groundwater flow velocity magnitude and direction in shallow volcanic aquifers of Ethiopian highlands. Chapter 4 discusses groundwater flow velocity estimation using the ^{222}Rn technique. This chapter mainly focuses on how a single well measured ^{222}Rn deficit/recovery (i.e. the ratio of ^{222}Rn concentration in the water well (C_{ww}) to the ^{222}Rn concentration in the background aquifer (C_{gw})) to estimate flow velocity in a well (V_{ww}). This theoretical velocity is used to estimate groundwater flow velocity (V_{gw}) based on the horizontal convergence factor (α) obtained from the water well radiuses (r_1, r_2 and r_3) and hydraulic conductivities (k_1, k_2 and k_3). Chapter 5 presents testing the applicability of the ^{222}Rn technique in HPWs functionality monitoring. The ^{222}Rn-derived groundwater flow velocity and the ^{222}Rn recovery are used to identify the performance of HPWs in different functionality categories. This chapter also addresses how results obtained from the ^{222}Rn technique and hydraulic properties obtained from pumping test data are complemented in the functionality classes. Chapter 6

presents concluding remarks, which summarize the aquifer productivity in a large igneous province of Ethiopia, the ^{222}Rn technique and the geospatial technique in estimating groundwater flow velocity and testing the applicability of the ^{222}Rn technique in water wells functionality monitoring. Issues requiring further recommendations and research activities are forwarded.

Chapter Two

2. Variation in hydraulic structure with respect to age and depth of a large igneous province in Ethiopia

2.1. Introduction

Eight percent of the earth's surface (terrestrial and seafloor) is made up of volcanic rocks. Volcanic aquifers serve as an important source of drinking and productive water globally. Large igneous provinces occur in the Deccan Trap (Mahoney, 1988), Karoo (Cox, 2000), Siberia (Zolotukhin & Al'mukhamedov, 1988), Columbia River (Hooper, 1982), Parana-Etendeka (Piccirillo et al., 1988), and East Africa (Mohr & Zanettin, 1988; Mohr, 1983) and North Atlantic (Dickin, 1988) (Figure 1). Unlike basement aquifers, which show distinct decreasing aquifer productivity with increasing aquifer depths (Bianchi et al., 2020; Dewandel et al., 2006; Deyassa et al., 2014; Howard et al., 1992; Maréchal et al., 2004), the depth and age wise variations in volcanic aquifers are least understood.

Data on the hydraulic structure of volcanic rocks has several important bearings as inputs to global scale groundwater models and in the groundwater resources development and management sector. Global scale groundwater models that account for the lateral flow of groundwater are rare and emerged only recently (de Graaf et al., 2017), but the accuracy of the models is challenged by the lack of a coherent representation of the vertical distribution of hydraulic conductivity (K) of the subsurface in different geological settings across the globe. The vertical variations in K in volcanic rocks of Nevada, USA were investigated that there is the influence of depth, alteration, rock type and overburden pressure on the heterogeneity of K values showing that the shallow part of the flow system has higher K values than the deeper flow systems (Jackson & Fenelon, 2022); the K variations are dependent on hydraulically interconnected fracture networks (Allocca et al., 2022). However, in carbonate aquifers, the K variation with depth is controlled by solute concentration and flow rate, where high K is found in low solute concentration in fresh water zone than in the deeper aquifer (Worthington, 2021). The complex permeability of volcanic rocks to confining pressure in Taupo Volcanic Zone, New Zealand, is due to the

intricate dissolution, veining and recrystallization of textures that leads to a wide variety of pore shapes and sizes (Cant et al., 2018). Volcanic mountains in high latitude regions and their immediate fronts have up to now relatively low borehole data density (Somers & McKenzie, 2020) since they are not the prime locations for drilling wells due to expected lower yields (Bresciani et al., 2018) and low population density. In contrast, African mountains are densely populated, necessitating the sinking of thousands of boreholes in highland volcanic terrains. For instance, in Ethiopia alone, several thousands (>1000) deep boreholes have been sunk to depths exceeding 300 m and reaching 980 m. Pumping test data from these boreholes could provide important information on the vertical variation in K, with the aim of improving global groundwater flow models in volcanic terrains.

In recent decades, the target depth for groundwater drilling has increased (GebreEgziabher et al., 2022; Thaw et al., 2022). The primary driver of deepening target depth in drilling is the overexploitation of shallow groundwater. Especially in arid environments, the shortages of annual rainfall, variation in climate, decreased local and regional recharge to the groundwater system can significantly affect aquifer productivity. In the volcanic aquifers of Ethiopia, significant recharge and groundwater flow mechanism from mountainous regions are characterized by the regional deep lateral subsurface groundwater flow system to the low elevated discharge zones of the rift margins and main Ethiopian rift systems which are characterized by semi-arid to arid environments. Such semi-arid to arid zones are highly dependent on groundwater resources due to lack of surface water. Based on the assumption that increased drilling depth can increase the yield of aquifers, government financed deep drillings were conducted to depths of exceeding 500m in various volcanic aquifers in Africa. Considering groundwater's resilience to climate change, tapping into deep groundwater resources for adaptation is increasingly advocated (UNICEF, 2021).

Making use of unprecedented pumping test data on volcanic aquifers in Ethiopia, the objective of the current work is to analyse the depth and age wise variation in the hydraulic structure of volcanic rocks and produce a conceptual framework of the hydraulic structure. The aim of the work is to produce key hydraulic data on volcanic aquifers and inform

groundwater managers to make appropriate decisions in determining the depth of drilling for water supply in volcanic terrains.

2.2. Materials and Methods

2.2.1. Site Description

The volcanic terrain in Ethiopia covers 65% of its land mass (Figure 2). The Ethiopian flood basalt covers an area of 600,00 Km^2 with an estimated volume of 350,00 Km^3 (P. Mohr & Zanettin, 1988a; Paul Mohr, 1983). The volcanic rocks were recently classified into the lower basal sequences (LB), the upper basal sequence (UB), the broad-based volcanic shield capping the plateau (SV), the Rift Margin Volcanics (RMV) and Quaternary scoriaceous basalt (QV) (Kieffer et al., 2004). The RMV is composed of LB, UB and QV rocks but is distinct by its location at the intersection of the tectonically active NNW-SSE running Ethiopian Rift Valley (ERV) and the E-W running Yerer Tullu-Welel volcano-tectonic lineament (YTVL) (Abebe et al., 1998).

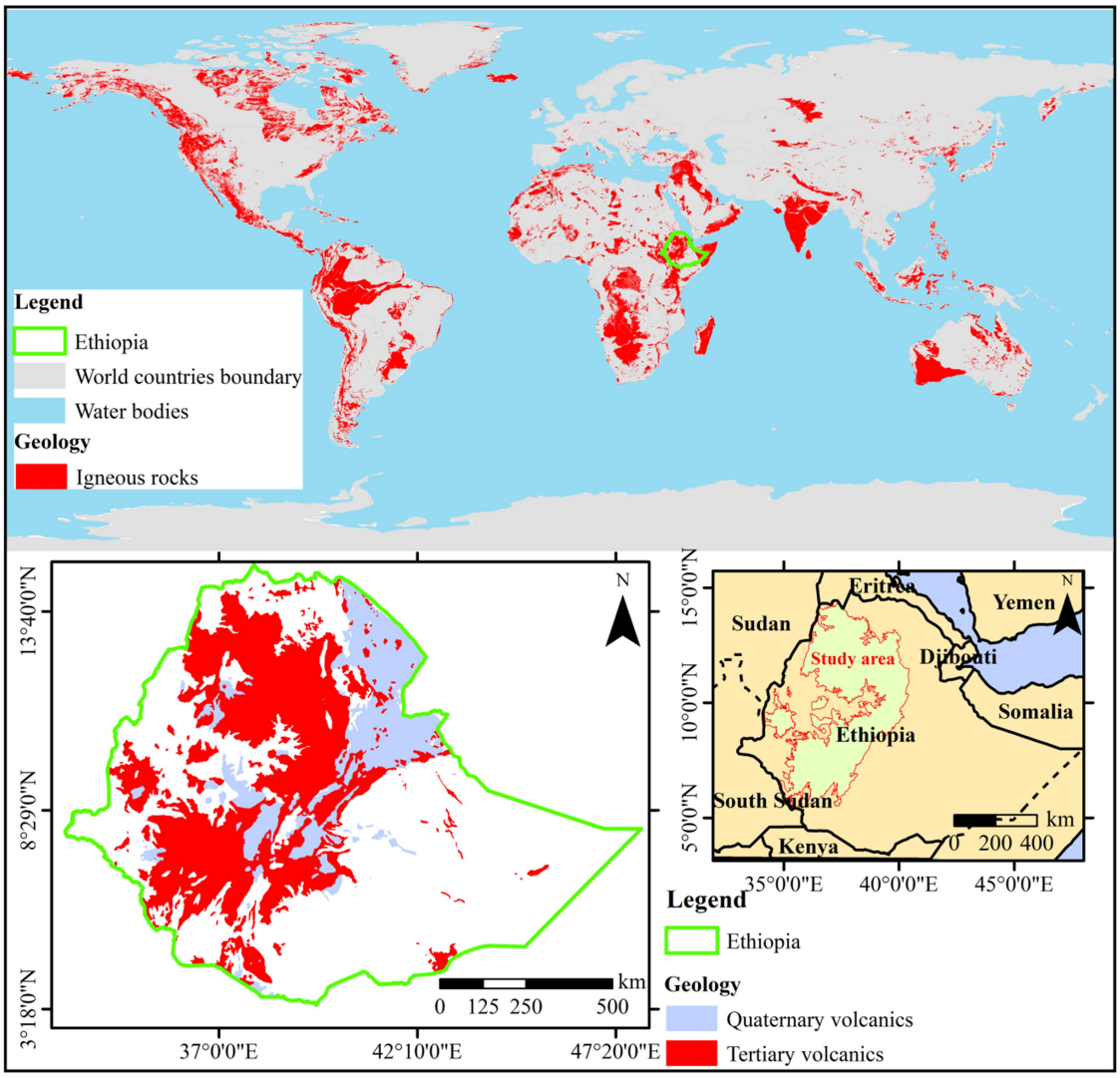

Figure 2.1: Global occurrence of igneous rocks modified from (USGS, 2000), location map of study area and volcanic map of Ethiopia

Mirroring the geologic classification, the volcanic rocks were classified into four hydrostratigraphic units (Kebede, 2013a). These are: 1) The basal sequence of lower basalt (LB), characterized by rugged topography, deep weathering and low permeability; 2) The upper basal sequence (UB) of large flood basalt, known by flat-topped, slightly to highly weathered, characterized by dual porosity, confined conditions. In the deeper volcanic aquifers, the well yields are associated with regional fault lines and permeable volcanics and interbedded permeable sediments (Ayenew et al., 2008a). 3) The RMV volcanics are characterized by deep-seated regional faults that crossed each other (YTVL and MER),

comprising fractured basalts and ignimbrites. 4) The QV is characterized by scoraceous basalt and scoria and central volcanoes. Intercalations of rhyolitic volcanic rocks with welded and unwelded ignimbrite provide confinement in all the units (Yitbarek et al., 2012).

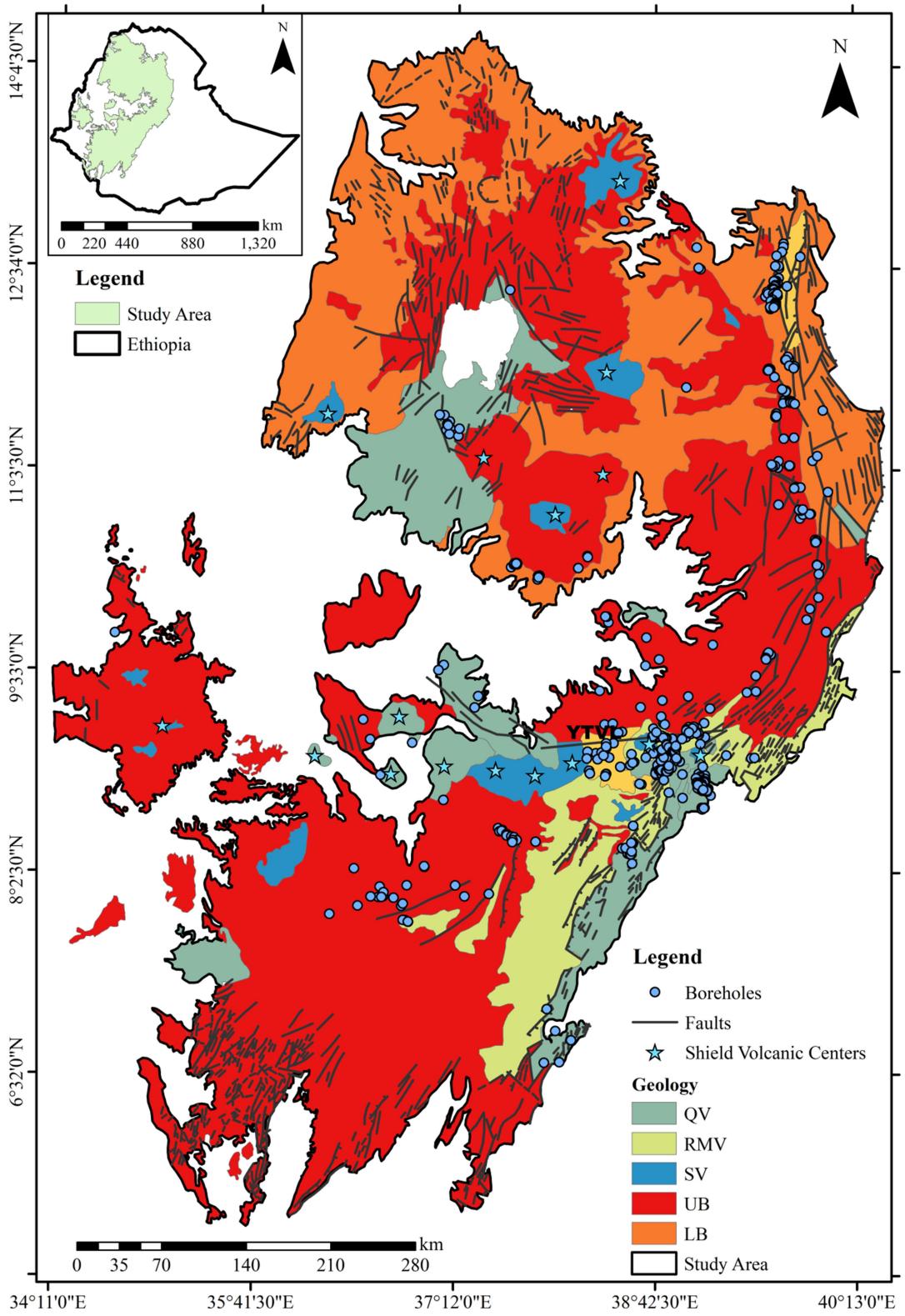
N
0 220 440 880 1,320
km
Legend
Study Area
Ethiopia
14°4'30"N
12°34'0"N
11°3'30"N
9°33'0"N
8°2'30"N
6°32'0"N
34°11'0"E
35°41'30"E
37°12'0"E
38°42'30"E
40°13'0"E
YTVL
Legend
Boreholes
Faults
Shield Volcanic Centers
Geology
QV
RMV
SV
UB
LB
Study Area
0 35 70 140 210 280
km

Figure 2.2: Hydrogeological map modified based on four major aquifer classes: a) LB = the lower basal sequence (Eocene Lower basalt), b) UB = the upper basal sequence (Oligocene to Miocene flood basalts), c) SV = the broad based volcanic shield, d) RMV= the Rift margin volcanics (Miocene to Pliocene volcanics) and e) QV= the quaternary volcanics

2.2.2. Pumping test data Collection and Aquifer classification

The pumping test data has been collected from multiple well fields. We collected single well constant discharge, step drawdown, and recovery test data records on 517 deep boreholes and 42 shallow wells from various government ministries. Well diameter varies between 6 inches for shallow wells and 8 to 28 inches for deep wells. While the deep wells are evenly distributed across the four hydrostratigraphic units, the shallow wells fall in four districts with different geologies. Volcanic aquifer pumping test data were analysed for the four rock age classes (Eocene LB, Oligo-Miocene UB, Miocene RMV and Quaternary QV) to determine hydraulic properties (T, K, Sc and Q). The salient features of the boreholes (nLB=23, nUB=254, nRMV=91 and nQV=191 boreholes) such as well depth, static water level, other hydraulic properties and geologic age group were used in the aquifer productivity analysis.

2.2.3. Pumping test data analysis

The pumping tests were analysed by constant discharge, recovery and step-drawdown tests. Because of the lack of observation wells we used single well pumping and recovery test method. The constant-discharge rate pumping test was analysed using (Theis, 1935) and (Cooper & Jacob, 1946) approximation methods considering the confined aquifer state in all the wells. Recovery data were analysed using the residual drawdown method. The specific capacity was determined from the ratio of well yield (Q) divided by the drawdown in the pumping well (i.e. Q/S). The transient flow of groundwater to the well was determined by the following equations for the drawdown of the well (Theis, 1935). The step-drawdown data were analysed using the single-well method of Rorabaugh (1953).

2.3. Results

2.3.1. Hydraulic properties Statistics

The statistical summary of hydraulic properties for the aquifer classes is presented in Table 1. The results indicate that the static water level reaches up to 199 m b.g.l (below ground level) in some wells of UB aquifers. The T values ranged between 0.02 - 9830 m^2/day and its mean values for the rock age classes ranged from 168.1 - 903.8 m^2/day. The K values ranged from 0.001 - 5130 m/day, showing the mean values are between 5.5 to 101.3 m/day. The S_c ranged from 0.01 to 2501.05 (L/min)/m, with the mean value between 36.82 and 100.55 (L/min)/m. The Q ranged from 1 to 150 L/s with the mean ranged between 20.59 to 60.3 L/s. The maximum T and Q are observed in the QV, while the lowest T and Q are observed in the LB. The hydraulic properties (T, and Q) show outliers of high values in the younger QV and RMV aquifer classes as compared to the older UB and LB ones. The absence of higher outlier values in the older aquifer units (LB) is most likely related to the preferential disappearance of secondary permeability and homogenization of volcanic aquifer hydraulic properties due to thick overlying different basaltic flow episodes of flood basalt and with increased age (Kebede, 2013b).

The cumulative frequency plot illustrates that there is a high percentage of high Q and T in the QV aquifer classes, while the lowest frequency of low Q and T values was observed in the LB aquifers (Figure 3a and b). Less than 5% of wells in all aquifer classes show a K value exceeding 50 m/day (Figure 3c). Consequently, 20% of wells show S_c values of less than 120 (L/min)/m (Figure 3d).

Table 2.1: The statistical summary of hydraulic parameters of water wells

Summary	Aquifer Classes	Depth(m)	SWL (m b.g.l)	Q (L/S)	K (m/day)	T (m^2/day)	Sc (L/Min)/m)
Min	LB	62.5	0	2	0.8	6.65	0.08
	UB	35.6	0	1	0.001	0.02	0.02
	RMV	68.6	0	2.5	0.01	0.91	0.03
	QV	18.6	0	7.25	0.02	0.84	0.01
Mean	LB	229.24	8.7	20.59	5.45	168.14	46.06
	UB	180.36	86.69	30.86	7.59	411.86	100.55

	RMV	393.49	43.88	45.83	101.32	850.01	45.34
	QV	402.35	92.49	60.3	53.2	903.81	36.82
Median	LB	186	8	17.25	3.75	79.20	1.03
	UB	150	86.5	20	1.68	122	13.66
	RMV	402	44	38.3	1.36	113	1.47
	QV	440	92	58	3.01	225	1.98
Sd	LB	119.25	5.58	16.27	4.65	182.99	71.40
	UB	114.74	62.20	28.10	25.99	756.02	253.96
	RMV	114.35	26.04	31.29	586.09	1882	265.77
	QV	155.51	53.79	30.91	310.36	1865.57	173.7
Max	LB	500	17	66.17	12.3	696	268.2
	UB	882	199	121	283.39	5570	2501.05
	RMV	598	84	117	5130	9720	2501.05
	QV	623	185	150	3930	9830	1764.71

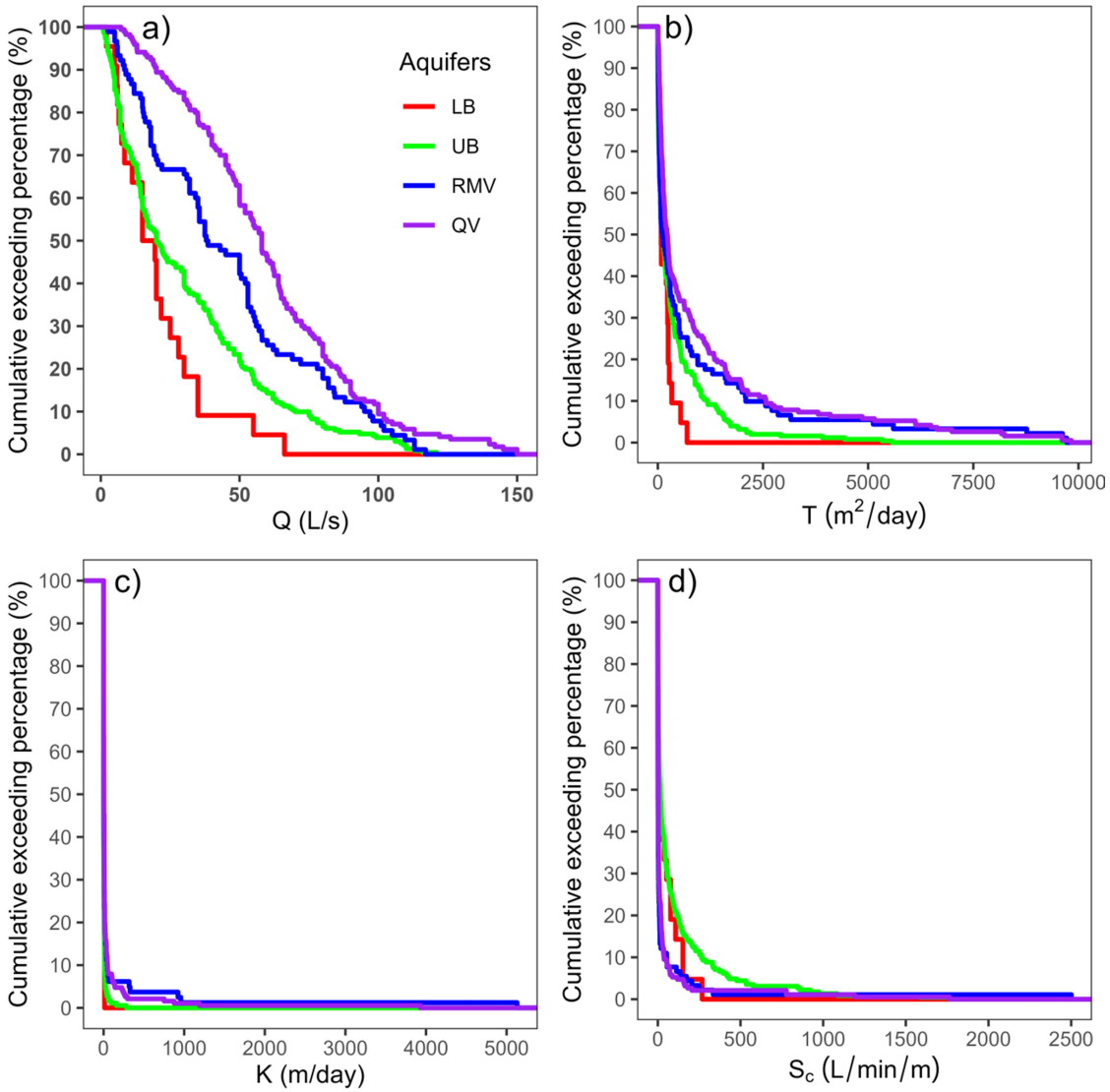

Figure 2.3: Cumulative frequency distribution of hydraulic properties in aquifer classes of Ethiopian volcanic aquifers. a) The percentage of wells whose Q equals/exceeds that shown in the wells. b) The percentage of wells whose T equals/exceeds that shown in the wells. c) The percentage of wells whose K equals/exceeds that shown in the wells, and d) The percentage of wells whose S_c equals/exceeds that shown in the wells.

2.3.2. Depth wise variation in aquifer properties

In many instances, volcanic aquifers show a depth wise decrease in K because of overburden pressure, which tends to reduce fracture aperture and pore space size (Jackson & Fenelon, 2022). There are also instances where non-systematic variations of hydraulic

properties with depth have been reported (Worthington, 2021). Non-systematic variation is the result of vertical heterogeneity in aquifer lithology, degree of weathering and secondary mineralization. In the current work, the aquifer properties analysis against depth indicates high variability and poor fit between T and Q, with depth when considered for all aquifer classes (Figure 4a - b) inconsistent with observations made elsewhere in volcanic aquifers (Jackson & Fenelon, 2022; Worthington, 2021). However, at the local scale mainly in the UB aquifer class the decreasing T and Q with depth was observed in some deep wells (eg: The Sululta plain deep wells), consistent with observations made by (Allocca et al. (2022); Jackson & Fenelon, (2022) . The studied volcanic aquifers are heterogeneous in nature and composed of complex intercalations of massive basalts, fractured basalts, ignimbrites, and minor volcanic ashes (Ayenew et al., 2008a; Furi et al., 2012; GEBRE, 2010; Kebede, 2013b; Kebede et al., 2005; Mamo, 2015; Nigate et al., 2017; Yitbarek et al., 2012). The variation in aquifer lithology contributes to the lack of systematic depth wise variation in hydraulic properties. The result indicated that there is no clear general trend of depth-wise variation in the hydraulic properties of aquifer classes (Figure 4a and b). The other contributing factor is the lateral variation in the hydraulic properties owing to variations in the degree of fracturing, lithological variation, and density of lineaments. These lateral variations contribute to non-systematic depth wise variation of the hydraulic properties when the hydraulic values derived for the different locations of the same aquifer class are compared for depth wise variation analysis.

2.3.3. Age wise variation in aquifer properties

The age wise (also lateral, as the rocks crop out in different regions) variations in aquifer properties are systematically compared to the depth-wise variations. The aquifers show a significant variation in the hydraulic properties with age confirming various previous observations made elsewhere globally (Brace, 1980, 1984; Ma et al., 2016a; Saar & Manga, 2004). The old (Eocene) LB aquifer is characterized by the lowest K Q and T as compared to the other younger aquifer classes (Figure 5a and b). The LB aquifer is a deeply weathered, thinly bedded basaltic aquifer with a strong thermal alteration. The thermal alteration includes the formation of quartz and calcite veins and mineralization by zeolites and chlorites (Ollier, 1988). With a smaller range of values and near absence of outlier

hydraulic values, the aquifer shows higher homogeneity compared to the other aquifers. The low value of K and T as well as the aquifer homogeneity are most likely the result of deep weathering and alteration. The Oligocene-Miocene UB aquifer shows narrow ranges of T (Figure 5b) due to complex hydro-stratigraphy, thick sequences of eruption episodes intermingled with unconsolidated pyroclastics and clay layers, while the outliers indicate the fracture-related high T aquifer. The highest T in the UB aquifer was observed in < 150m deep well, while the lowest T was observed in the deepest well associated with the thick massive basaltic formation. The Oligocene-Miocene UB aquifer shows the next narrow ranges of Q and T with relatively frequent outlier values but not as pronounced as in the other younger classes. All the outlier values (high T and Q) in the UB aquifers are from the shallow layer of the aquifer (Figure 5a and b). T and Q are relatively high compared to the older Eocene LB which shows a clear sign of decreasing T with age.

The Miocene RMV aquifer shows the medium to high range of Q and T values. The outliers of high T values are associated with regional and local faults in fractured aquifers (Figure 5a and b). The QV aquifer is characterized by the highest aquifer productivity when compared with all other volcanic aquifers. The highest value of T was observed in scoraceous basaltic formations, while the lowest T was in pyroclastic deposits and reworked overlying unconsolidated units. The outliers of T and Q in QV show the productive scoraceous basaltic aquifers controlled by quaternary structures (Figure 5a and b). The highest T and Q in the youngest QV aquifers are due to the primary porosities in the quaternary scoraceous basaltic formations not filled with mineral grains, not altered, interconnected grain matrix, fracture networks of volcanic rocks, recent quaternary structures (local and regional faults), sequences of eruption episodes and weathering intensity. QV shows slight increments of Q and nearly constant variation of T with age and depth of the aquifer (Figure 4a and b). Generally, the overall volcanic aquifers' productivity variations age-wise of each aquifer classes show a weak correlation that does not show significant changes as observed from the P-value and R^2 values of all volcanic aquifer classes (Figure 4a and b). The volcanic aquifer classes (from the oldest LB to the youngest QV) are exposed to the surface in different regions showing lateral variations at different localities where they have no single vertical litho-stratigraphic sections exposed in one

region. For example, the LB aquifer is exposed to the surface only in the northern part of Ethiopia. However, there is no lateral continuation of this unit in the central and southern part of the study area because it is deeply buried under thick successions of other volcanic classes. Similarly, the UB aquifer formed thick succession of flood basalts with various eruption episodes in different regions. The RMV and QV also comprise thick succession of different phases of volcanic layers at the central part of the study area. In general, it is difficult to find the vertical lithologic section in one single borehole because of the lack of drilled borehole that penetrated through all aquifer classes.

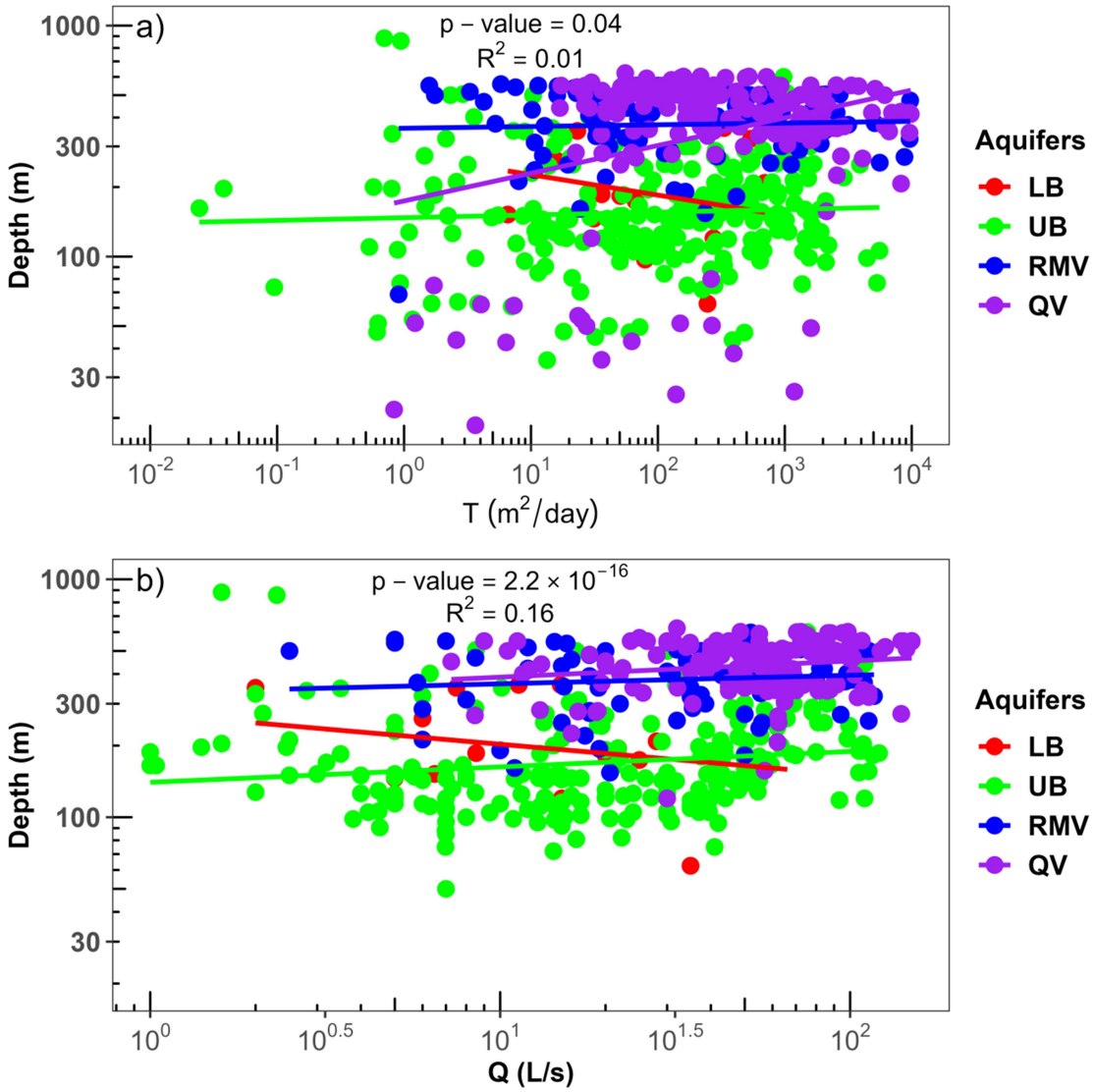

Figure 2.4: The scatter plot depicting four volcanic aquifer classes: LB= the lower basal sequences, UB= the upper basal sequence , RMV= the rift margin volcanics and QV=the Quaternary volcanics a) The scatter plot of T against water well depth and b) the Q against water well depth.

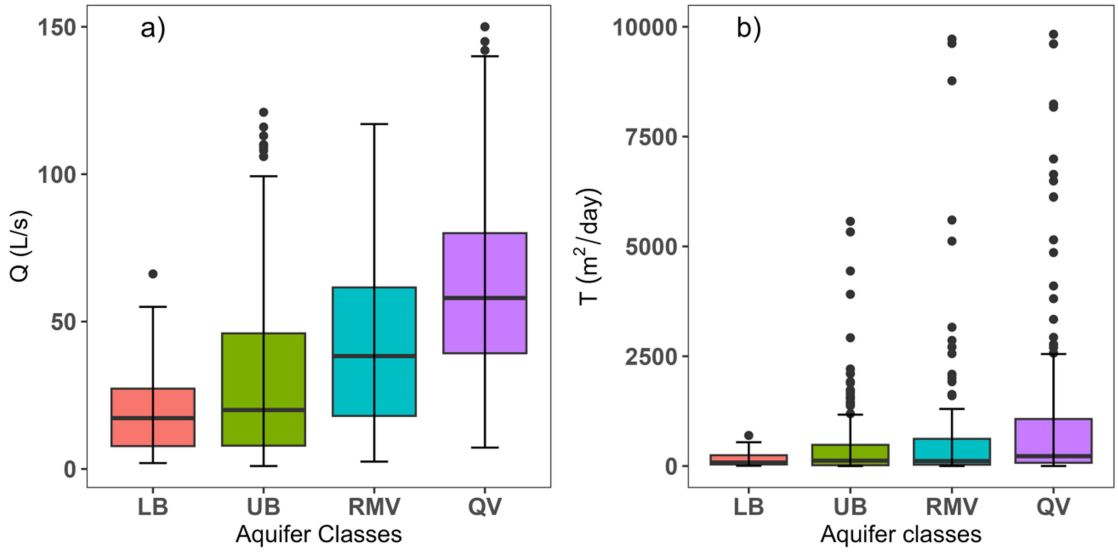

Figure 2.5: The box plot of volcanic aquifer classes a) the Q against aquifer classes and b) the T against volcanic aquifer classes.

2.4. Discussion

2.4.1. Implications for water well drilling and productivity analysis

The age and depth wise analysis of volcanic aquifers in the Ethiopian highlands is of vital importance to managing groundwater resource exploration and water well drilling programs. Water suppliers are challenged with the question of what the drilling depth should be to obtain a sufficient volume of water for water supply. Among local water supply agencies, there is the assumption that deep drilling in volcanic aquifers can increase borehole yields. However, the results from this work reveal that the hydraulic properties (Q and T) of the volcanic aquifers have no clear vertical trends with increasing water well depth. The lack of any depth wise trend in aquifer productivity and T suggests these parameters are controlled by local geologic conditions including, the complex interfingering of different lithologies, fracture networks, the presence of regional and local structures, etc. This means reliance must be made on local knowledge of geology and evidence from geophysics to determine drilling depth.

However, the age wise variation in aquifer productivity is significant. Older formations are less productive compared to younger formations. This is also in agreement with observations in Djibouti whereby the younger volcanic aquifers show a higher T than the older volcanic layers (Mohamed Jalludin & Razack, 2004). Eocene LB is characterized by the lowest productivity due to the deep weathering and alteration that led to the filling of fractures and matrix porosity with secondary infilling materials. The variation in K, T and Q within the Eocene LB is limited owing to the homogenization of the aquifer by weathering and alterations. Water suppliers must expect a low yielding aquifer if boreholes are to be sited in the Eocene LB aquifer, local high productivity zones are unlikely to be crossed in this unit. The Oligocene-Miocene UB is characterized by a higher yield compared to the LB but is characterized by low yields compared to the other younger units. The UB is characterized by thickly bedded multiple eruption layers of basalts intermingled with clay layers, unconsolidated pyroclastics and impermeable rhyolites and trachytes. Some wells show good productivity (Figure 4a and b) at shallower depths fractured basaltic formations. Local high productivity zones can be encountered in this unit.

The late Miocene RMV of medium to high productivity is associated with fractured basalts and ignimbrite and is intensively affected by two major faults, the YTVL and Main Ethiopian Rift (MER) faults that formed deep aquifer systems expressed as the hydrogeological window (Kebede et al., 2008). The highest aquifer productivity in the QV aquifer is associated with the highly fractured and weathered basalts, scoraceous basalts and scoria of recent quaternary eruptions and structures, as well as fracture networks that formed a high degree of water-bearing formation as previously reported in Kebede et al. (2005); Mamo (2015); Nigate et al. (2017). Comparing the productivity of the different formations, it can be concluded that the younger formations are more promising for future groundwater development providing higher borehole yields such as groundwater for agricultural production.

2.4.2. Conceptual hydrogeological frame work of volcanic aquifers and implications for groundwater flow models

Global scale groundwater models that account for the lateral flow of groundwater are emerging recently (de Graaf et al., 2017), but the accuracy of the models is challenged by

the lack of a coherent representation of the vertical distribution of hydraulic conductivity (K) of the subsurface in different geological settings across the earth's surface. Considering volcanic aquifers cover a substantial part of the continental and oceanic crust, hydraulic structure data on volcanic rocks will help the modelling effort in assigning appropriate mean K values and their vertical and lateral distribution in volcanic rocks. The current work reveals that the hydraulic structures of volcanic rocks are heterogeneous and local factors control the vertical hydraulic structure of the rocks. Depth is not a very good predictor of hydraulic conductivity and transmissivity as there is no clear correlation between depth and T (and K) up to the depth of 1000 meters. Against the widely held notion that K decreases with depth in crystalline rocks because of hydrostatic and geostatic pressures (Bianchi et al., 2020; Dewandel et al., 2006; Deyassa et al., 2014; Maréchal et al., 2004), the dataset from the volcanic province under investigation reveals no such observation. However, the ages of the lithology are a good predictor of the hydraulic properties (Figure 6), noting that the vertical section presented here does not represent a single well. There is an unconformity between vertical litho-stratigraphic formations that also varies in lateral extent. The vertical variations in K values show a heterogeneous distribution that becomes homogenized at the older LB unit. With age, aquifer properties will become homogenized. Fracture porosity, which would have contributed to high variability in the hydraulic properties, is lost to alteration filling with the ageing of rocks. While there are growing datasets on the depth wise variation in the hydraulic properties (Jackson & Fenelon, 2022; Ma et al., 2016b; Saar & Manga, 2004; Worthington, 2021), the hypothesis that K and T vary globally with rock age necessitates a concerted effort to compile the hydraulic properties of rocks across the globe based on age group.

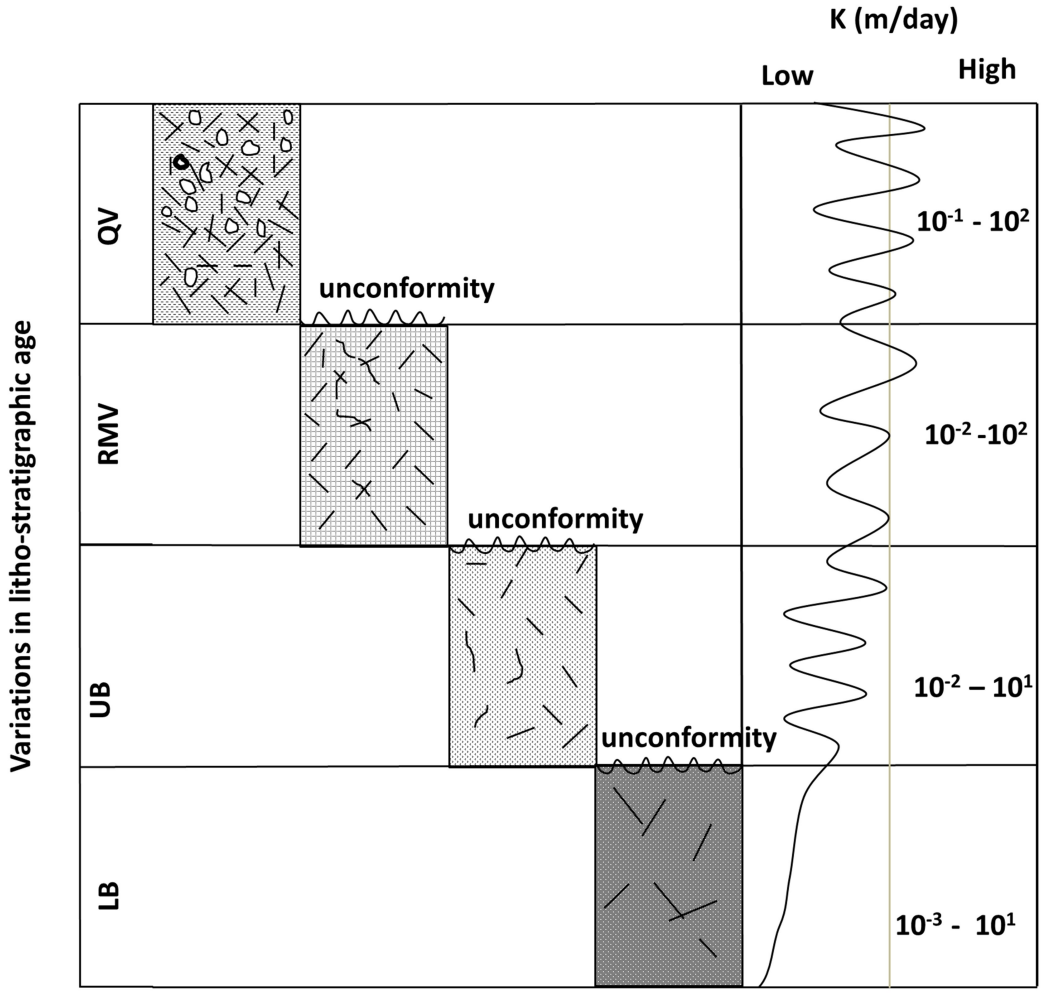

Figure 2.6: The conceptual hydrogeological model in Ethiopian volcanic aquifers depicting aquifer productivity variation with age wise. The x-axis shows the ranges in k of aquifers and y-axis shows the age-wise classification of each volcanic aquifer classes.

2.4.3. Comparison of results with global volcanic aquifers

In the global volcanic aquifers, including Ethiopia, deep drillings were conducted based on the assumption that they would have higher productivity at higher depths and older ages than the shallower and youngest volcanic products. However, the Ethiopian volcanic aquifer productivity shows a weak correlation of aquifer productivity against the depth and age of aquifer classes due to complex hydrogeological systems. The regolith layer overlaying the basaltic units formed a shallow groundwater flow system in the upper Blue

Nile basin, providing water supply for hand-pump wells of the rural water supply, showing decreasing water yield in the basaltic layer (Walker et al., 2019a). This is not in agreement with the current work that shows the shallow fractured and weathered quaternary volcanic layers provide good productivity compared to the underlying massive flood basalt and the overlying regolith layer of thick clay units in the volcanic aquifers.

Comparing the current result to the global volcanic aquifers (Table 2), we show that volcanic formation age is a good predictor of aquifer property. In Djibouti, volcanic aquifers show decreasing productivity with increased age. The younger stratiform series show a higher T than the older Dalha Series (M. Jalludin & Razack, 1994), in agreement with our observation. Similarly, the oldest Eocene Deccan traps in India show the decreasing potential of aquifer productivity with age (Gupte, 2010). The weathered portion of the youngest lava flows formed the local and intermediate aquifer productivity (Vincent & Joshi, 1986), while low productivity is observed in the much lesser primary porosity and vesicles are filled with secondary minerals (Singhal, 1997). The oldest Deccan trap aquifer shows the lowest aquifer productivity as compared to the younger basalts of Ethiopian volcanics, Hawaiian islands and Columbia Snake River basalt. The Miocene age Columbia Snake River basalts are the most productive aquifer, providing an average T of 10^4 m^2/day, while productivity decreases in the coherent and denser deeper basaltic units (Kahle et al., 2011; Piersol & Sprenke, 2015; Porcello et al., 2009). The Columbia River basalt aquifer has similar characteristics to the younger QV, high productivity Ethiopian volcanic aquifers.

Table 2.2: A comparison of aquifer characteristics of the Ethiopian trap series with some other volcanic regions

country	Place/Area	Formation	Age	T (m^2/day)	Reference
Spain	Gran Canaria	Old basalts	Miocene	5-180	(Custodio, 1985)
		Modern basalts	Post Plieocne	40-200	
India	Karnataka	Deccan Trap	Early Eocene	10-180	(Adyalkar & Mani, 1974; Deolankar, 1980)
	Andhra Pradesh			1-198	
	Maharashtra			0.1 to 500	
USA	Columbia	Basalt		$1x10^3$ to $1.8x10^5$	(Walton &

	Snake Rivers			(av. $1x10^4$)	Stewart, 1961)
	Oahu, Hawaii	Tholeiitic	Pliocene	15000 (in dyke free zone)	
		Basalt		1500 in the marginal dyke zone	
Mexico		Fissured basalt	Pliocene to Holocene	605-865	
Ethiopia	Lower basalt	Basalt	Eocene	0.02 to 696	Current study
	Upper basalt	Basalt, rhyolite and ignimbrite	Oligo-Miocene	0.53 to 5,570	
	Rift margin volcanics	Basalt and Ignimbrites	Late Miocecene	1.5 to 9,720	
	Quaternary volcanics	Scoraceous Basalt	Quaternary	16.9 to 9,830	
Djibouti	Stratiform series		Pliocene to Pliestocene	129.6 to 49,248	(M. Jalludin & Razack, 1994)
	Dalha series		Miocene to Plieocene	0.25 to 1,382.4	

2.4.4. Implication for groundwater resources management and modelling

Systematic groundwater resource exploration and exploitation requires prior knowledge of hydrogeological settings in the vast highly populated regions of volcanic terrain. The age and depth-wise analysis of the Ethiopian volcanic aquifers is exhibited by complex hydrogeological settings with no clear correlation between the depth of drilling and aquifer productivity. Complex volcanic layering formed by different eruption episodes, inter-fingering of clay layers and paleo-soils with volcanic layers, topographic settings, structural effects and local conditions of the aquifer system controls the aquifer productivity. Increasing the depth of drilling to get higher aquifer productivity appears not to be a convincing argument for drilling deeper. Future groundwater development efforts for productive use can target the younger volcanic rocks. Deeper drilling in older rocks may not produce exceptionally high borehole yields and fractures and secondary permeability tend to disappear with rock ages. The limitations of this work are the lack of borehole data

in various volcanic terrains for both shallow and deep wells and the full scarcity of data from shield volcanoes to characterize the aquifers' hydraulic properties. Furthermore, the main Ethiopian Rift system and the south eastern Ethiopian Plateau are not included in the analysis of this study to frame the general hydrogeological set up of the entire Ethiopian volcanic aquifers.

2.5. Summary and concluding remark

Our analysis reveals that formation age is one of the primary controls on the hydraulic properties of volcanic rocks. This finding implies the need for a global compilation and inter-comparison of the hydraulic structures of volcanic rocks. The pattern in depth wise variation may be similar (i.e., week correlation between depth and hydraulic properties) across various age groups globally; however, each age group has a statistically distant hydraulic property from the other age group. Volcanic rocks have been known to occur on Earth's surface for billions of years, necessitating an inter-comparison of hydraulic properties with age.

The current work also has local groundwater management significance. The productivity of Ethiopian volcanic aquifers aged from Eocene LB to Quaternary characterized by complex hydro-stratigraphy was investigated by depth and age-wise using litho-stratigraphy and hydraulic properties. The aquifer properties show that the T and Q of major aquifer classes ranged from LB (0.02 to 696 m^2/day and 1 to 66 L/s), UB (0.53 to 5570 m^2/day and 1 to 121 L/s), RMV (1.5 to 9,720 m^2/day and 2.5 to 117 L/s) and QV (16.9 to 9830 m^2/day and 7.25 to 150 L/s), showing the general unclear trend of decreasing or increasing aquifer productivity with increased drilling depth and age. The age-depth-wise aquifer productivity analysis shows that

1) The depth wise variation of aquifer productivity showed weak correlation (P-value = 0.04 and R^2 = 0.01 for T and P-value = $2.2*e^{-16}$ and R^2 = 0.16 for Q) in all aquifer classes which have no clear pattern with increased drilling depth. The aquifer classes (deep QV and RMV aquifers) show increased productivity, LB shows decreasing productivity and UB shows unclear patterns of aquifer productivity with increased water well depth.

2) The Eocene LB aquifer system with its limited lateral extent and overlain by thick, massive flood basalts that hindered the vertical recharge to the LB, shows the lowest productivity as compared to all other aquifer systems.
3) The Oligocene to Miocene UB aquifer shows a weak correlation of aquifer productivity with drilling depth and age due to complex multiple eruption phases of volcanic layers intermingled with clay layers and paleosols, topographic settings and geological structures. However, exceptional cases were observed in the deepest well which shows very low productivity in massive basaltic units.
4) The Miocene RMV is the second most productive deep aquifer system, showing a weak correlation with depth and age, while some of the deep wells in RMV are highly productive compared to the shallower depth in a fractured basalts and ignimbrites that are controlled by the major regional fault systems of YTVL and MER.
5) The youngest QV is the most productive aquifer system, serving as the source for shallow and deep wells, showing high productivity in highly fractured and weathered basalt, scoraceous basalt and scoria fall deposits.
6) Deep drilling into QV and RMV, although there is complexity in hydro-stratigraphy, encountered a more productive aquifer system than LB and UB. Detail geophysical studies and fracture density analysis are recommended to develop full insights into the depth and wise aquifer productivity analysis. This work helps to understand the general flow model and merit-based groundwater wells effective drilling depth in the broad volcanic aquifers of the Ethiopian highlands.

Chapter Three

3. Estimating Groundwater Flow Velocity in the Shallow Volcanic Aquifers of Ethiopian Highlands Using a Geospatial Technique

3.1. Introduction

Groundwater has a crucial role as a source of water supply in several parts of the World's rural and urban centers. The strategic importance of groundwater for water supply is due to its resilience to more frequent and extreme drought, increased variability in precipitation, sustaining climate change adaptation strategies and groundwater-related ecosystems in sub-Saharan Africa including Ethiopia (MacAllister et al., 2020; Macdonald et al., 2019; Taylor et al., 2013). Shallow groundwater in sub-Saharan Africa represents a neglected opportunity for promoting small-scale irrigation activities (Gowing et al., 2020). Since rainfall-dependent agricultural activities have been affected by seasonal variations of climate effects, shallow groundwater can be used as an alternative source for small-scale irrigation. Despite its importance for the water supply, the shallow groundwater of Ethiopian highlands has been less investigated. Furthermore, there are un-sustainability and low-yielding hand pump boreholes and rapid transit of contaminated water due to damaged headwork and poor construction that deteriorates groundwater quality (Banks et al., 2021) and decreasing aquifer productivity and multi-faceted failures of the hand pump boreholes in the shallow aquifers of Ethiopian highlands (Macdonald et al., 2019). Therefore, understanding groundwater flow velocity has paramount importance in revealing the hydrogeological settings and sustainable groundwater management.

Shallow volcanic aquifers of Ethiopian highlands were tapped by hand pump wells as a vital source of water supply for significant statistics of populations in the remote communities of Ethiopia. However, the shallow volcanic aquifers are manifested by depletion of water level due to the response to climate change effects and reduction in groundwater recharge during long dry seasons. Likewise, an increased abstraction of groundwater due to the high population demand for water supply has also caused

groundwater depletions (Fenta et al., 2020). This in turn can affect the hydraulically interconnected aquatic environments dependent on shallow groundwater flow systems.

The shallow volcanic aquifers of Ethiopian highlands comprised moderate to high productivity in a fractured and weathered tertiary to Quaternary basalts, alluvial deposits and thick weathered regolith (Kassune et al., 2018; Mamo, 2015; Nigate et al., 2017, 2020; Walker et al., 2019a) in the Lake Tana basin. Similarly, basalt and alluvial deposits were characterized by good productivity, while localized aquifers of rhyolite, trachyte, pyroclastic and welded ignimbrites depict low productivity aquifer system (Yitbarek et al., 2012) in the Becho plain and along Awash River banks. Hence, detailed hydrogeological studies of aquifer characteristics and groundwater flow dynamics have a paramount importance for the proper management of shallow volcanic aquifers.

Groundwater flow velocity estimation is fundamentally important in hydrogeological studies for a variety of purposes including monitoring and predicting contaminant movement and pluming from recharge to the discharge zone, estimating cleanup times, studying recharge, designing permeable reactive barriers (PRBs), and interpreting groundwater movement in regional aquifer systems (Devlin et al., 2009). Furthermore, measurements of groundwater flow velocity help to identify the dynamics of groundwater flow and its response to stress, optimize water resources management and calibrate groundwater flow and transport modelling and characterize engineering structures associated with groundwater (Bakx et al., 2023). With the increasing dependence on groundwater resources and geothermal resources, the measurement of groundwater flow velocity magnitude and groundwater flow direction is becoming more and more refined (Li et al., 2019).

There are several methods of groundwater flow velocity estimation. The Darcy-based method is the low-cost and effective method that performs groundwater flow velocity estimation at the local and regional scale by using conventional aquifer characterization of water level survey, hydraulic conductivity and effective porosity (Devlin, 2020). The groundwater flow velocity can be estimated by thermal response test (Chae et al., 2020), radioactive tracer Technetium-99m (Ahmad et al., 2008), groundwater flow velocimeter using point dilution technique to measure in-situ groundwater flow velocity (A. Englert,

2003), the measurement of contact resistance using formation resistivity and solute flow theory related to the change in concentration with the time of a solute to estimate a groundwater flow velocity (Lile et al., 1997) and borehole hydraulic testing to compute flow velocity in un-faulted fractured aquifers (Medici et al., 2019). The in-well groundwater flow velocity methods are point dilution methods(Brouye, 2003; Drost et al., 1968); Passive flux meter(Hatfield et al., 2004), in-well point velocity probe (Osorno & College, 2016), colloidal borescope (Kearl et al., 1998), heat pulse flowmeter (Liu et al., 2023), direct velocity techniques (Essouayed et al., 2019b). The ^{222}Rn isotope is also a proven technique to estimate groundwater flow velocity (Cook et al., 1999; Hamada, 2000; Schubert et al., 2011). The estimation of groundwater flow velocity using the geospatial technique has a significant ecological advantage as it uses the measurements of natural groundwater flow systems without introducing artificial tracers. However, another method like the tracer method (e.g. point-dilution method) applies artificial tracers which might affect the quality of groundwater along the flow and groundwater-related ecological systems. Similarly, groundwater flow velocity estimation using the natural ^{222}Rn isotope technique has no effect on the groundwater quality and related aquatic environments, while it might have inaccurate results due to inappropriate ^{222}Rn sampling (^{222}Rn the water well and in the aquifer).

The geospatial technique is used to estimate the groundwater velocity at a large scale depending on the four essential maps (groundwater elevation head, effective porosity, saturated thickness, transmissivity) and borehole history and this method has been conducted in shallow unconsolidated aquifers and fissured-karst aquifers (T. O. Abdullah et al., 2020; Al-Madhlom et al., 2020). However, the groundwater flow velocity estimation in volcanic aquifers has been rarely investigated, particularly in Ethiopian volcanic settings. Therefore, the purpose of this work is to investigate aquifer hydraulic parameters from pumping test data analysis, examine the history of water wells and estimate groundwater flow velocity using geo-spatial technique in shallow volcanic aquifers of Ethiopian highlands. This work helps in understanding the groundwater flow dynamics, contaminant pluming, aquifer response to stress, sustainable groundwater development and

management in rural water supply and small-scale irrigation activities in shallow aquifers of Ethiopian highlands.

3.2. Materials and Methods

3.2.1. Geology and Hydrogeology

The study sites (Figure 1) are situated in shallow volcanic aquifers of four major basins of Abay, Awash, Ziway Lake and Ghibe basins. The geology of study sites (Figure 1b to 1e) comprises volcanic rocks of Oligocene to Quaternary formations. The Mecha site (Figure 1b) is situated in the source region of the Abay Basin. The major geologic units are Quaternary basalts associated with cinder cones, Quaternary alluvium in flat-lying topography and marshy areas and weathered features of tertiary basaltic formation (P. A. Mohr, 1967; P. Mohr & Zanettin, 1988a). The Miocene basaltic formation is characterized by medium to low productivity fractured aquifer, while Quaternary basalt, alluvium and inter-granular aquifers show high aquifer productivity (Kebede et al., 2005; Mamo, 2015; Nigate et al., 2017, 2020; Walker et al., 2019b). The Ejere site (Figure 1c) is situated in the Awash River Basin. It comprises the Miocene basalt, trachyte and Quaternary alluvial sediments (P. A. Mohr, 1967; Peccerillo et al., 2007; Woldegabriel et al., 1990). The Miocene basalt aquifers that are regionally overlain by ignimbrite units and alluvial deposits (Ayenew et al., 2008a; Berehanu et al., 2017; Demlie et al., 2007; Kebede et al., 2008; Yitbarek et al., 2012). The tertiary trachyte is characterized by low permeability localized aquifers, while the Quaternary alluvial deposits in the Awash River banks depict high productivity.

The Sodo site (Figure 1d) is situated in the Ziway Lake Basin. The geology of this site is the tertiary weathered basaltic formations intercalated with welded to partially welded pyroclastic flows of ignimbrite, rhyolitic and trachytic lava domes (Abebe et al., 1998; Ayalew et al., 2002; Boccaletti et al., 1998; Peccerillo et al., 2007; Woldegabriel et al., 1990) and the Quaternary formations of pyroclastic, lacustrine sediments and the alluvium unit of reworked materials of volcanic origin. The top weathering products were serving as a source of shallow groundwater and springs. The Quaternary basalt and scoria show high productivity as compared to the tertiary basaltic formation, while the trachyte, rhyolite,

lacustrine deposits and pyroclastic flow show low productivity (Alemu, 2017; Ayenew et al., 2008a; Furi et al., 2011; Yitbarek et al., 2012). The Abeshege site (Figure 1e) is situated in the Gibe Basin. This site is characterized by tilted and horizontally stratified hexagonal columnar jointing and thick weathering features of Oligocene basaltic formations. Whereas, the welded pyroclastic Flows are characterized by densely welded and lithic fragments associated with rhyolitic lava flows intercalated with ash and unwelded tuffs(Abbate et al., 2015; Ayalew et al., 2002; Beccaluva et al., 2009; Kieffer et al., 2004a; Lebas & Mohr, 1970; Peccerillo et al., 2007; Sembroni et al., 2016). The flood basaltic formation and welded to partially welded pyroclastic flows show variable transmissivity and yield of the aquifers where the weathered and fractured units are characterized by good water-bearing formation.

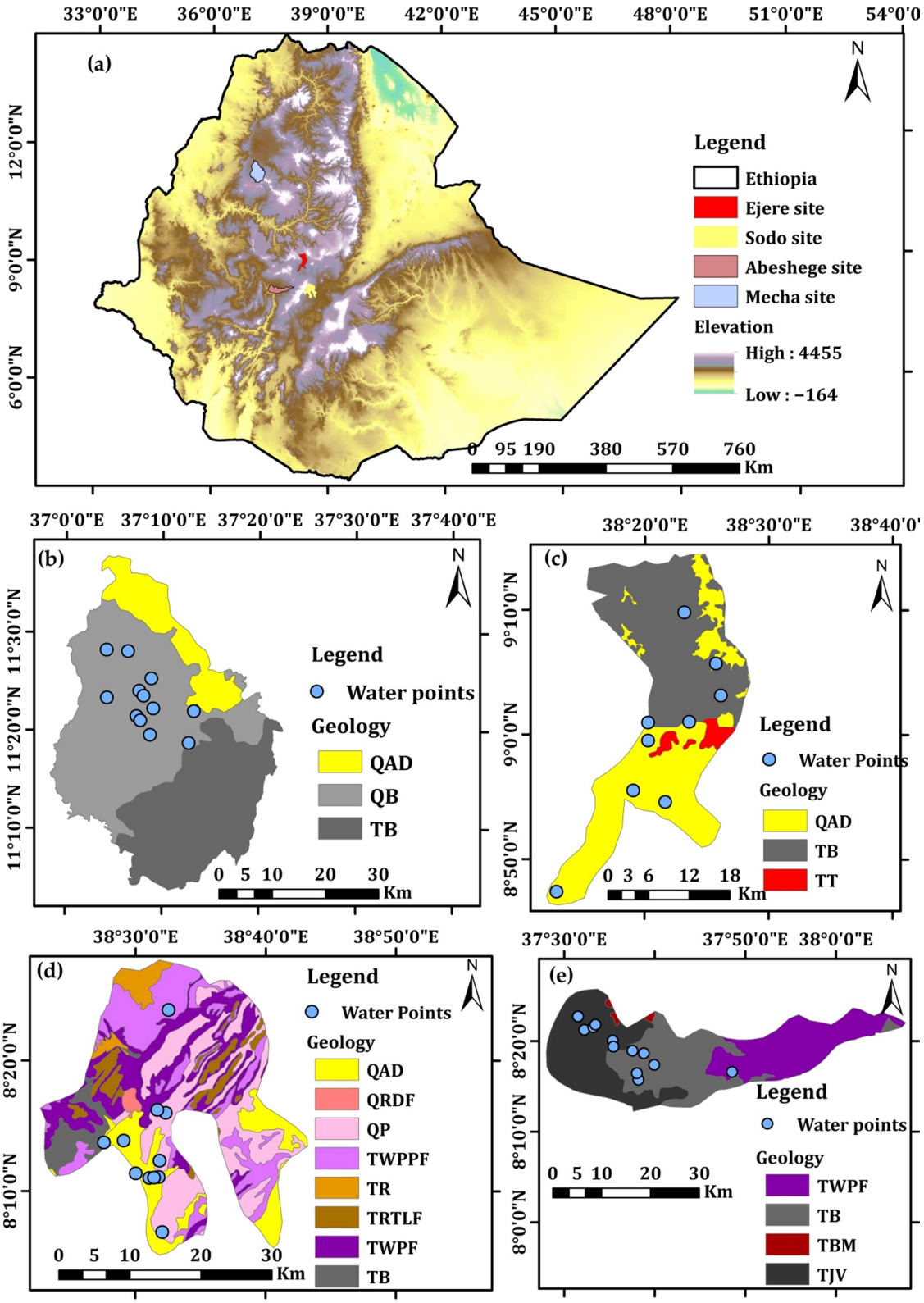
(a)
33°0'0"E
36°0'0"E
39°0'0"E
42°0'0"E
45°0'0"E
48°0'0"E
51°0'0"E
54°0'0
12°0'0"N
9°0'0"N
6°0'0"N
N
Legend
Ethiopia
Ejere site
Sodo site
Abeshege site
Mecha site
Elevation
High : 4455
Low : −164
0 95 190 380 570 760
Km
(b)
37°0'0"E
37°10'0"E
37°20'0"E
37°30'0"E
37°40'0"E
11°30'0"N
11°20'0"N
11°10'0"N
Legend
Water points
Geology
QAD
QB
TB
0 5 10 20 30
Km
(c)
38°20'0"E
38°30'0"E
38°40'0'
9°10'0"N
9°0'0"N
8°50'0"N
Legend
Water Points
Geology
QAD
TB
TT
0 3 6 12 18
Km
(d)
38°30'0"E
38°40'0"E
38°50'0"E
8°20'0"N
8°10'0"N
Legend
Water Points
Geology
QAD
QRDF
QP
TWPPF
TR
TRTLF
TWPF
TB
0 5 10 20 30
Km
(e)
37°30'0"E
37°50'0"E
38°0'0"E
8°20'0"N
8°10'0"N
8°0'0"N
Legend
Water points
Geology
TWPF
TB
TBM
TJV
0 5 10 20 30
Km

Figure 3.1: a) location maps of four study sites in Ethiopia, b) Geological map of Mecha site, c) Geological map of Ejere site, d) Geological map of Sodo site and e) Geological map of Abeshege site. The lithological units are: QAD = Quaternary alluvials, lacustrine and soil deposits, QB= Quaternary basalt, TT = tertiary trachyte, QRDF = Quaternary rhyolitic domes and flows, Quaternary pyroclastics, TR= tertiary rhyolite, TRTLF = tertiary rhyolite and trachyte lava flows, TWPPF = tertiary welded to partially welded pyroclastic flows, TWPF = tertiary welded pyroclastic flows, TB= tertiary Miocene flood basalt, TBM= tertiary Oligocene flood basalt and TJV = tertiary volcanics (basaltic and rhyolitic composition) of Oligocene flood basalt.

3.2.2. Pumping Test Data analysis

In all study sites, the pumping test data was collected from shallow hand pump wells by the Hidden Crises project. The minimum and maximum depths of the boreholes ranged between 18.6 and 84.3m respectively. We conducted pumping test data analysis on 42 hand pump boreholes to compute aquifer hydraulic parameters like transmissivity (T), hydraulic conductivity (K) and specific capacity (Sc). The detailed history of water wells, hydraulic parametres and effective porosity are given in the appendices. The summary of all hydraulic parameters obtained from pumping test data analysis and calculated effective porosity are presented in Table 1.

Table 3.1: Summary of water wells history, hydraulic parameters and calculated effective porosity

Sites		SWL	BH Depth	Saturated Thickness (b)	T(m^2/day)	Specific Capacity (Sc)	Effective Porosity (Equation (8))
Abeshege	Min	11.17	43.5	11.61	9.5×10^{-2}	0.099	0.12
	Mean	35.26	64.1	29.6	5.33×10^{3}	186.8	0.18
	Max	62.16	84.3	53.3	9×10^{2}	845.55	0.26
Ejere	Min	5.94	35.6	17.86	1.17	1.72	0.16
	Mean	16.92	62.66	34.46	1.19×10^{2}	68.28	0.19
	Max	32.82	50.7	47.74	4.81×10^{2}	265.49	0.24
Mecha	Min	2.42	21.75	11.43	8.35×10^{-1}	1.96	0.16
	Mean	10.44	44.31	33.21	4.1×10^{2}	327.17	0.21
	Max	23.06	61.34	58.92	1.61×10^{3}	1764.71	0.28

	Min	10.35	18.6	3.59	9.07×10^{-1}	1.52	0.16
Sodo	Mean	25.26	46.68	21.06	7.47×10^{1}	38.65	0.19
	Max	52	80	47.12	3.96×10^{2}	163.04	0.23

The pumping test data analysis was carried out using AquiferTest Pro 10 software using a constant discharge rate and recovery test methods. The time against drawdown data was plotted on the log-log scale in the Neuman's type curve superimposed on the type curve until the data points matched (Neuman, 1975). The Theis Model (Theis, 1935) considers the radial flow presented in the following equations (1).

$$S(r,t) = \frac{Q}{4\pi T} W(u) \qquad (1)$$

Where, s(r, t) is the drawdown at the radial distance r from the well at time t after pumping commenced, $u = \frac{r^2 S}{4Tt}$ is the dimensionless quantity that varies with the r distance from an observation well at time t, T is the transmissivity (m^2/day) and Q denotes the discharge rate (m^3/day), and S is the storativity (dimensionless) and W(u) is the dimensionless exponential integral known as well function which can be approximated as equation (2):

$$W(u) = \int_u^{\infty} \frac{e^{-y}}{y} dy = -\gamma - ln^u + u - \frac{u^2}{2.2!} + \frac{u^3}{3.3!} - \frac{u^4}{4.4!} + \cdots \qquad (2)$$

The well function W (u) and 1/u is determined from the Theis curve matching technique. The T and S were obtained from the time-drawdown curve fitting for both linear and log-log plots to obtain the hydraulic parameters using the following equations (3 and 4).

$$T = \frac{2.3Q}{2\pi \Delta s} \qquad (3)$$

$$S = \frac{2.25Tt_0}{r^2} \qquad (4)$$

The behaviour and productivity of the water well were determined using the specific capacity as the discharge ratio per unit drawdown expressed as (L/min)/m (Fitts, 2013) in equation (5).

$$Sc = \frac{Q}{S_w} \qquad (5)$$

The values of effective porosity of all boreholes were obtained from specific capacity data using the following equation (6) (Ahuja et al., 1989; Razack, M., & Huntley, 1991; Wilkinson, 2012).

$$\varphi i = \frac{\ln(\sqrt{(\frac{Q}{s})^{0.67}} + 1.8)}{5} \qquad (6)$$

Where φ_i is the dimensionless initial effective porosity, Q is the water well yield in m^3/day, s is the drawdown in m, b is the saturated thickness in m and Q/s is the specific capacity in (m^3/day)/m. Whereas, the average effective porosity was obtained from an iterative process of generating the fit solution and re-applying them to the initial effective porosity arrived at the following equation (7).

$$\varphi_e = 0.1301 + (0.1544\varphi_i) - (0.0165{\varphi_i}^2) \qquad (7)$$

Where φ_i is the initial effective porosity and φ_e is the effective porosity. Equation 7 is re-iterated to obtain the final equation used to calculate effective porosity from only specific capacity is determined by using the following equation (8). This equation is used to estimate effective porosity since the relationship between specific capacity and effective porosity is fitted by R^2 = 1.0 and it is applicable in all hydrogeological environments. However, the main limitation of using this relationship to estimate effective porosity is the inaccuracy of results which arises if the pumping test and water level data are not recent and not properly collected.

$$\emptyset_e = 0.15108 * \left(\frac{Q}{s}\right)^{0.0826} \qquad (8)$$

Therefore, for the purpose of this work effective porosity is determined using equation (8). The current data shows that the specific capacity-based computation of effective porosity

used the logarithmic equation that estimates the initial effective porosity. The correlation analysis shows that R^2 = 0.84 for initial effective porosity against specific capacity plot. Therefore, the re-iteration initial effective porosity data to generate the final effective porosity equation (8) which has R^2 =1 showing a good fit as elaborated in the figure 2.

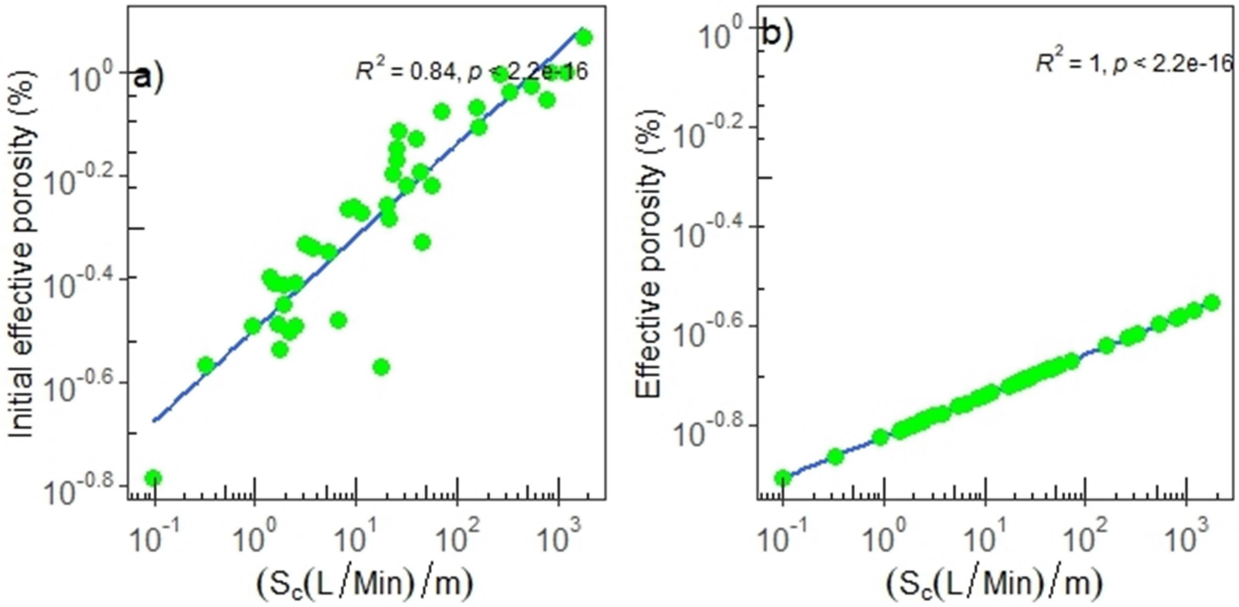

Figure 3.2: a) the initial effective porosity against specific capacity and b) the effective porosity against specific capacity plot. The green points show the data and the blue line is the regression line.

The seepage velocity is calculated by dividing the Darcy flux by the effective porosity, as shown in equation 9 (Gupta, 2017).

$$V = -\frac{T}{bn_{eff}}\frac{\Delta h}{\Delta s} \qquad (9)$$

Where V is groundwater flow velocity (m/day), T is transmissivity (m^2/day), b is the saturated thickness of the aquifer and $\frac{\Delta h}{\Delta s}$ is the hydraulic gradient. The hydraulic gradient estimation which is represented in the groundwater elevation head may have uncertainties such as avoiding closely spaced water well measurements to obtain variations in hydraulic heads, highly permeable sediments showing a small differences in the hydraulic head, differing screen length in the well forms poor hydraulic interconnections of geologic units, geological barriers or clogged well screen for measurements in the well which are not

interconnected, deep groundwater system or seawater intrusion into the aquifer might form different measurements in the well. The groundwater flow velocity estimation considers the homogeneous and isotropic conditions of the aquifer. The results obtained from this method represent the aquifer conditions at the large scale, while the local scale level estimation of groundwater flow velocity needs single well method.

3.2.3. Geospatial technique

The data of water wells collected from all study sites such as water well locations, the static water level in meters below the ground surface (m.b.g.s.) that represents the distance between the ground surface and the static water level in the borehole, the transmissivity of the aquifers (m^2/day), effective porosity (dimensionless in percentage) and saturated thickness of the aquifers (m). The homogeneity of the units of the input data was considered during the data processing. The transmissivity value was obtained from pumping test data analysis. The saturated thickness of the aquifer was obtained from the depth of the water table to the bottom of the aquifer. The effective porosity was computed from a specific capacity. In groundwater flow velocity estimation, three criteria must be fulfilled prior to the use of the input raster maps. These are: 1) the raster maps must have the same extent and cell size, 2) the raster maps must be floating point and 3) the raster maps should be dimensionally homogeneous (i.e. consistent units for all data) (Environmental Systems Research Institute (ESRI), 2015).

All four raster maps (groundwater elevation head in meters above sea level (masl), transmissivity, effective porosity and saturated thickness) were produced by considering the raster cell size for all four layers in a kriging-type interpolation. The transmissivity, effective porosity and saturated thickness were directly used as an input in the Arc map, spatial analyst tool box, groundwater in Darcy velocity command window. Since a static water level raster map cannot be used directly, the command window requires a groundwater head elevation raster map (water table elevation). The groundwater head elevation raster map was prepared by subtracting the static water level raster map from the digital elevation map (DEM) of the study area which can be performed by using the Map Algebra/Raster calculator within the spatial analyst tool.

3.3. Results

3.3.1. Geospatial Analysis of hydrogeological features

3.3.1.1. Groundwater elevation head and water table contour map of all study sites

The groundwater elevation head and water table contour map in all study sites were presented in Figure 3a – 3d. The water table contour maps showed the groundwater flow direction in all study sites. In the Mecha site (Figure 3a), groundwater elevation head and water table contour showed shallow depth in the Quaternary alluvial deposits, reworked soil materials and Quaternary basaltic formations, while the deeper groundwater table is observed in the fractured tertiary basaltic formations. In the Ejere site (Figure 3b), the groundwater table showed shallow depth in the alluvial deposits situated in the Becho plain along the Awash river bank, but the deeper groundwater table is observed near the plateau and escarpments. The Sodo site (Figure 3c) groundwater table showed shallow depth in the areas situated near the bottom of the escarpment and along the rift direction in fractured basalt and Quaternary alluvial deposits. Whereas, the deeper groundwater table depth is observed in the plateau areas in basaltic and rhyolitic units. In the Abeshege site (Figure 3d), shallow groundwater tables are observed in the Ghibe river discharge zone in the basaltic formations and thick overburden units, while deep groundwater tables are observed in the plateau regions in the fractured basaltic units and welded pyroclastic units.

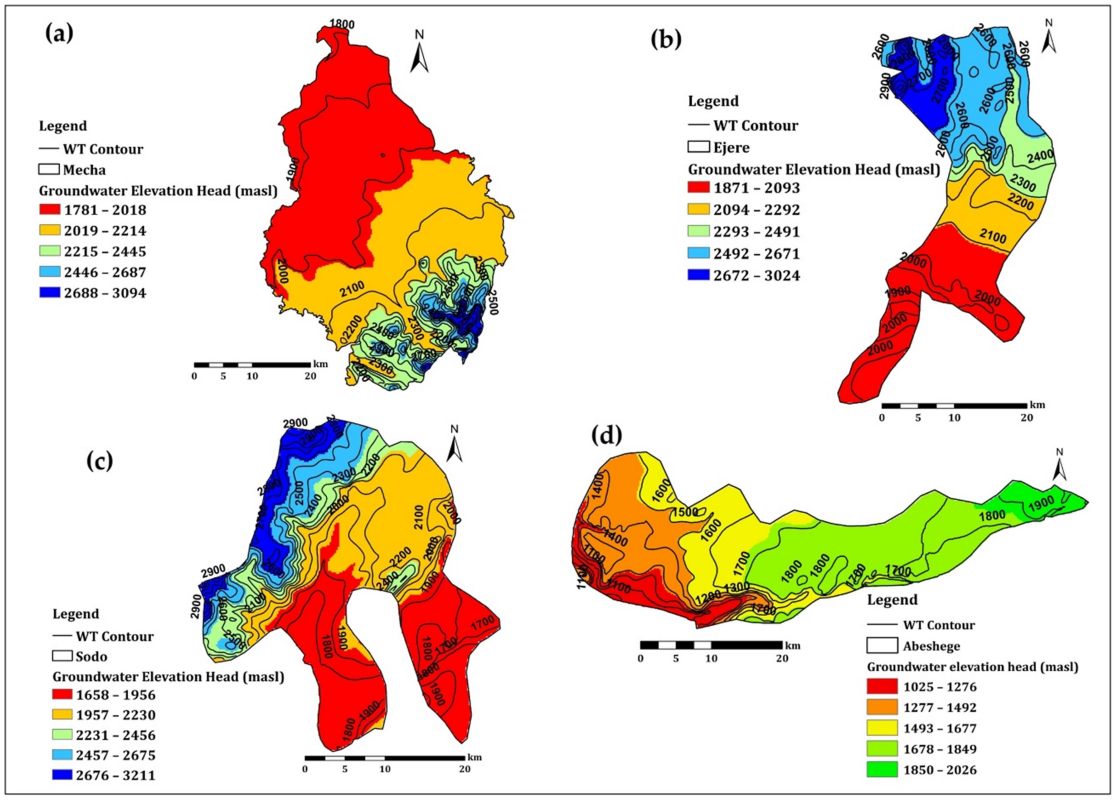

Figure 3.3: Groundwater elevation head and water table contour map depicting groundwater flow direction: a) Mecha site, b) Ejere site, c) Sodo site and d) Abeshege site

3.3.1.2. Mecha Site

In the Mecha site, the groundwater elevation head ranged from 1,781 to 3,094 masl (Figure 4a). The groundwater elevation decreases to the north and north western part of this site showing the depressed low elevated regions near Lake Tana. Such shallow groundwater elevation is associated with the discharge zone to Lake Tana Graben. Whereas, the southern and south eastern parts showed the elevated regions of the plateau sector showing deeper groundwater elevation head. Furthermore, the deeper groundwater elevation head is associated with the geological settings that show deep ground groundwater circulation in a massive fractured basaltic formation at the southern part of the area, while the shallower groundwater elevation is observed in the quaternary alluvial and lacustrine formations near the Lake and in the depressed regions.

The effective porosity values of this site ranged between 15.99% and 27.97% as presented in (Figure 4b). The effective porosity is higher in the northern part of the Mecha site,

particularly in the Quaternary volcanic formations and in the inter-granular aquifers. In the southern part of the Mecha site, the massive and less fractured volcanic aquifers showed the lowest value of effective porosity.

The saturated thickness of the Mecha site ranged between 11 and 59 m (Figure 4c). Thick saturated layers are observed in the central part of the area mainly in the Quaternary basaltic formations. The thin layers of saturated aquifers are found in the lacustrine alluvial soils near the Lake Tana region. However, the wider areas in the southern part showed intermediate saturated thickness in the fractured tertiary basalt and Quaternary volcanic formations.

The transmissivity of the aquifer in this site as obtained from the pumping test data analysis varies from 2 to 1,610 m^2/day (Figure 4d). These show the highest values are at the central part of the study site while the lowest range of transmissivity was observed at the north western and eastern part of the Mecha site. High transmissivity values are associated with the Quaternary basaltic and alluvial deposits, while the lowest transmissivity is observed in the massive basaltic units and lacustrine deposits.

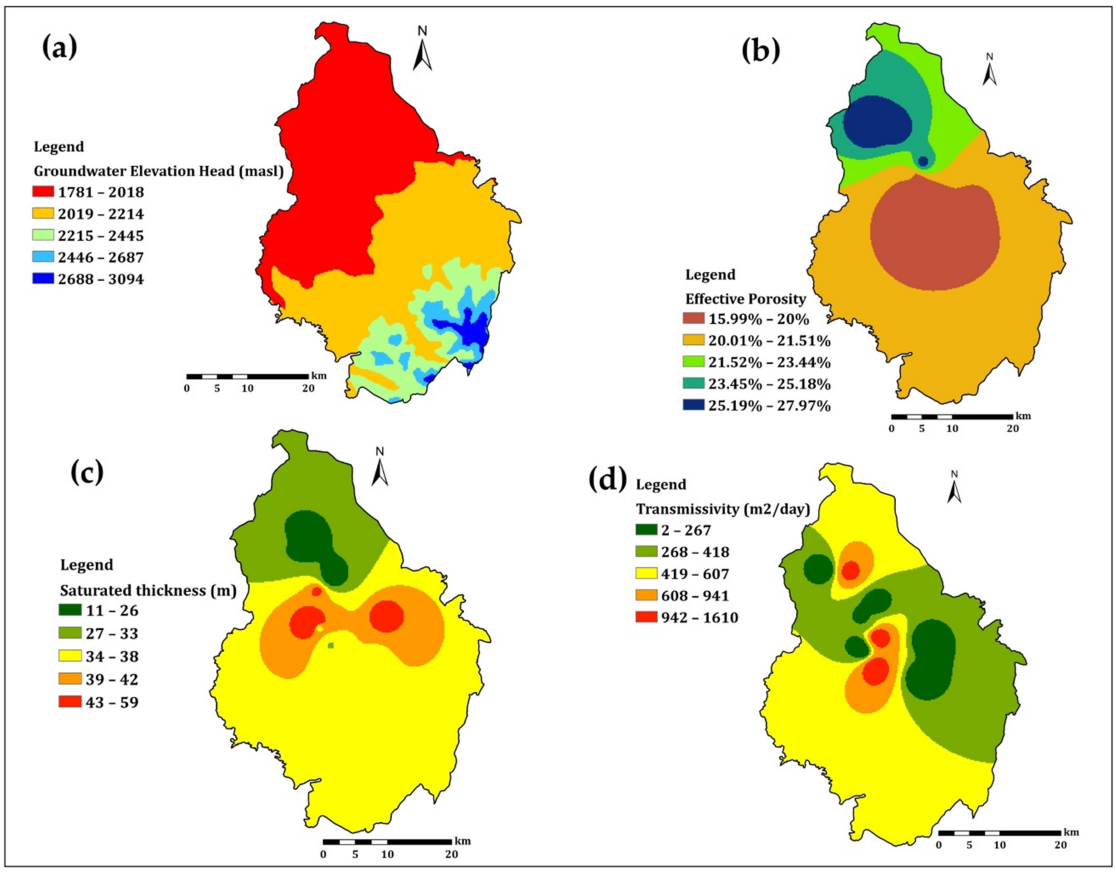

Figure 3.4: Four raster maps of the Mecha Site: a) Groundwater elevation head, b) Effective Porosity of the aquifer, c) Aquifer saturated thickness and d) The transmissivity map

3.3.1.3. Ejere Site

In the Ejere site, the groundwater elevation head was governed by the surface elevation of the study site that ranged from 1,876 to 3,024 masl (Figure 5a). The highest groundwater elevation head is observed in the northern part of the site where the topographic setting has a significant role mainly in the basaltic formation on the top of the plateau sector. Whereas, the shallow groundwater elevation heads are observed in the depressed areas of the Becho plain and in the Awash River banks within the alluvial deposits.

The effective porosity values varied from 17.4% to 26.7% (Figure 5b). The highest effective porosity is observed at the central part in the fractured basaltic formations affected by the structures and in the southern part of the study site in the highly permeable alluvial deposits in the Becho plain and Awash River bank. Whereas, low values of effective

porosities are observed at the northern part of the study site associated with the intermediate to massive basaltic formations.

The saturated thickness of the Ejere site showed values ranging between 18 and 48 m (Figure 5c). The highest value of saturated thickness is observed at the pockets areas of the northern and central parts of the study site showing the heterogeneity of aquifer thickness distribution due to variations in weathering and fracture units. However, the eastern and the south western part of the region show a saturated thickness of less than 36m in alluvial deposits and basaltic formations.

The transmissivity values in the Ejere site varied between 1 and 481 m^2/day (Figure 5d). The highest transmissivity values are observed in the small pocket of the central part of the study site in the tertiary basaltic aquifer which is highly influenced by the geological structures and topographic effects. Whereas, the northern part showed the lowest transmissivity which is influenced by the massive tertiary basaltic units and the central part is identified by less fractured trachytic deposits.

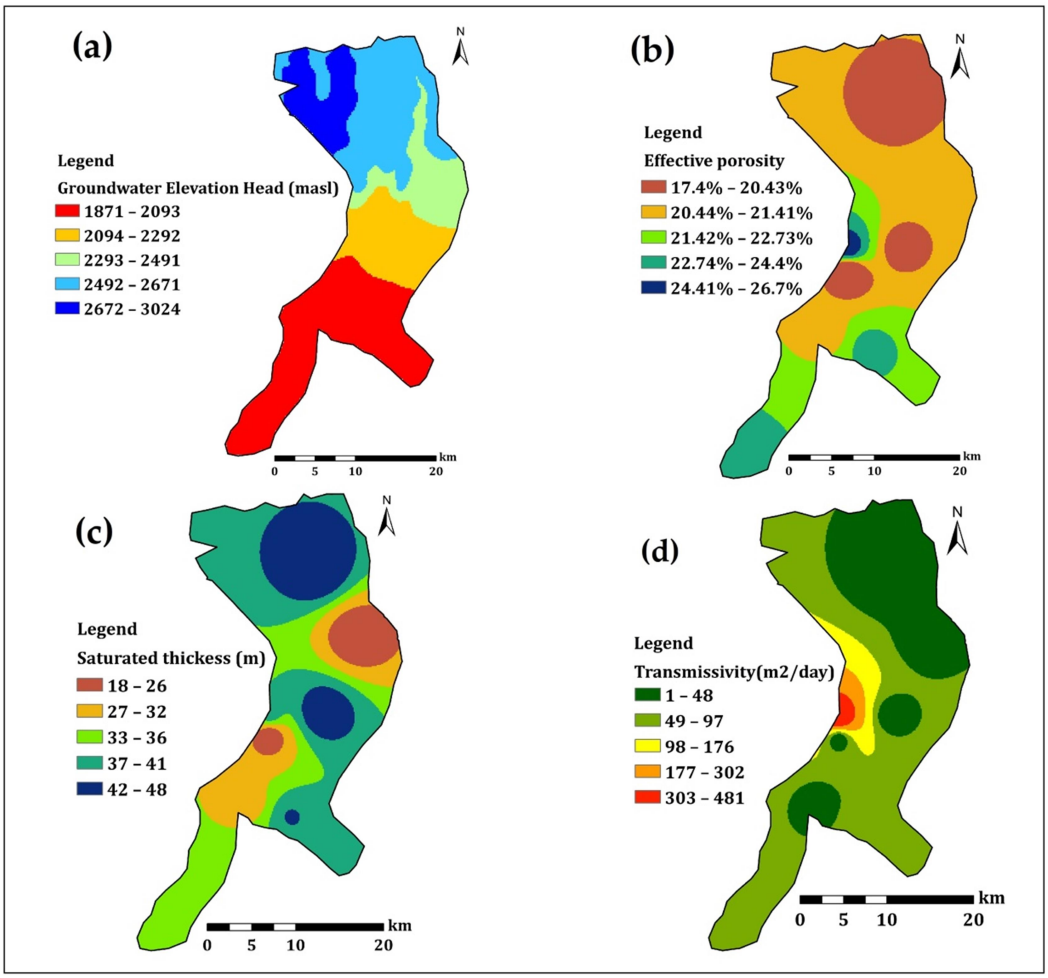

Figure 3.5: Four raster maps of the Ejere Site: a) Groundwater elevation head, b) Effective Porosity of the aquifer, c) Aquifer saturated thickness and d) The transmissivity map

3.3.1.4. Sodo Site

The Sodo site groundwater elevation head ranged between 1,658 and 3,211 masl (Figure 6a). The northern and western parts of the site showed deeper groundwater elevation head in the topographically elevated region of the Guraghe Mountain dominantly covered by less fractured tertiary volcanics of the basaltic and welded rhyolitic domes. The southern and eastern parts of the site show shallow groundwater elevation head at the bottom of the escarpment and the depressed areas covered by pyroclastic materials.

The effective porosity of the Sodo site ranged between 17% and 24.97% (Figure 6b). The low values of effective porosity are associated to the welded and partially welded rhyolite,

pyroclastic deposits and less fractured tertiary basaltic formations. The southern part of the area showed the highest effective porosity associated with fractured and weathered volcanics along the fault escarpment showing the effects of geological structures.

The saturated thickness of the aquifer in the Sodo site varied from 4 to 47 m (Figure 6c). The south western part of the site showed the maximum saturated thickness associated with the fractured and weathered volcanic formations. The eastern and southern parts exhibited a medium range of saturated thickness in partially welded rhyolite and less fractured rhyolitic and pyroclastic formation, while the northern part showed the lowest saturated thickness of the aquifer on the top of the mountain where the aquifer is shallow at recharge areas.

The transmissivity of the Sodo site ranged between 1 and 263 m^2/day (Figure 6d). The highest values of transmissivity is observed in the small pocket of the southern part of the area along the fractured zone at the bottom of the Guraghe mountain that is subsequently affected by geological structures in basaltic and rhyolitic formations. Whereas, the vast areas of the northern, north western and the southern part of the site showed medium to low transmissivity in a low permeability welded to partially welded rhyolitic, trachytic formations and pyroclastic materials. Similarly, the top part of the Guraghe Mountain showed less fractured basaltic formations indicating a low range of transmissivity.

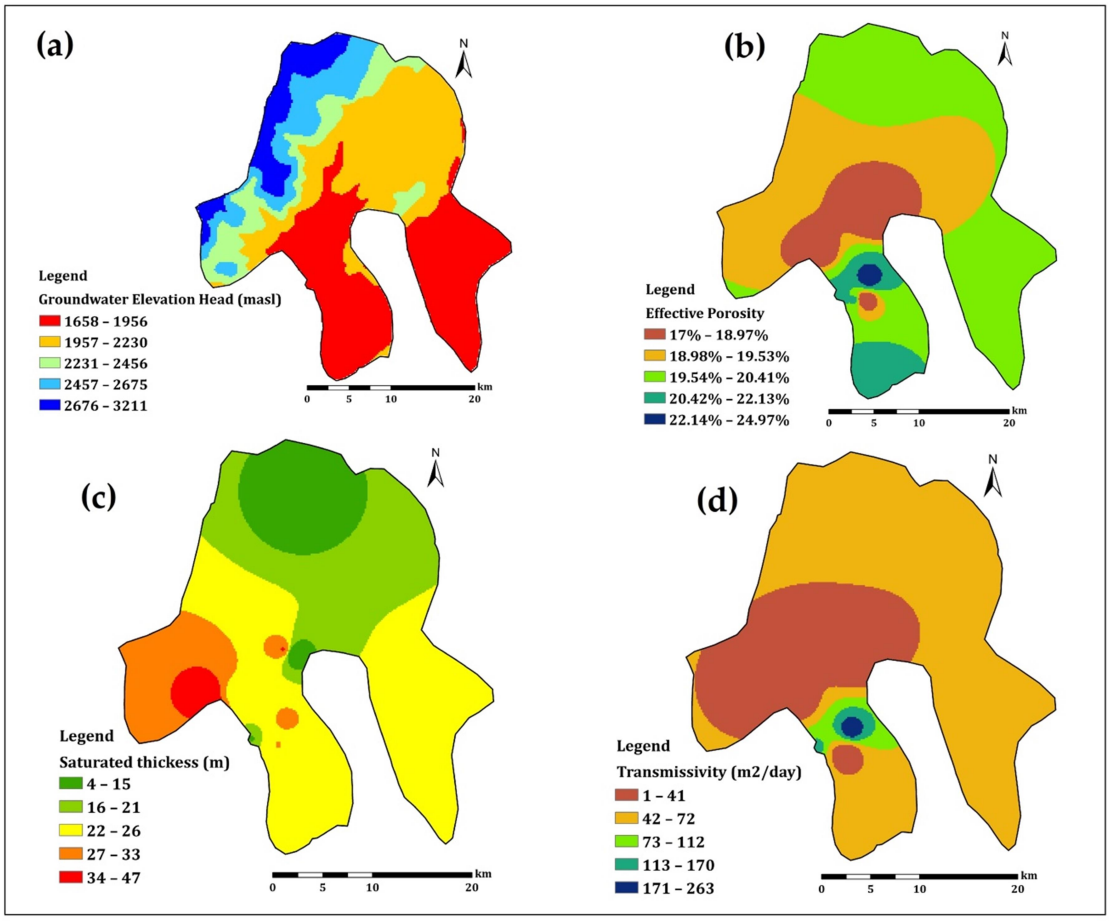

Figure 3.6: Four raster maps of the Sodo Site: a) Groundwater elevation head, b) Effective Porosity of the aquifer, c) Aquifer saturated thickness and d) The transmissivity map

3.3.1.5. Abeshege site

The groundwater elevation head in the Abeshege site ranged between 1,025 and 2,026 masl (Figure 7a). The groundwater elevation head is shallower in the western and south western part of the study area indicating the discharge zone near the margin of river gorge in the Ghibe basin except in a few areas affected by a series of geological structures that allowed the deeper groundwater flow. Whereas, the deeper groundwater elevation head in the eastern part of the study area is associated with deep regional groundwater flow from the plateau escarpments to the outlet at the Ghibe basin.

The effective porosity in the Abeshege site varied from 13.5% to 26.7% (Figure 7b). The highest effective porosity is observed in localized small areas of highly fractured basaltic

formation. The western part and small pockets at the center of the study site show the lowest effective porosity in less fractured and less weathered tertiary basaltic formations. Welded pyroclastic and massive volcanic formations with low fracture networks showed a medium range of effective porosity.

The saturated thickness of the Abeshege site ranged between 12 and 53 m (Figure 7c). The highest value of saturated thickness was observed at the western periphery and central part of the study site in fractured basaltic formations. The low saturated thickness at the centre is associated to the fractured part of the basaltic unit and the top weathered part of the aquifer. The medium range of saturated thickness is in the basaltic and pyroclastic units.

The Transmissivity of the Abeshege site varied between 1 and 5,307 m^2/day (Figure 7d). The highest transmissivity value was recorded in the small patchy area affected by the series of geological structures in the basaltic formations. The medium range of transmissivity is associated with the partially welded formation and fractured basaltic units. Whereas, the low values are observed at the north western part and at the central part of the site in welded pyroclastic materials and in massive tertiary basaltic formation.

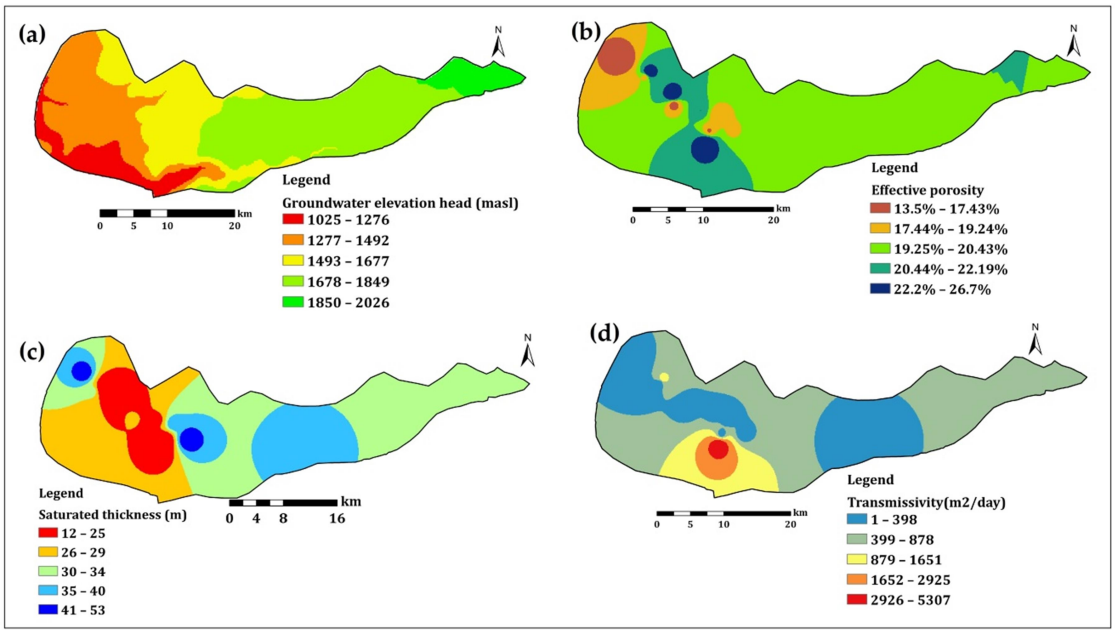

Figure 3.7: Four raster maps of the Sodo Site: a) Groundwater elevation head, b) Effective Porosity of the aquifer, c) Aquifer saturated thickness and d) The transmissivity map

3.3.2. Groundwater Flow Velocity Estimation

The groundwater flow velocity in the Mecha site ranged between 0 to 47.31 m/day (Figure 8). The highest groundwater flow velocity is observed in the south eastern part of the study site indicating the effects of elevated topographic features, the geology and geological structures in the tertiary basaltic formations allow an increasing groundwater flow velocity magnitude. Furthermore, such groundwater velocity decreases towards the north in the discharge zone of the Lake Tana basin. The dominant areas of the study site showed a low range of groundwater flow velocity magnitude mainly in the depressed flat plat plains of the basin except in some volcanic spatter cones sparsely distributed in the site. Furthermore, low groundwater flow velocity is associated with the alluvial and lacustrine deposits. The groundwater flow direction is towards the northwest into Lake Tana following the regional groundwater flow.

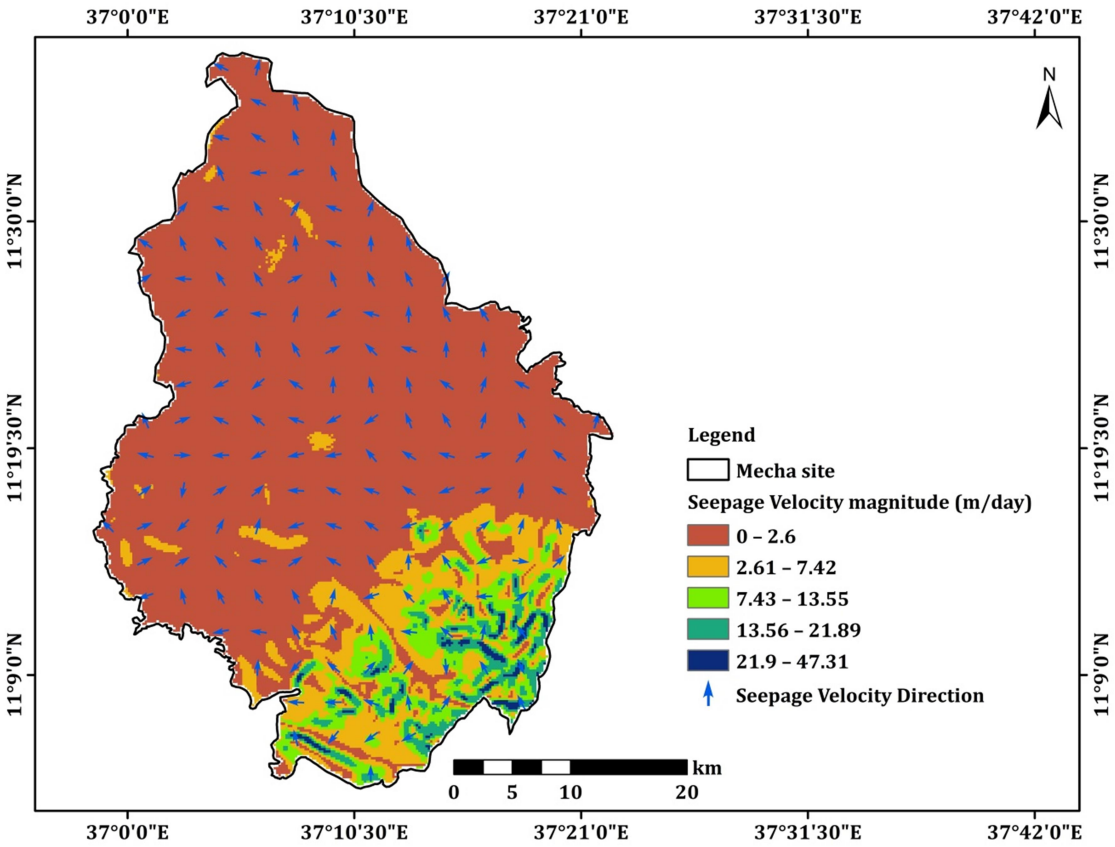

Figure 3.8: The groundwater flow velocity magnitude and direction of the Mecha site

The Ejere site groundwater flow velocity showed values from 0 to 7.47 m/day (Figure 9). The highest groundwater flow velocity magnitude is observed at the central and north western part of the site in fractured and weathered volcanic units affected by geological structures. Whereas, the dominant part of the study site indicates low values of groundwater flow velocity magnitude in a less fractured massive tertiary basaltic formation and trachytic units in the north eastern and the depressed Becho plain that exhibit the alluvial deposits. Furthermore, in low groundwater flow velocity regions there are low effects of geological structures. As compared to all other study sites, the Ejere site shows low ranges of groundwater flow velocity magnitude. The groundwater flow velocity direction is towards the south following the regional groundwater flow direction from the plateau sectors to the Becho plain.

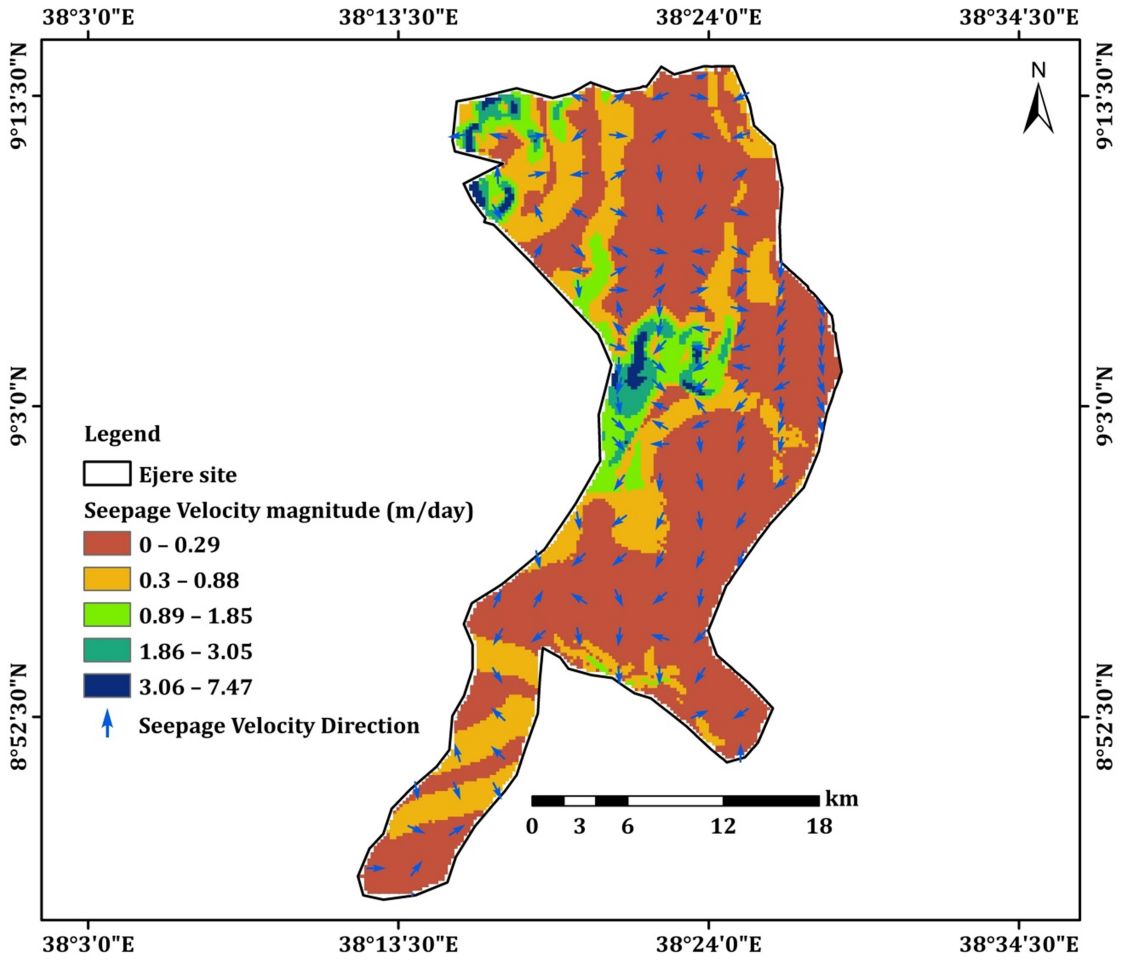

Figure 3.9: The groundwater flow velocity magnitude and direction of the Ejere site

The groundwater flow velocity in the Sodo site ranged between 0 and 22.36 m/day (Figure 10). The highest groundwater flow velocity magnitude is observed in the north western part of the area where the effects of topography and geological structures are high in the fractured basaltic and rhyolitic formations. The dominant regions of the study site are below 0.79 m/day showing low groundwater flow velocity controlled by the low permeability welded to partially welded pyroclastic materials, rhyolite, trachyte and low extent of less fractured basaltic units. Furthermore, a few areas in the southern part also exhibit low permeability in lacustrine deposits. The groundwater flow velocity direction also indicates the regional groundwater flow direction from the Guraghe Mountain to the Rift floor.

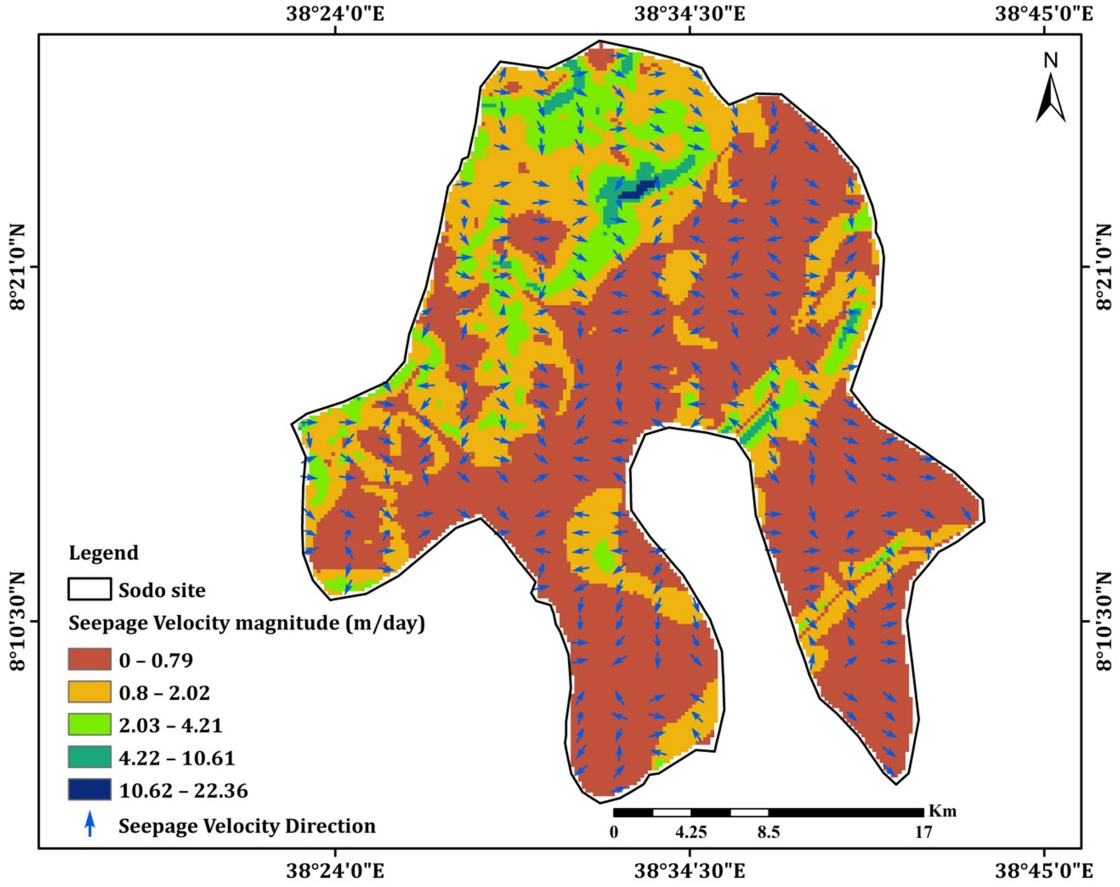

Figure 3.10: The groundwater flow velocity magnitude and direction of the Sodo site

The Abeshege site groundwater flow velocity ranged between 0 and 195.35 m/day (Figure 11). The highest groundwater flow velocity magnitude at the southern part of the site is

observed in fractured tertiary basaltic units where the effects of topographic features and geological structures are high. Furthermore, such high-velocity region is situated near the discharge zone of the Ghibe basin exhibiting the incising of deep gorges associated with a series of structural networks. However, the dominant regions of this study site in partially welded pyroclastic flows and tertiary basaltic formations with low fracture networks showed groundwater flow velocity magnitude ranging below 6.13 m/day. The groundwater flow velocity direction is towards the west and the south west to the Ghibe basin following the regional flow system.

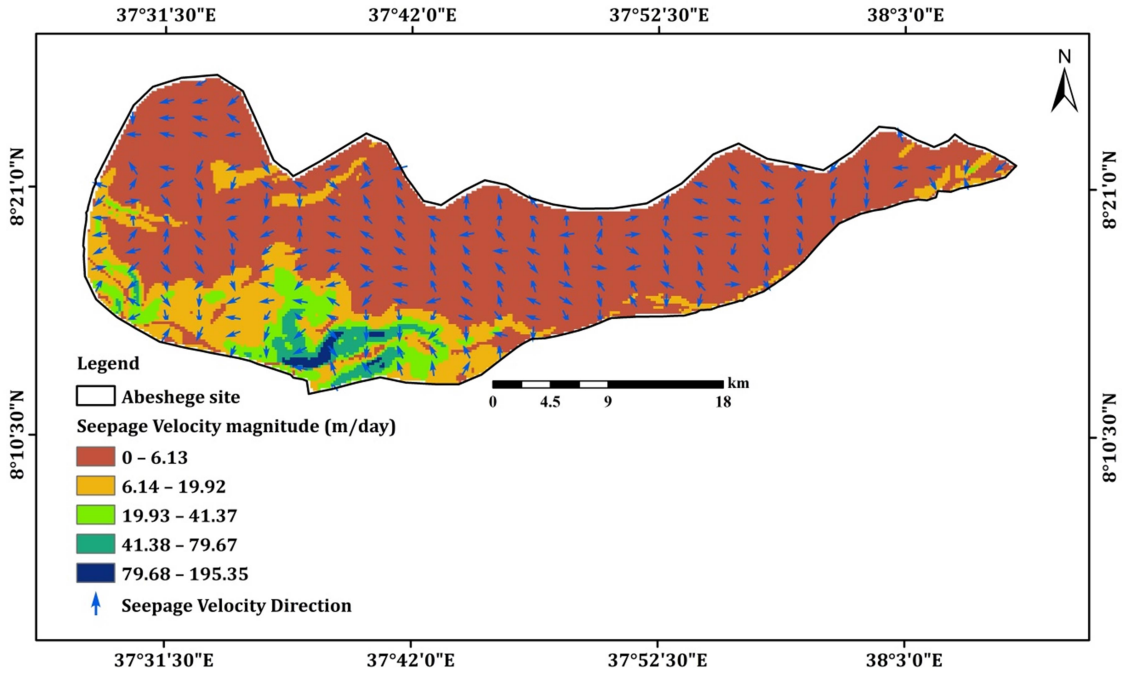

Figure 3.11: The groundwater flow velocity magnitude and direction of the Abeshege site.

3.4. Discussion

3.4.1. Geospatial technique in groundwater flow velocity estimation

Shallow volcanic aquifers are the most reliable water resource that serves most of the Ethiopian volcanic highlands. However, such strategic resources are susceptible to seasonal climatic effects related to the nature of rainfall, contaminations due to unprotected hand pump wells and wastewater discharge in urban areas and stress associated with over pumping lowering groundwater levels (MacAllister et al., 2020; Macdonald et al., 2019;

Maurice et al., 2019). The groundwater flow velocity estimation in the shallow volcanic aquifers has vital importance in characterizing the aquifer response to seasonal changes, groundwater flow dynamics and contaminant transport and optimizes groundwater flow modelling. Previous studies reveal that there has been no investigation on groundwater flow velocity estimation in the Ethiopian shallow volcanic aquifers. The current work is conducted in shallow volcanic aquifers systematically selected from major basins to estimate groundwater flow velocity. The geospatial technique conducted in this work was successfully applied in shallow volcanic aquifers to estimate groundwater flow velocity magnitude and direction.

In the Mecha site, high groundwater elevation head show a significant correlation with high groundwater flow velocity. The groundwater flow velocity shows a similar trend to transmissivity in areas surrounding Koga dam. The transmissivity and effective porosity in the depressed plain near Lake Tana are controlled by Quaternary deposits, shallow water levels in the discharge zone, hydraulic interconnection of surface water with groundwater and irrigation return flow. The higher range of transmissivity and effective porosity are associated with the highly permeable Quaternary basalt aquifer, while the medium to low range of transmissivity and effective porosity are associated to tertiary basalt, Quaternary reworked soil and lacustrine deposits. The shallow aquifer saturated thickness is associated to the nature of the shallow water table in the the Koga Dam irrigation return flow effect and effects of the discharge zone. These results are in agreement with the previous investigations in the Lake Tana Graben (Kebede et al., 2005; Mamo, 2015; Nigate et al., 2017, 2020).

In the Ejere site, groundwater flow velocity magnitude shows a similar trend with groundwater elevation head, effective porosity and aquifer transmissivity. The groundwater elevation head is controlled by surface topographic elevation which shows higher values at the plateau and escarpment region of the site and low values around Becho plain. The effective porosity is higher in the permeable thick alluvial aquifer of the Becho plain near the Awash River Bank, while the effective porosity is low in the massive basaltic and trachytic formations. Similarly, high transmissivity is associated with the fractured tertiary basalt and Quaternary alluvial deposits, while low transmissivity value is

associated with the massive less fractured basalt and trachytic units. As compared to all other study sites, the Ejere site is characterized by a very low range of groundwater flow velocity magnitude. This might be associated with the less fractured and less weathered tertiary basalt and trachytic units. This result is in agreement with previous works conducted in the Upper Awash basin (Ayenew et al., 2008a; Berehanu et al., 2017; Yitbarek et al., 2012).

In the Sodo site, high groundwater flow velocity in the Guraghe Mountain range is controlled by geological structures and topographic effects. However, low groundwater flow velocities in all other regions of the Sodo site are characterized by the nature of hydro-stratigraphic units of pyroclastic, rhyolites, trachytic and lacustrine deposits. The groundwater flow velocity and transmissivity show a similar trend of low to medium range which indicates the nature of pyroclastic and lacustrine deposits. The higher effective porosity and transmissivity are associated with the fractured and weathered basalt, rhyolite and alluvial deposits of high permeability aquifer, while the lower value is associated with the massive less fractured rhyolite domes and basaltic formations of the escarpment and the top of Guraghe Mountain.

In the Abeshege site, groundwater flow velocity shows a similar trend with effective porosity and aquifer transmissivity. The highest value of groundwater flow velocity and transmissivity are observed in the fractured and weathered basaltic formation as compared to the other three sites. The high values of groundwater elevation head are controlled by the regional hydraulic gradient and topographic settings surrounding the Ghibe basin discharge zone. The highly weathered and fractured basaltic unit is characterized by the highest transmissivity and groundwater flow velocity, while the welded pyroclastic deposits show slightly medium to low transmissivity and groundwater flow velocity. Furthermore, this site is known by large tributary rivers of Ghibe such as Wabe and Walga that cross through this study area and wide agricultural fields.

An estimated groundwater flow velocity orders of magnitude is higher in fractured media than granular media based on aquifer settings like in sands (0.1 to 1 m/day), sand and gravel (0.1 to 10 m/day), fractured rock (1 to 100 m/day) and Karst (1 to 500 m/day) (Aley, 2002; Cherry, 1990). The estimated groundwater flow velocity results in the current

work are in agreement with the high groundwater flow velocity magnitude in fractured aquifers and low-velocity magnitude in intergranular and alluvial sediments. Similarly, this work shows the results of effective porosity which are in agreement with the previous work that shows in granular media and fractured rocks (Morris, D.A. and Johnson, 1967).

3.4.2. Importance of groundwater flow velocity estimation in groundwater resources management

The groundwater flow velocity estimation is important to understand the nature of aquifer productivity, sustainability of groundwater resources, groundwater flow dynamics, engineering structures associated with groundwater, hydrogeochemical evolution and contaminant transport, groundwater responses to stress, and optimizing water resources management and calibrating groundwater flow models (Bakx et al., 2023). The use of groundwater flow velocity provide essential information to predict the arrival times of contaminants, groundwater mixing, residence times and contaminant mass flux across boundary at various aquifers and surface water bodies (Devlin, 2020; Hall, 1993; Li et al., 2019). Various groundwater flow velocity estimation methods have been conducted based on the single borehole applied(Hall, 1993; Matsumoto et al., 2020; Piccinini et al., 2016b; Poulsen et al., 2019; Vienken et al., 2017) and environmental tracer test (Hamada, 2000; Schubert et al., 2011), direct velocity measurement (Essouayed et al., 2019b; Kearl et al., 1998; Labaky et al., 2009) and regional scale level Darcy-based and geospatial methods (T. Abdullah et al., 2021; T. O. Abdullah et al., 2020; Al-Madhlom et al., 2020; Mazor & Nativ, 1992).

The geospatial-based groundwater flow velocity estimation can be applied in shallow volcanic aquifer that in turn has a vital role in groundwater resources management mainly for hand pump wells in rural water supply. Therefore, the geospatial technique can be a promising tool to estimate large-scale groundwater flow velocity in the shallow volcanic aquifers of the Ethiopian highlands. The present work would help to practice conducting the method in many other parts of Ethiopian basins at different levels. However, the major challenge is the scarcity of hydraulic parameters data in various basins due to the expensive nature of conducting pumping tests mainly during post-water well construction.

3.5. Concluding remark

Shallow volcanic aquifers of Ethiopian highlands (Mecha, Ejere, Sodo and Abeshege sites) were systematically selected to estimate groundwater flow velocity by using the geospatial technique. The pumping test data analysis was conducted to compute hydraulic parameters (T, K and Sc), the borehole history (depth, static water level and drawdown) and four input raster maps (groundwater elevation head, effective porosity, aquifer saturated thickness and transmissivity maps) were compiled to estimate output resultant maps of groundwater flow velocity magnitude and direction.

The groundwater flow velocity in the selected sites varied between 0 to 47.31, 0 to 7.47, 0 to 22.36 and 0 to 195.35 m/day in Mecha, Ejere, Sodo and Aeshege respectively. The Abeshege site showed the highest transmissivity and groundwater flow velocity as compared to all other three sites. This is associated with a thick fractured and weathered basaltic aquifer. In the Mecha site, the groundwater flow velocity of the aquifer shows slightly higher values next to the Abeshege site which is associated with Quaternary basaltic formation and alluvial deposits in the Lake Tana Graben. In the Sodo site, the groundwater flow velocity shows a medium range of distribution in the pyroclastic and lacustrine deposits as compared to other sites, except in a few pocket areas of higher velocity controlled by rugged topography and geological structures. In the Ejere site, groundwater flow velocity shows the lowest value as compared to all other sites in less fractured and weathered basaltic and trachytic aquifers, while slight increments of groundwater velocity magnitude are observed in the thick alluvial deposits of the Becho plain.

This work has significant importance in supporting other methods of groundwater flow velocity. Groundwater flow velocity estimation has an important role in understanding groundwater resources management, sustainability of groundwater resources, groundwater flow dynamics and contaminant transport. Thus, we give a remark to employ this method in understanding groundwater resources of shallow volcanic aquifers of Ethiopian highlands that help as a major source of rural water supply.

Chapter Four

4. Groundwater Flow Velocity Estimation Using ^{222}Rn Technique in Shallow volcanic aquifers of Ethiopian highlands

4.1. Introduction

Groundwater Resources have been prioritized than surface waters in the vast areas of Ethiopian regions due to the buffering capacity of the seasonal changes and relatively less probability to contamination. In the Ethiopian highland, shallow volcanic aquifers have been used as a source of water supply for domestic and small scale irrigation purposes. Shallow aquifers are one of the trustworthy resources in the vast areas of rural and urban centres of Ethiopia (Gowing et al., 2016, 2020; Walker, 2017; Walker et al., 2019a), serving as a major source of groundwater that can be easily accessed by shallow hand pump wells and springs.

Shallow groundwater in sub-saharan Africa (50 to 60 m depth) supports domestic demand and is a neglected opportunity for sustainable use of small scale agriculture (Walker et al., 2019b). The shallow and very shallow volcanic aquifers are formed in Miocene and Quaternary formations situated in alluvial plains and along the river beds of the Eastern Ogaden, Danakil depression, lower Omo valley, Southern Sidamo, Gambella and Western Gonder areas (Kebede, 2013). These shallow aquifers comprise the tertiary and quaternary volcanic deposits and thick weathering profiles of regolith and alluvial deposits (Ayenew et al., 2008a; Furi et al., 2012; Kebede, 2013b; Kebede et al., 2005; Nigate et al., 2020; Walker et al., 2019a) in all selected study sites.

Previous works reveal that in the global volcanic aquifers including Ethiopia, there is a clear indication of the declining of the aquifer and failures of water wells (Macdonald et al., 2019). Moreover, there are different causes of water wells failures that are mainly associated to the aquifer productivity, groundwater flow velocity and the water well performance problems like clogging, water well construction problems and materials selected for well completion (Bonsor et al., 2015; Owor M, MacDonald AM, Bonsor HC,

Okullo J, Katusiime F, Alupo G, Berochan G, Tumusiime C, Lapworth D, Whaley L, 2017; Owor et al., 2017).

Aquifer characterization to determine hydraulic properties was conducted during water well construction through pumping test data analysis. However, after water well construction, there is no continuous monitoring of the aquifer hydraulic parameters. Therefore, monitoring the nature of these groundwater resources aquifer productivity and groundwater flow velocity to identify the causes of the water wells failures and declining of the performance rate needs establishing systematic methods. The methods to identify the sources of such problems are rarely employed mainly during post-water well construction.

There are several methods to estimate groundwater flow velocity. Borehole Point Dilution Method uses salt tracer introduced into the well and Inflow of groundwater into the well measured as a resulting decrease in tracer concentration as a function of time (Drost et al., 1968; Hall, 1993; Piccinini et al., 2016a). Point Velocity Probe (PVP) used a device applied in screened wells, where a small volume of tracer is introduced through the injection system and the velocity of the tracer is estimated based on arrival of the tracer at a detector (Berg & Gillham, 2010; Kempf et al., 2013; Labaky et al., 2007, 2009; Osorno & College, 2016). Passive Flux Meter(PFM) is a permeable cylinder down-hole device designed to measure the magnitudes of horizontal groundwater specific discharge and Contaminant mass flux in porous media (Hatfield et al., 2004; Klammler et al., 2007). Colloidal Bore scope method employed direct observation of particles in the well screen to the measured velocities are averaged (up to 2400m/day) to obtain a mean Darcy flux (Kearl, 1997; Kearl et al., 1998). Direct Velocity Tool(DVT) was tested for velocities ranging from 5 to 30 cm/day with short measurement time of 5–10 minutes (Essouayed et al., 2019a).

Heat Pulse Flow meter is a thermal transmission in the open portion of the well screen that induces a thermal signal proportional to the Darcy flux (Kerfoot and Massard, 1985; Zlotnik & Tartakovsky, 2018). The unit is best deployed with velocities greater than 50 cm/day). In-situ Permeable Flow Sensor uses a thermal perturbation technique of a cylindrical heated device that is in contact with the porous media at the velocity measurement point to measure groundwater flow velocity (ranging from 0.5 to 90 cm/day) (Doetsch et al., 2012; Kempf et al., 2013).

The ^{222}Rn isotope is one of the proven techniques to estimate the groundwater flow velocity (Hall, 1993; Hamada, 2000; Hoehn & Von Gunten, 1989; Mayer et al., 2016; Schubert et al., 2011; Thao et al., 2017), to characterize the subsurface information of the hydrostratigraphic nature, to identify the surface water-groundwater interaction and depth at which groundwater is influenced by surface water, groundwater residence time. The ^{222}Rn technique uses ^{222}Rn concentration in groundwater which decreases with a half-life of 3.824 days after the supply stops. This method works using ^{222}Rn recovery that is obtained from the ratio of ^{222}Rn concentration in groundwater before (C_{gw}) and after it flows into a well (C_{ww}), the water well radius (r), radon decay constant ($\lambda = 2.1x\mathbf{10^{-6}}\ \boldsymbol{s^{-1}}$), horizontal convergence factor (α) and water velocity in a well (V_{ww}) to estimate groundwater flow velocity in the aquifer.

Estimating groundwater flow velocity has several key contributions in groundwater resources management that is significantly important in hydrogeological studies to quantify recharge, estimate clean-up times, design permeable reactive barriers, characterize both groundwater and contaminant movement in aquifer systems (Labaky et al., 2009). The contributions of this work have wide applicability in understanding transport zone near source zone, governs groundwater flow direction, contaminant concentration pluming, residence time and to support remedial design. The key Advantages of using radon as a tracer to determine groundwater flow velocity in a single well tests is due to the low cost methodological approach, avoidance of artificial tracer injection into the aquifer, necessity of only one groundwater well, Possibility of immediate availability of results. Nevertheless, potential sources of error might be due to the poor sampling, inadequate hydraulic connection of the well because of clogging screen and unsuitable well diameter resulting in excessively long or short well water residence times and practical approach to support in-depth theoretical considerations (Schmidt & Schubert, 2007; Schubert et al., 2011).

Groundwater resources in various basins of Ethiopia lack detail information of aquifer hydraulic properties, flow dynamics, nature of complex structural controls, storage capacity and aquifer response to changes associated to climate seasonal and anthropogenic effects. Therefore, the purpose of this study is to estimate groundwater flow velocity that

helps understand groundwater flow dynamics using ^{222}Rn as a proxy in the shallow hand pump wells of the Mecha, Ejere, Sodo and Abeshge sites in Ethiopian highlands during post water well construction. This work used ^{222}Rn technique to estimate groundwater flow velocity at a single-well level. This work helps to pave the way for decision making in groundwater resources development, management and monitoring the status of water wells during post water well construction.

4.2. Description of Study area

The study sites (Mecha, Ejere, Sodo and Abeshge) are situated in the Abay, Awash, Ghibe and Ziway Lake basins respectively. The climate, geology and hydrogeology of each site are discussed in the following section providing a further emphasise.

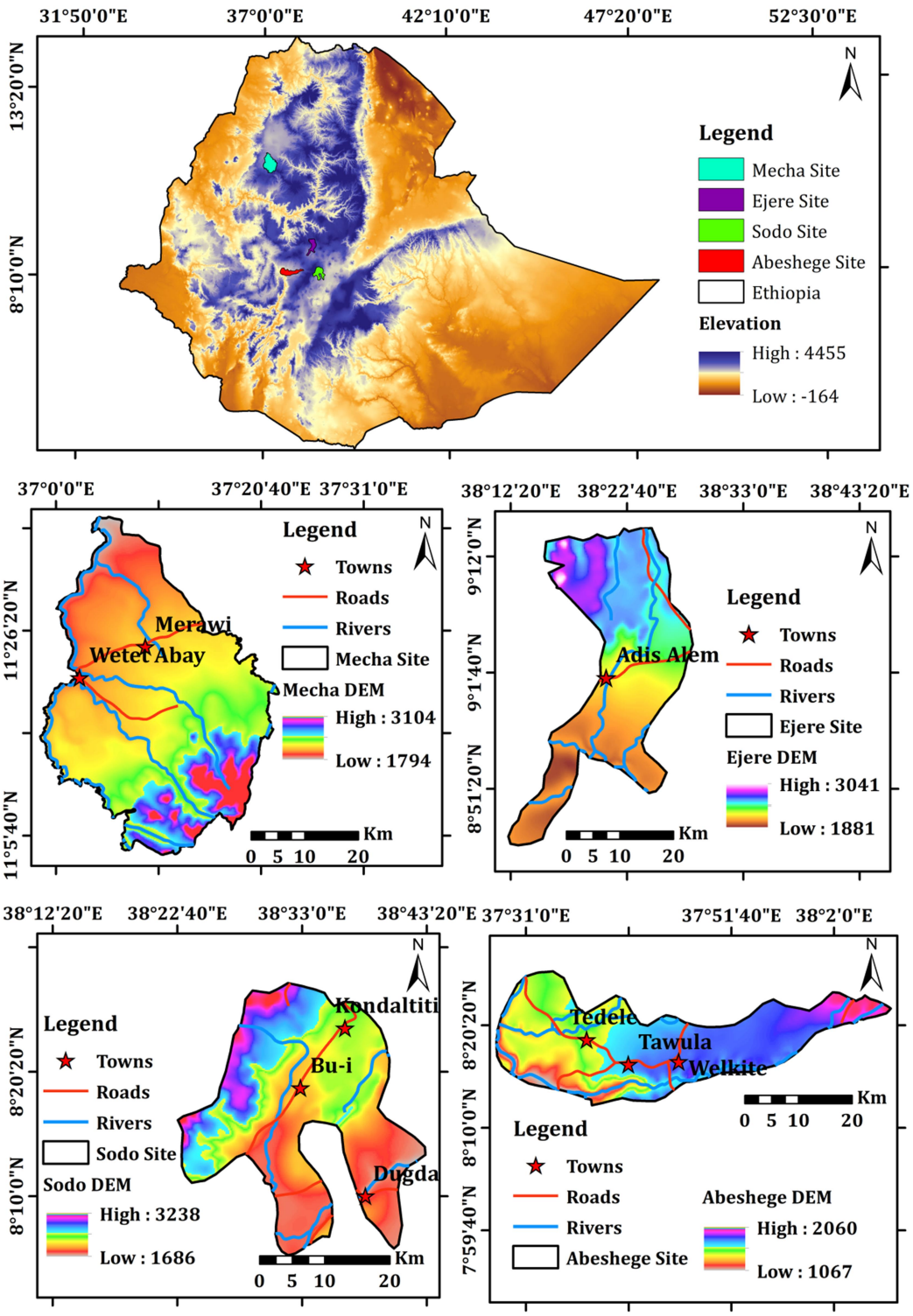

Figure 4.1: Location Map of the Study area

4.2.1. Mecha site

The Mecha site is situated in the source region of the Abay Basin at southern part of Lake Tana (Figure 2). It is found in the climate region of the tropical highland monsoon of one rainy season from June to September. The annual average temperature of Marawi and surrounding areas is 20^0C that ranges from 15^0C to 20^0C, showing hot months in December, January and February and relatively low in August and July. The rainfall distribution is controlled by northward and southward movement of inter-tropical convergence zone (ITCZ). The annual precipitation at Marawi station is 1572.3 mm/year.

The regional geological setting comprises shield volcanoes, flood basalts and Quaternary volcanics exposed near Tana Lake and associated few exposures of alluvial sediments (Ayalew et al., 2002; Kieffer et al., 2004b; Pik et al., 1998). The major volcanic exposures of the regional geology were characterized by Ashengie formation, Aiba basalt, Tarmaber-Gussa Formation, Ignimbrite, Rhyolite with minor tuffs, plateau basalt, the young aged Scoria fallouts forming cones near Bahir Dar and alluvium in the flat lying areas. In the Mecha site, the major geologic units are Quaternary basalts, quaternary alluvium and Tarmaber formation (P. Mohr & Zanettin, 1988a). The Tarmaber basaltic Formation situated in the vast south and south eastern part of the Mecha site, is characterized by weathered features with medium to coarse-grained textures. The Quaternary basalt is associated with cinder cones and broad-based gentle sloping circular to elliptical hills in the central and western part of the study area. Whereas, Quaternary soil is found in a flat lying topography and marshy areas in the northern part near to the shore of Tana Lake.

The hydrogeology of Mecha site is characterized by low productivity fracture aquifer of the Tarmaber formation in the southern and south eastern part, highly productive quaternary basaltic aquifer in the central and Shallow aquifers of the quaternary thick soil formation with inter-granular aquifer are in the northern part of the study area (Kebede et al., 2005, 2017; Mamo, 2015; Nigate et al., 2020; Walker et al., 2019a).

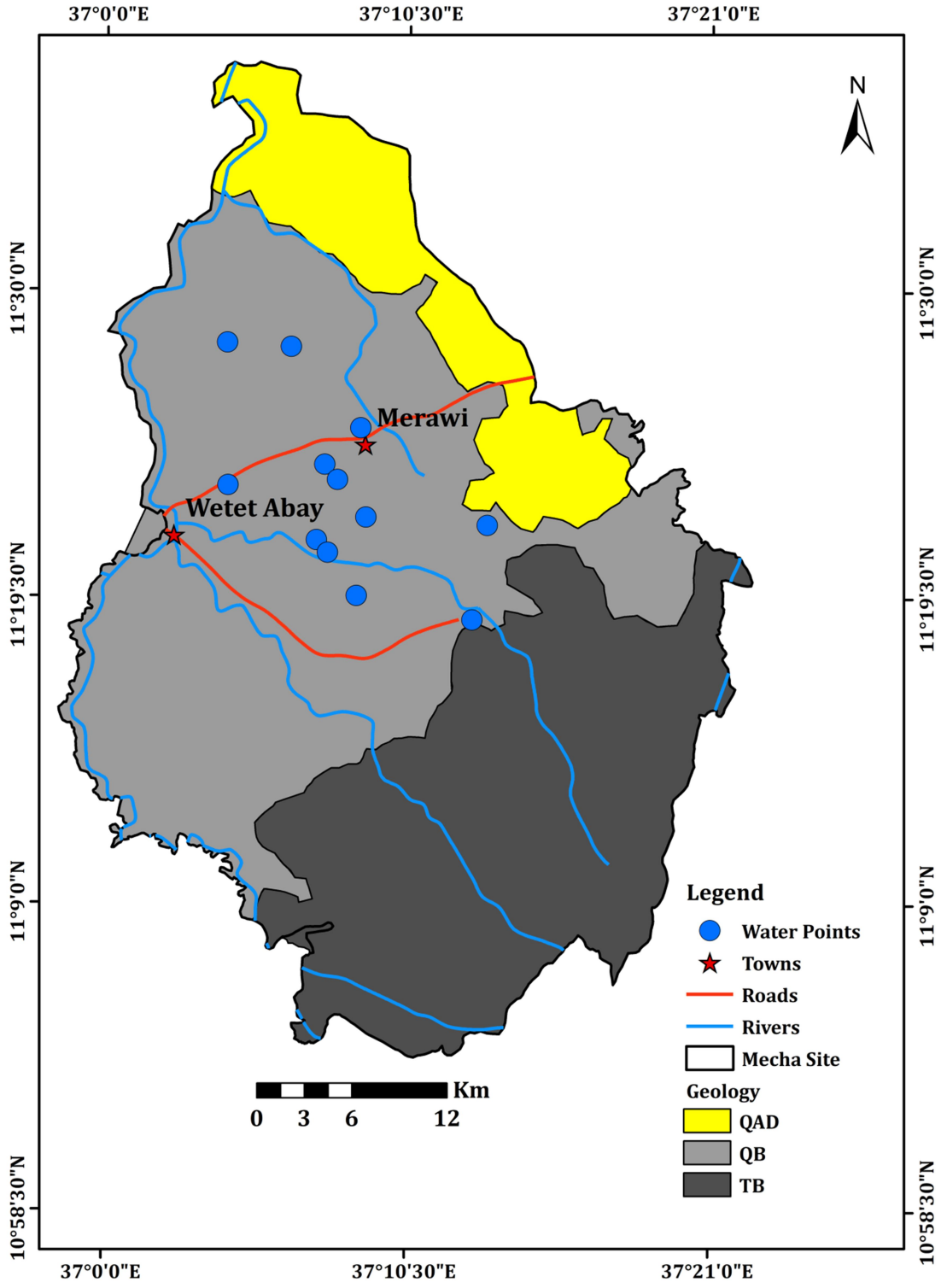

Figure 4.2: Geological Map of Mecha District and water sampling points

4.2.2. Ejere site

The Ejere site is situated 45km west of Addis Ababa in the Awash River Basin at the northern part of the major flat lying Becho Plain (Fig.3). The climatic condition of area is characterized by moisture source of the Atlantic Ocean and Indian Ocean currents as a source of precipitation. The main rainfall is experienced during summer season from June to September during the Atlantic and Indian Ocean coverage of the Ethiopian highlands. The mean Annual rainfall in the entire basin of the Awash basin is from 1190 to 1090 mm/year in the escarpments to less than 950mm in the lowland areas. The mean annual temperature of the region is 13 to 20^0C.

The geology of Ejere site comprises the upper basalt, Wechecha trachyte and Quaternary alluvial sediments (P. A. Mohr, 1967; Peccerillo et al., 2007; Woldegabriel et al., 1990). The upper basalt covered the northern part of the area, the Addis Ababa and surrounding Akaki forming both confined and unconfined aquifers regionally overlien by ignimbrite units and alluvial of Becho plain (Ayenew et al., 2008b; Azagegn et al., 2015; Berehanu et al., 2017; Demlie et al., 2008; Kebede et al., 2008; Yitbarek et al., 2012). The Wechecha Trachyte forms the volcanic centers and ridges near Ejere and surrounding areas regionally characterized by low permeability localized aquifers except in weathered and fractured zones. In most areas it acts as the aquiclude between lower and upper basalts. The quaternary alluvial sediments covered the vast regions of the southern part of Ejere site; thick overburden with high productivity in the Becho plain near to the Banks of Awash River accumulated alluvial deposits. The E-W trending Volcano-tectonic regional lineament of the Addis Ababa – Ambo fault zone crosses this study site.

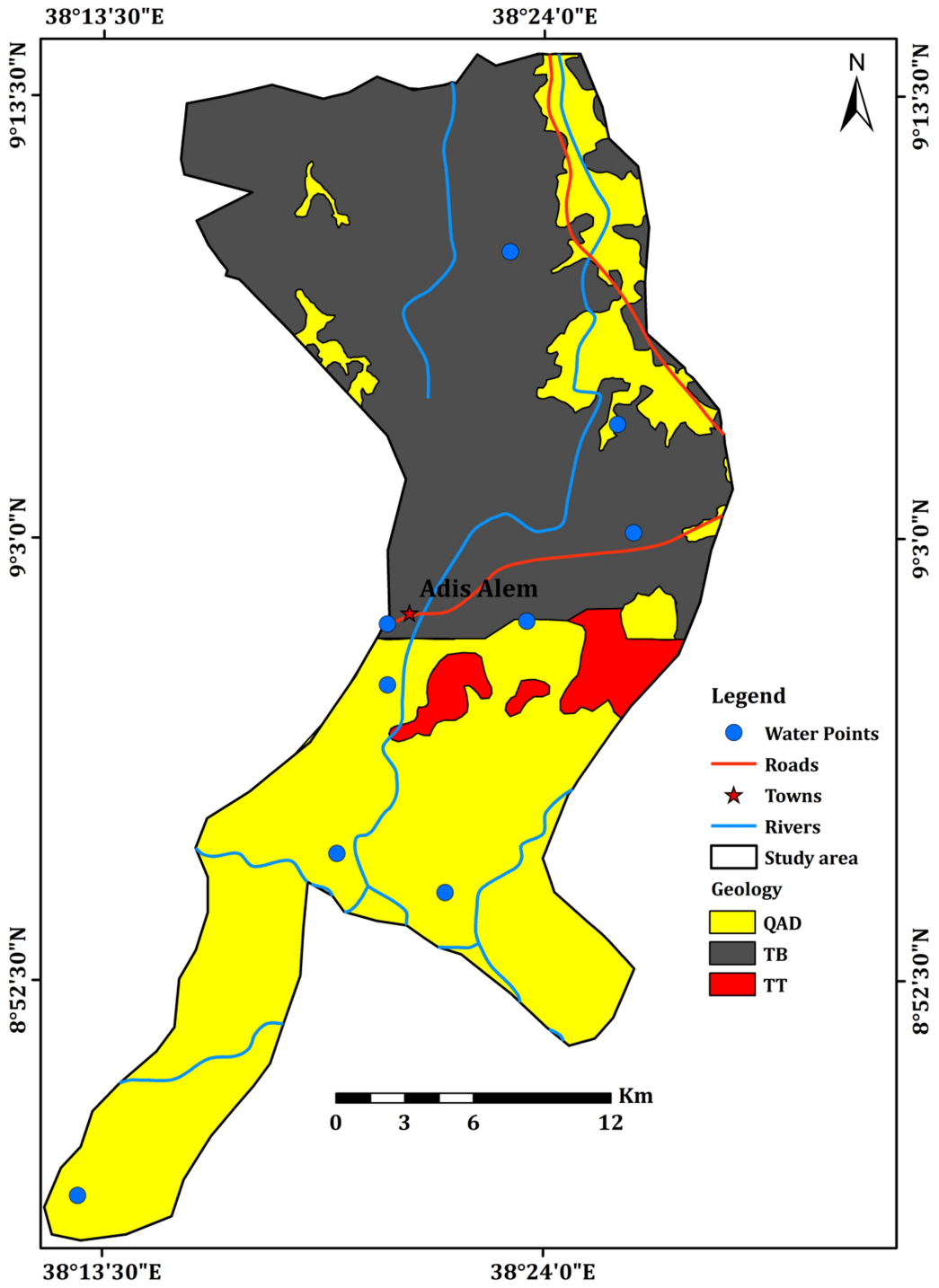

Figure 4.3: Geological Map of Ejere District and water sampling points

4.2.3. Sodo site

The Sodo site is situated 85 km at the south of Addis Ababa in the Ziway Lake Basin (Figure 4). The climatic condition of the area is influenced by the bimodal rainfall seasons that show the main rainy season is from June to September and the short rainy season lies between March and May, whereas, from October to February, it is sunny and dry season of very little rainfall. The nearest station Butajira shows the mean annual rainfall of 1,062 mm/year. The temperature shows slight increasing from the escarpment to the rift showing the altitudinal effect with the average monthly temperature ranged from 11.3 to 26.3^{0}C.

The geology of the Sodo site comprises the Aiba-Alaji basalt exposed at the escarpment of the Guraghe Mountain characterized by compact, medium to coarse grained textures and showing some weathering features that are intercalated with pyroclastic rocks (Abebe et al., 1998; Ayalew et al., 2002; Peccerillo et al., 2007; Woldegabriel et al., 1990). The fine grained Guraghe-Anchar Basalt (~300m thickness) shows vesicles filled with secondary minerals and is also intercalated with minor rhyolitic sequence. The welded pyroclastic flows consist of welded ignimbrite with minor intercalation of basaltic lava flow and lithic fragments associated with rhyolitic lava flows, ash and tuff. Whereas, the welded to partially welded pyroclastic flows show fine-grained, densely welded ignimbrite to poorly welded pyroclastic and lithic fragments associated with rhyolitic lava flows, intercalated ash and unwelded tuff. The rhyolitic and trachytic lava domes are intercalated with ash and tuffaceous deposits. The Rhyolite is exposed at the marginal escarpments of the Guraghe Mountain, that represents the product of the central volcano and some exposures of ash and unwelded tuff on the top and fine-grained lava flow and pyroclastic deposits interbedded with basaltic lava flows at the base of the volcano. The pyroclastic deposit is characterized by fine-grained poorly welded volcanic ash flow and fall deposits and lithic fragments associated with pumice and rhyolitic lava flows. The rhyolitic domes are associated with obsidian lava flows intercalated with fine ash and unwelded tuff. The lacustrine sediments are exposed in the rift floor mainly representing the silt, sand units and sediments of volcanic origin, pumice, volcanic ash, obsidian, rhyolite and basaltic rock fragments showing intercalation with pyroclastic fall deposits in some regions. The

alluvium unit is commonly characterized by reworking of the materials from volcanic origin.

Regional hydrogeological studies reveal that the volcanic aquifers are controlled by the porosity, fractures and weathering intensity, that comprises both primary and secondary structures as a good groundwater reservoir. The top weathering products of the volcanic rocks were serving as a source of shallow groundwater and springs. The regional aquifer classification shows that the volcanic aquifers of the plateau basalt (Aiba basalt and Guraghe-Anchar basalt) shows good range of transmissivity and yield of the aquifer as compared to other hydrogeological units like welded and unwelded pyroclastic deposits, rhyolitic lava flows and domed, ash falls and flows in the Sodo site. Aquifers of trachyte and rhyolite shows the least productivity in the study area, where the lacustrine deposits, pyroclastic flow are followed and the highest productivity is observed in scoria and basalt (Alemu, 2017; Ayenew et al., 2008a; Furi et al., 2011; Yitbarek et al., 2012).

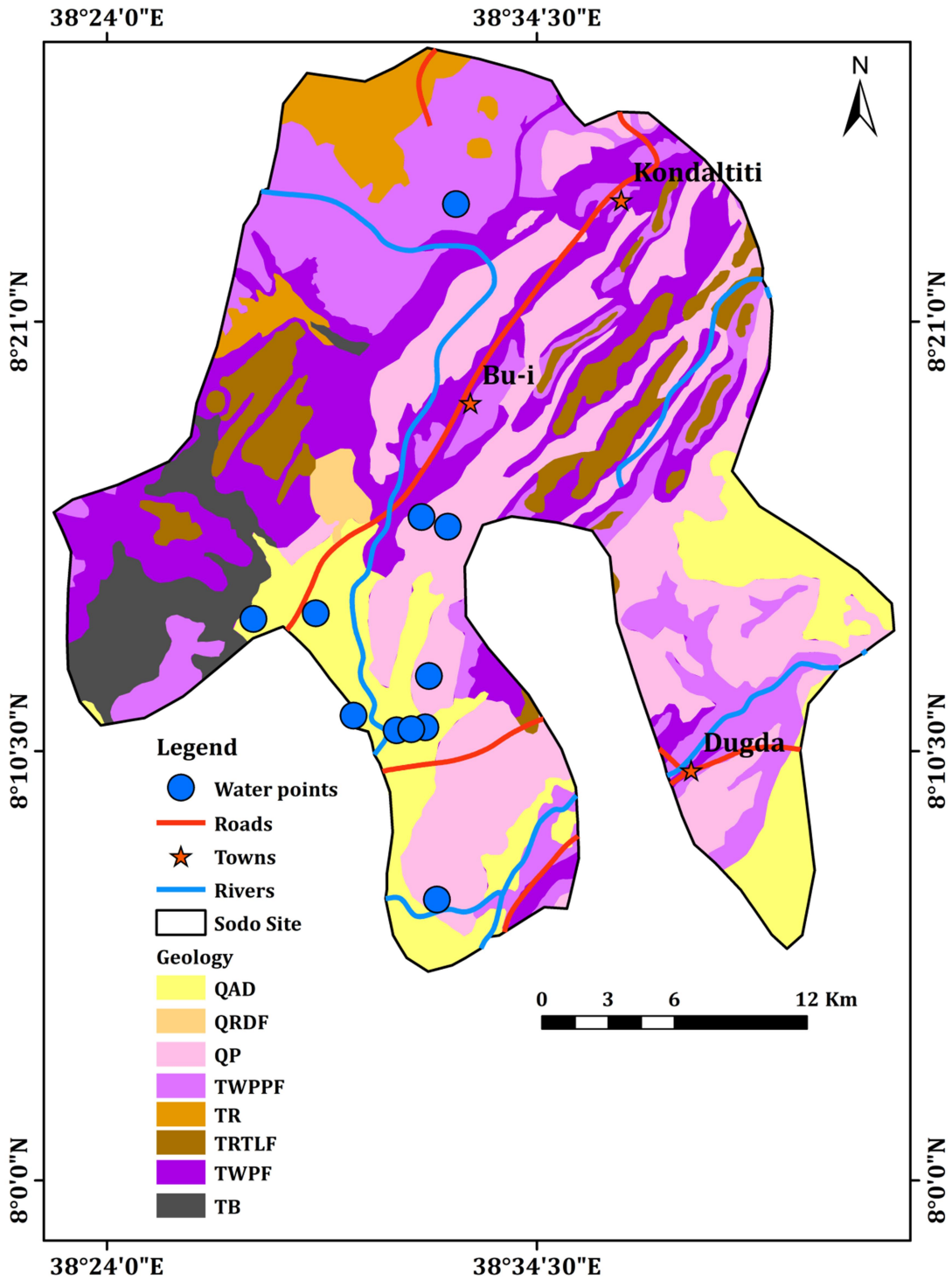

Figure 4.4: Geological Map of Sodo District and water sampling points

4.2.4. Abeshege site

The Aeshege site is situated in the Gibe Basin of the Guraghe zone at 150km south of Addis Ababa (Figure 5). The climatic condition of this site is under the influence of the ITCZ rainfall distribution that shows the highest rainfall season during the months of June to September and low rainfall season during the March to May with general bimodal type of rainfall. The hydrological networks such as Wabe River, Kulit River and Walga River are the Major tributaries of the Ghibe Basin draining in the study area.

The geology of this site comprises the Oligocene flood basalt of Jimma Lower Basaltic unit exposed around the Ghibe River and at the gorges of its main tributaries. It is characterized by medium to course-grained and partly weathered basaltic unit horizontally stratified in various areas, tilted in few areas and hexagonal columnar jointing. This unit is exposed at the gorges of the Kulit, Walga and Wabe Rivers. The Oligocene to Miocene basaltic unit covered the central part of the study site, is characterized by weathered features. The Miocene basaltic unit is exposed in the north western part of the site, is also characterized by some weathering features and covered by thick product of the regolith. The welded to partially welded pyroclastic Flows is the Pliocene volcanic product that covered the vast areas surrounding Welkite town and its north eastern part. This pyroclastic flow is characterized by weathered densely welded and lithic fragments associated with rhyolitic lava flows intercalated with ash and unwelded tuffs (Abbate et al., 2015; Ayalew et al., 2002; Beccaluva et al., 2009; Kieffer et al., 2004b; Lebas & Mohr, 1970; Peccerillo et al., 2007; Sembroni et al., 2016).

The regional hydrogeological studies reveal that the major aquifer units are formed in trap series flood basalts and the welded to partially welded pyroclastic flows. The good water bearing formations in the Abeshege site is situated in areas of these volcanic aquifer classes of highly weathered basalt aquifer with high variability of transmissivity and yield of the aquifer.

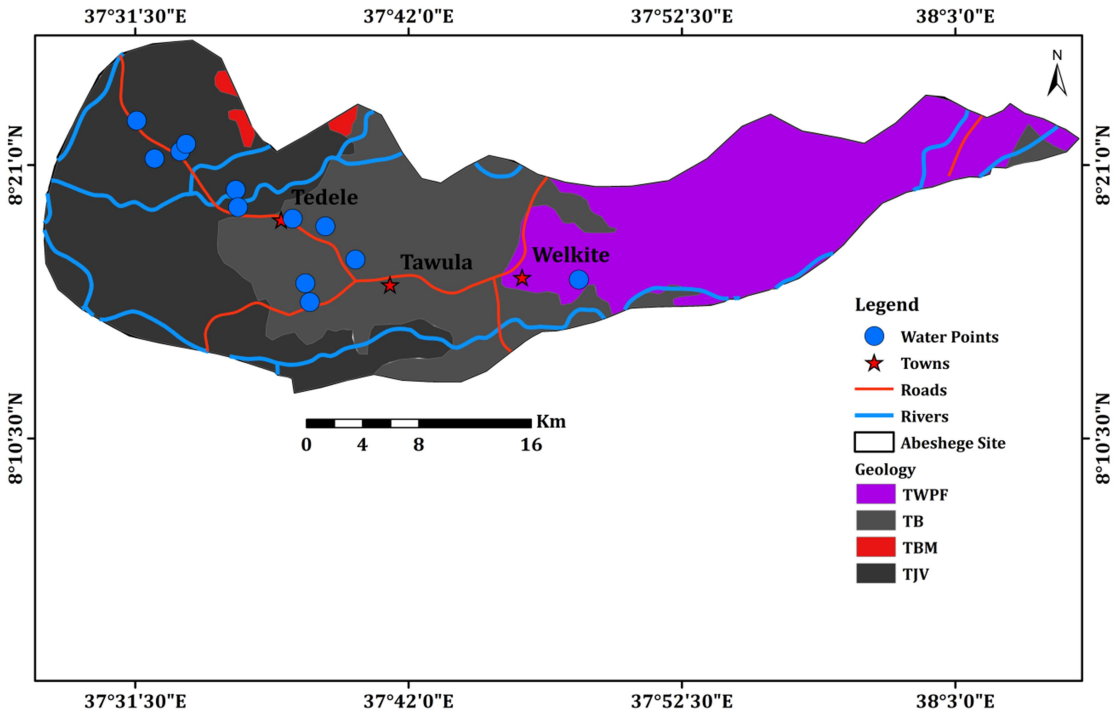

Figure 4.5: Geological Map of Abeshge District and water sampling points

4.3. Methodology

4.3.1. Theoretical background

The Radon (^{222}Rn) is chemically inert and its natural occurrence in groundwater makes it suitable for a single-well tracer due to its abundant occurrence in groundwater in every aquifer matrix from radioactive decay of ^{226}Ra. The ^{222}Rn (short half-life of 3.82days) natural background concentration in groundwater can be determined by the net ^{222}Rn emanation in to the water-filled pore spaces, the specific porosity of the aquifer matrix and its bulk density. After immediate loss from the contact of the aquifer matrix, when groundwater enters in to the monitoring well, ^{222}Rn decay is no longer balanced by ^{222}Rn production and results in a fast concentration decrease in the well water.

The ^{222}Rn deficit/recovery can therefore be used as a quantitative measure of its residence time in the well and thus for determining the groundwater flow velocity. Where the ^{222}Rn decay constant (λ) is $2.1\text{x}10^{-6}\ s^{-1}$ and C_{ww} and C_{gw} are ^{222}Rn concentration in the water well and the aquifer after time t has elapsed. The characteristics of ^{222}Rn are its initial

concentration in the groundwater and its relatively fast decrease in the water well. The simplified mathematical approaches, assumed perfectly mixed water column in the screened well section (Cook 1999). The Convergence of groundwater streamlines towards a well and its immediate surroundings were semi-quantitatively assessed that convergence causes flow velocities through the well and exceeds those through the aquifer by factors between 2 and 4 (Cook et al 1999). For an uncased borehole, they quantitatively suggested a factor of 2 and an assumption that is in accordance with the theoretically derived result.

4.3.2. Mathematical Approach

Under steady-state flow condition, the residence time of groundwater in a well depends on the radius (r) of the well and on the velocity of the groundwater flow passing through it. Since the well radius is known, the radon deficit (C_{ww}/C_{gw}) can be used as a direct quantitative measure for groundwater flow velocity (V_{gw}) through a well. The cross-sectional area A of the well subdivided in to subareas (dA) and each with a length of 2x and infinitesimally small width of y. From trigonometric, each sub-area has a length of $2x=2r\cos\theta$ and width $y= du\cos\theta=r\cos\theta d\theta$, with u being a circumference of the well and du is infinitesimally small segment of it (Hamada, 2000).

Parameteres	Descriptions
r	Water well radius
A	Water well cross-sectional area
λ	Radon decay constant
t	Water residence time
C_{ww}	Radon concentration in a water well
C_{gw}	Radon concentration in groundwater
V_{ww}	Groundwater flow velocity in a well
V_{gw}	Groundwater flow velocity in the aquifer
α	Horizontal convergence factor
r1,r2,r3	Radius of filter screen, outside of filter screen and radius of the filter pack
K_1,k_2,k_3	Hydraulic conductivity of the filter screen, filter pack and the

aquifer

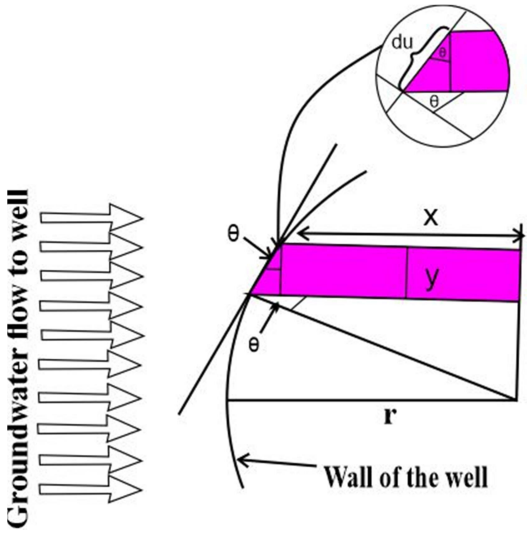

Figure 4.6: Schematic sketch of sub-area (dashed red) of the sectional area of the well with length of 2x = 2rcosϴ and with y = rcosθdθ (Modified after Hamada (2000)).

For each sub-areas ($dC_{ww}d_A$), the ^{222}Rn inventory depends on the initial ^{222}Rn concentration of the groundwater entering the well (C_{gw}), average ^{222}Rn concentration in a well (C_{ww}), the velocity of water in a well (V_{ww}), the ^{222}Rn decay constant ($2.1x\mathbf{10^{-6}}\ \boldsymbol{s^{-1}}$) and t the time (s). The decrease of the initial Radon equilibrium concentration in the groundwater (natural Rn background $\mathbf{C_{gw}^{\infty}}$) because of the absence of ^{222}Rn production is quantified in equation (1):

$$\mathbf{C_{ww}^{t} = C_{gw}^{\infty} e^{(\lambda t)}} \ldots\ldots\ldots\ldots\ldots\ldots\ldots\ldots\ldots\ldots\ldots\ldots\ldots\ldots\ldots\ldots\mathbf{1}$$

$$\boldsymbol{dC_{ww}^{t} dA = r\cos\theta\, d\theta \int_{0}^{t} C_{gw}^{\infty}\, e^{\lambda t} V_{ww}\, dt} \qquad \ldots\ldots\ldots\ldots\ldots\ldots\mathbf{2}$$

The water residence time for each subarea can be expressed as:

$$\boldsymbol{t = {2r\cos\theta}/{v}} \ldots\ldots\ldots\ldots\ldots\ldots\ldots\ldots\ldots\ldots\ldots\ldots\ldots\ldots\ldots\ldots\ldots\ldots\mathbf{3}$$

$$\int_0^t C_{gw}^{\infty} e^{-\lambda t} V_{ww} dt = -\frac{1}{\lambda} C_{gw}^{\infty} V_{ww} \left(e^{-\lambda 2 r \cos\theta / Vww} - 1 \right) \ldots\ldots\ldots\ldots\ldots\ldots\ldots\ldots 4$$

The total amount of Rn-222 is calculated by integrating equation 3 for θ from $-\frac{\pi}{2}$ **to** $\frac{\pi}{2}$. The average Rn-222 concentration in a well per unit length is

$$C_{ww}^{t} = \frac{1}{\pi r^2} \int_{-\pi/2}^{\pi/2} r \cos\theta d\theta \left(-\frac{1}{\lambda} C_{gw}^{\infty} V_{ww} (e^{-\lambda 2 r \cos\theta / Vww} - 1) \right) \ldots\ldots\ldots\ldots\ldots\ldots 5$$

Re-arranging equation 5, the following equation is obtained:

$$\frac{C_{ww}^{t}}{C_{gw}^{\infty}} = \frac{V_{ww}}{\pi \lambda r} \int_{-\pi/2}^{\pi/2} \left(1 - e^{-\lambda 2 r \cos\theta / Vww} \right) \cos\theta d\theta \ldots\ldots\ldots\ldots\ldots\ldots\ldots\ldots 6$$

Equation (5) is similar to the following equation by Hamada 2000

$$\frac{C_{ww}^{t}}{C_{gw}^{\infty}} = \frac{1}{\pi} \int_{-\pi/2}^{\pi/2} \frac{1}{\mathcal{E}} \left(1 - e^{-2\mathcal{E} cos\theta} \right) \cos\theta d\theta \ldots\ldots\ldots\ldots\ldots\ldots\ldots\ldots 7$$

Where $\mathcal{E} = \lambda r / Vww$ ……..8

$$\alpha = \frac{8}{\left(1 + \frac{k_3}{k_2}\right) + \left\{1 + \left(\frac{r_1}{r_2}\right)^2 + \left[\frac{k_2}{k_1}\left(1 - \frac{r_1}{r_2}\right)^2\right]\right\} + \left(1 - \frac{k_3}{k_2}\right)\left\{\left(\frac{r_1}{r_3}\right)^2 + \left(\frac{r_2}{r_3}\right)^2 + \frac{k_2}{k_1}\left[\left(\frac{r_1}{r_3}\right)^2 - \left(\frac{r_2}{r_3}\right)^2\right]\right\}} \ldots 9$$

This shows that the easily measurable ^{222}Rn deficit $\left(\frac{C_{ww}^{t}}{C_{gw}^{\infty}}\right)$ detected in the water well (integrated over the whole sectional area) depends quantitatively on the known radius of the well (r), the known decay constant and the flow velocity through the well ($\mathbf{V_{ww}}$), which is the parameter of interest can be obtained. The aspect that are not considered (Hamada, 2000), because of different hydraulic conditions in the aquifer and well (filter screen and filter pack), groundwater flow is characterized by a convergence of the streamlines toward the well. Cook et al 1999 mentioned flow convergence around the well, but quantified it only for the case of an uncased borehole. Depending on the difference in the hydraulic conditions between the aquifer and the well, the velocity of the water well $\mathbf{V_{ww}}$ can be substantially higher than the groundwater flow velocity in the host aquifer $\mathbf{V_{gw}}$.

An empirical developed for the relationships between inflow width, well radius and introduced a horizontal convergence factor based on the well geometry and all relevant hydraulic conductivity data and radius (K_1, K_2, K_3, r_1, r_2 and r_3) as well as applying α, flow

velocity in the undisturbed aquifer ($\mathbf{V_{gw}}$) can be quantitatively related to the flow velocity determined inside the well ($\mathbf{V_{ww}}$) (Drost et al., 1968).

If the well is constructed without the filter pack or if K of filter pack is assumed equal to K of aquifer ($r_3 = r_2$ and $K_3=K_2$), then the above equation is simplified as:

$$\boldsymbol{\alpha = \frac{4}{1 + (\frac{r_1}{r_2})^2 + \left(\frac{k_2}{k_1}\right)[1 - (\frac{r_1}{r_2})^2]}} \ldots\ldots\ldots\ldots\ldots\ldots\ldots\ldots\ldots\ldots \mathbf{10}$$

If the well is an open borehole without any filter screen and filter pack ($r_3=r_2=r_1$ and $k_3=k_2=k_1$), the above equation is simplified to $\alpha = 2$, this relation is developed empirically (Cook et al., 1999). The groundwater flow velocity in the undisturbed aquifer ($\mathbf{V_{gw}}$) can be quantified using the flow velocity determined inside the well ($\mathbf{V_{ww}}$) based on equation (11).

$$\boldsymbol{V_{gw} = \frac{V_{ww}}{\alpha}} \ldots\ldots\ldots\ldots\ldots\ldots\ldots\ldots\ldots\ldots\ldots\ldots\ldots\ldots\ldots\ldots\ldots\ldots \mathbf{11}$$

The groundwater flow velocity estimation in a single well using this mathematical equation used the convergence of streamlines that considers non-linear 2-D integral equations that can be solved using numerical methods. To solve this equation iterative method of numerical integral with two unknown variables can be solved using genetic algorithm that can be determined by assigning upper and lower boundaries. Therefore, this complex integral equation for the purpose of groundwater flow velocity estimation is solved using matlab tool box for the integral function, its constraints and main script.

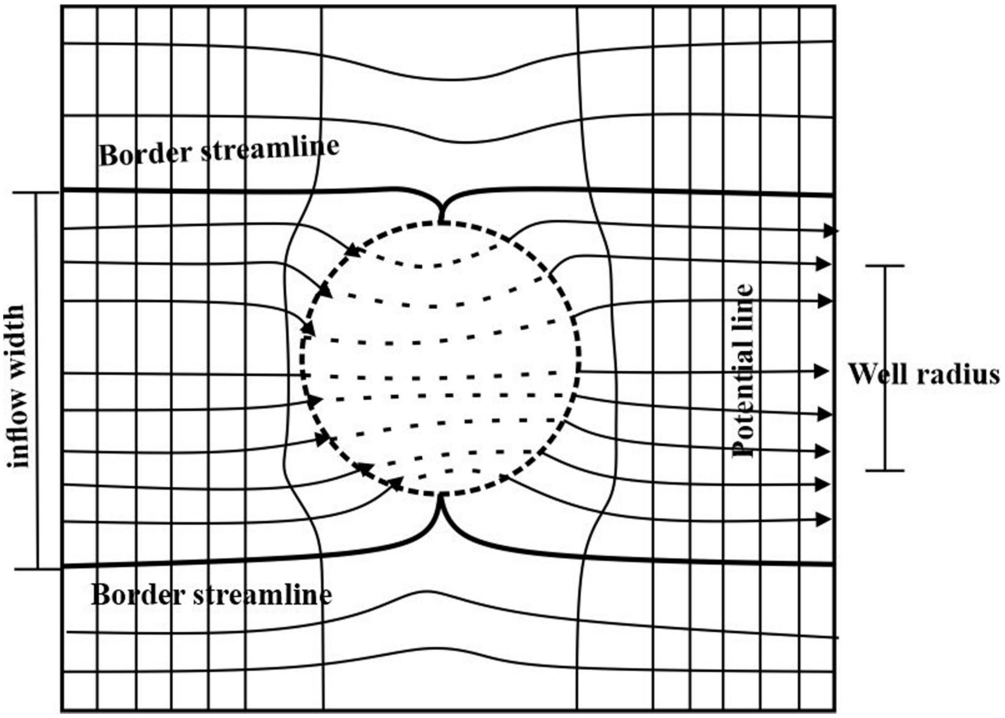

Figure 4.7: schematic diagram of the horizontal flow pattern showing the top view within and around a well central dotted line (modified after Andreas Englert (2003)).

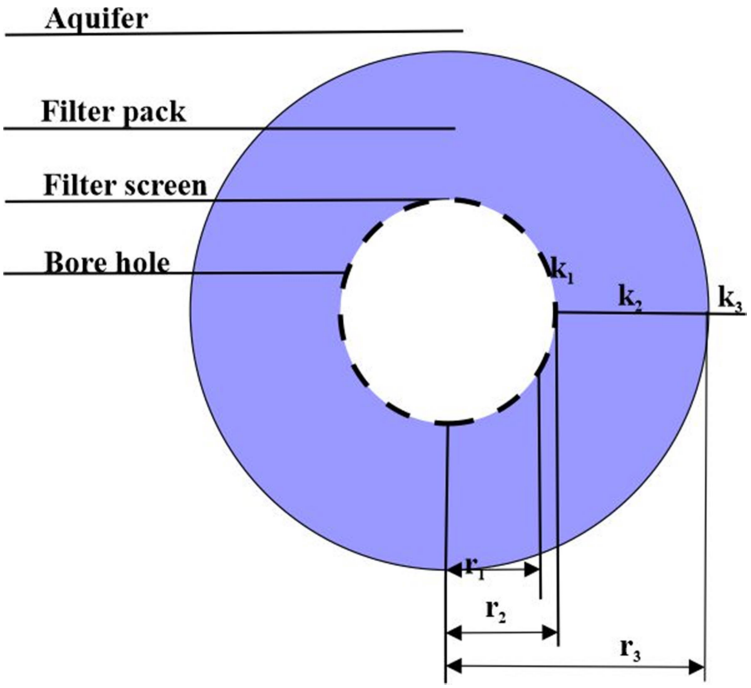

Figure 4.8: schematic diagram of horizontal cross-section of a screened well with filter pack (modified after (Drost et al., 1968)).

4.3.3. Water Sampling and Materials

The groundwater sampling was conducted in shallow hand pump wells currently serving as a source of water supply. All water samples were measured insitu for the concentration of ^{222}Rn in a well and aquifer in April, 2021. A RAD7 (Durrige Company Inc 2020) radon detector was fitted to a big bottle system for the quick survey of Radon. A 250 ml dark glass bottle was used to take the sample from the well by tightly capping the bottle to prevent the entrance of the air into water sample. The RAD7 consists of a drying tubes and desiccants. All sets were carefully attached to the filter and tubing, carefully removing plastic caps from small drying tube, attaching the filter to the inlet of RAD7, using small drying tube to collect air samples, purging for few minutes and then starting the test.

The ^{222}Rn concentration from the water well was sampled before purging stagnant water, whereas, ^{222}Rn concentration which represents the aquifer was sampled after significant purging of the water from the well. Counting is based on the principle of liquid-gas-membrane extraction (Schmidt & Schubert, 2007). During extraction, holly vinyl fibres were used to strip ^{222}Rn from water sample to a closed air-loop. The ^{222}Rn counting was conducted for overall period of 45 minutes for each water point in which each counting cycle takes place for 15 minutes. This was separately conducted for each samples from a well and aquifer of sampling sites. Three readings were recorded and an average of three measurements was taken as a representative to a specific site ^{222}Rn concentration in a well and an aquifer. The counting was recorded using the sniff technique that separately represent for both waters in a well and aquifer ^{222}Rn concentration analysis.

4.4. Results

4.4.1. Radon concentration and recovery

The summary of radon concentration in water well and aquifer, radon deficit/radon recovery, velocity in water well, groundwater velocity and residence time in a well are presented in Table 1. In the Mecha site ^{222}Rn concentration in water wells and aquifer ranged between 437 to 12,063 Bq/m^3 and 1480 to 22,184 Bq/m^3 respectively (Figure 9).

The highest ^{222}Rn concentration of the Mecha site was observed in the Mecha Tebelo (EME15), while the lowest ^{222}Rn concentration was observed in Mecha Amarit (EME13). The highest concentration of ^{222}Rn from Mecha Tebelo was observed in 30m deep shallow hand pump well. However, there is no distinct pattern that indicates the relationship between ^{222}Rn concentration and water well depth. In water wells of Mecha District, the highest ^{222}Rn recovery was observed in EME09, while, the lowest was observed in EME13. All other wells are in the range between 0.62 and 0.86.

Table 4.1: Radon concentration, Radon Deficit and groundwater velocities in water wells and aquifers and the water residence time in the well.

Sample ID	C_{ww} (Bq/m^3)	C_{gw} (Bq/m^3)	C_{ww}/C_{gw}	V_{ww}(cm/day)	V_{gw}(cm/day)	t(days)
EAE01	5470±522	13027±835	0.391	0.988	0.494	5.181
EAE02	14964±953	14968±961	0.999	138	69.1	0.0012
EAE04	8430±650	11573±751	0.766	4.19	2.09	1.47
EAE07	2800±368	4160±461	0.673	2.71	1.36	2.182
EAE08	4010±454	4150±462	0.966	34.6	17.3	0.18
EAE10	2970±391	3510±421	0.846	6.91	3.46	0.921
EAE11	3920±446	8540±674	0.459	1.26	0.628	4.29
EAE12	7940±627	9330±679	0.851	6.91	3.46	0.89
EAE13	1920±322	2080±332	0.923	13.8	6.91	0.44
EAE14	1400±277	1760±308	0.795	5.02	2.51	1.261
EEJ02	13992±902	21007±1020	0.762	4.07	2.03	1.5
EEJ06	13514±874	14954±943	0.834	6.01	3.01	1.0033
EEJ09	12549±825	13988±898	0.813	5.32	2.66	1.142
EEJ10	2860±384	3090±397	0.926	15.4	7.68	0.43
EEJ18	3610±429	4530±476	0.797	4.94	2.47	1.251
EEJ17	9930±700	11093±720	0.993	138	62.16	0.0415
EEJ20	4940±497	12064±792	0.411	1.06	0.528	4.9
EME01	8320±644	11573±739	0.759	4.07	2.03	1.52
EME02	12062±783	12543±807	0.923	13.8	6.91	0.44
EME05	4110±458	6080±552	0.676	2.82	1.41	2.16
EME07	3010±301	4610±481	0.653	2.47	1.23	2.35
EME09	4310±474	4590±483	0.939	19.8	9.88	0.35
EME12	4570±480	7370±603	0.62	2.19	1.1	2.634

EME13	437±164	1480±281	0.295	0.705	0.353	6.723
EME15	12063±86	21296±1010	0.572	1.84	0.922	3.081
EME18	6420±568	7500±610	0.856	7.68	3.84	0.86
ESD01	12541±797	13509±856	0.867	8.13	4.07	0.79
ESD04	1520±285	2850±381	0.533	1.61	0.804	3.465
ESD08	2750±377	5160±508	0.533	1.61	0.804	3.465
ESD09	3220±405	6940±586	0.464	1.26	0.628	4.232
ESD10	3150±212	8330±640	0.378	0.953	0.477	5.36
ESD11	2330±352	2770±381	0.841	6.58	3.29	0.953
ESD13	1850±313	3800±483	0.487	1.4	0.698	3.97
ESD16	7900±625	6000±546	0.756	4.07	2.03	1.54
ESD17	6750±598	7090±613	0.952	23	11.5	0.271
ESD20	2350±350	2750±379	0.855	6.91	3.46	0.87

In the Ejere site, results obtained from ^{222}Rn concentration ranged between 2,860 and 13,992 in water well and 3,090 to 22,189Bq/m^3 in an aquifer (Figure 9). Elevated concentration of ^{222}Rn was recorded in EEJ02, while the lowest concentration was observed in EEJ10. The ^{222}Rn recovery in all samples from water wells of Ejere site is in the range of 0.41 to 0.99. The highest ^{222}Rn deficit was observed in EEJ17, while the lowest was in EEJ20. The relationship between ^{222}Rn concentration and water well depth show a weak correlation.

In the Sodo site, ^{222}Rn concentration measurement from wells and aquifer are in the range of 1,850 to 12,541 and 2,750 to 13,509 Bq/m^3 respectively (Figure 9). The highest ^{222}Rn concentration was recorded in ESD01, while the lowest concentration is in ESD11. Water well depth has no significant effect on the distribution of ^{222}Rn concentration, except in one well with shallow depth (ESD01=25.3m) showing the highest range of ^{222}Rn concentration. The ESD19 (80m deep) indicates the lowest range of ^{222}Rn in water well. However, all other wells in this sampling site have distinct relationship with water well depth. The ^{222}Rn recovery in the Sodo site ranged between 0.378 and 0.952, where the highest value was measured in ESD17, while the lowest value is in ESD10.

In the Abeshege site, the ^{222}Rn concentration ranged between 1,400 and 14,964 Bq/m^3 in wells and 1,760 to 14, 968 Bq/m^3 in aquifers (Figure 9). The highest value of ^{222}Rn

concentration was recorded in EAE14, while the lowest ^{222}Rn concentration was observed in EAE02. In this study site, the ^{222}Rn recovery of all sampled wells was observed in the range of 0.39 to 0.99. The highest ^{222}Rn recovery was recorded in EAE02, whereas the lowest was in EAE01. The deepest well (EAE10 = 84.3m) in this site show ^{222}Rn concentration of 2,970 and 3,510 in well and aquifer, whereas, the shallowest well (EAE07=43.5m) has 2800 and 4160 Bq/m^3. The concentration of ^{222}Rn recorded in wells and aquifers and the depth of boreholes have no significant relationship.

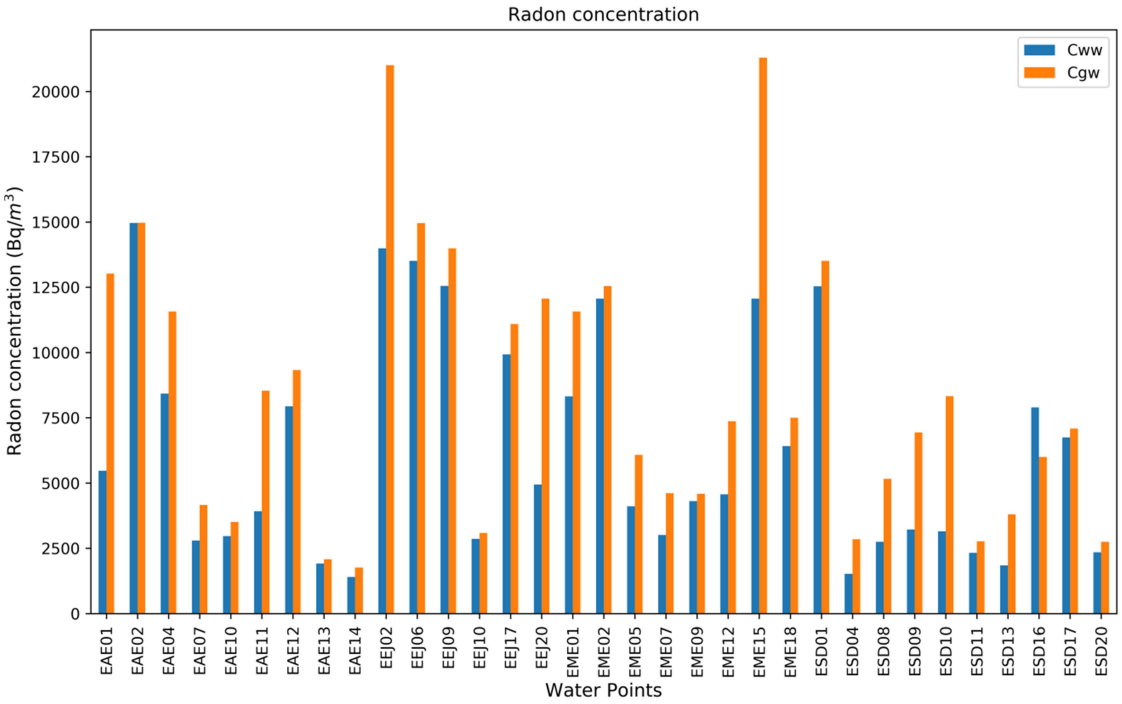

Figure 4.9: ^{222}Rn Concentration in groundwaters of all study sites

4.4.2. Groundwater flow velocity estimation

Groundwater flow velocity is estimated from ^{222}Rn deficit/recovery measured from ^{222}Rn concentrations in water well and the aquifer, Rn decay constant (λ), water well radius (r), the factor horizontal convergence factor (α) of flow streamline obtained from hydraulic conductivities of the aquifer, filter screen and the filter pack using equation 9 and 11 for each samples of the sampling sites.

The groundwater flow velocity in the Mecha site was ranged from 0.35 to 9.88 cm/day and the average groundwater flow velocity is 3.45cm/day. The highest value is observed in the EME09 and lowest value is in the EME13 (Figure 4.10). In this site there is a slightly low groundwater flow velocity as compared to the other three sites. This is associated to less effect of hydraulic gradients, surface topography and geological structures in the vast plains where many hand pump bore holes were situated. This area is exhibited by the shallow water table depth encountered by hand dug wells at each household level for the domestic purpose. Furthermore, there are various irrigated farm lands gaining the water from Koga dam along widely distributed hydraulic structures for various Keble's surrounding Marawi town.

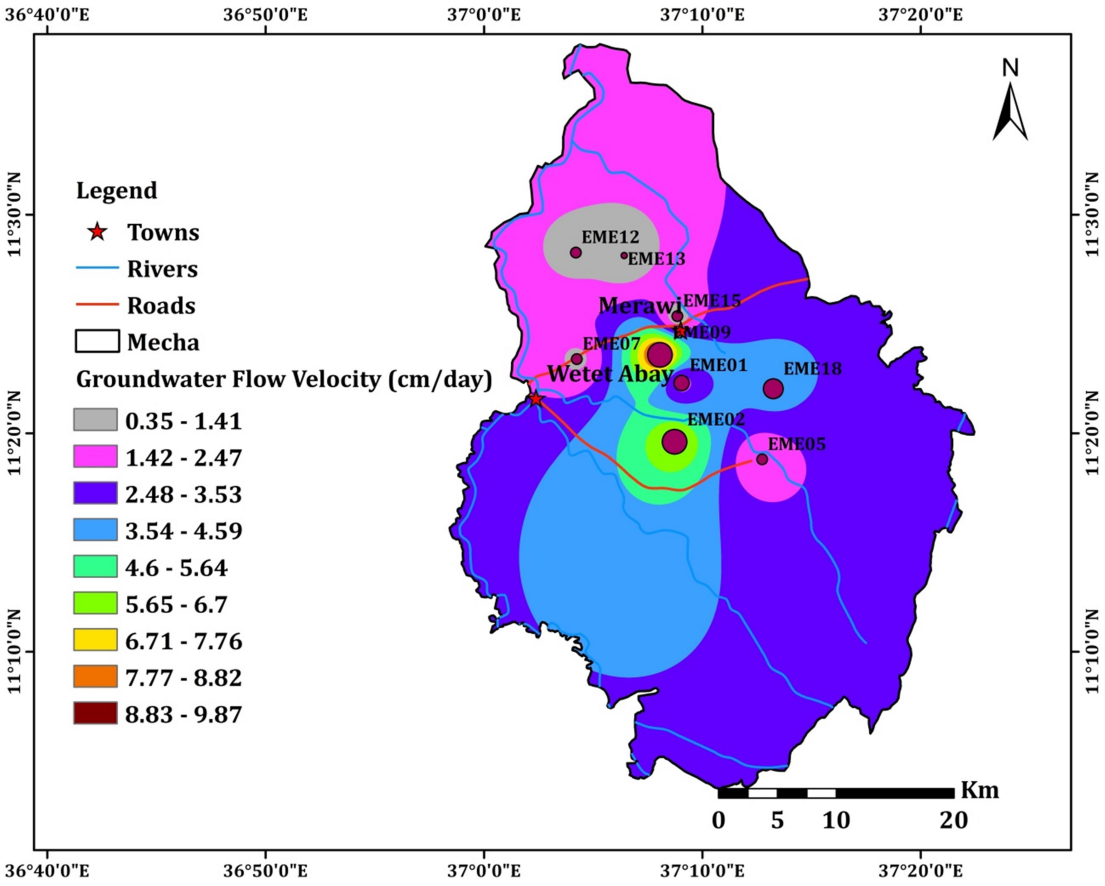

Figure 4.10: Groundwater flow velocity map of Mecha District

In the Ejere site, groundwater flow velocity ranged between 0.53 to 62.16 cm/day (Fig.11). The highest value is observed in the EEJ17 and the lowest value is in the EEJ20 where the average groundwater velocity is 17.46 cm/day. In the Ejere site groundwater flow velocity is controlled by surface topography of hydraulic gradient, lithostratigraphy and geological structures. In the Northern part of Ejere, elevated surface topography, fractured and weathered volcanic units played a significant role to increase groundwater flow velocity as observed in EEJ17 hand pump well. However, in the southern part of the site groundwater flow velocity is decreased due to the less effect of hydraulic gradients and hydrostratigraphic distribution. Wide range of thick alluvial deposits surrounding Awash river bank exhibits slight decrease of flow velocity as compared to the rugged topography with fractured nature of the northern part of the Ejere site.

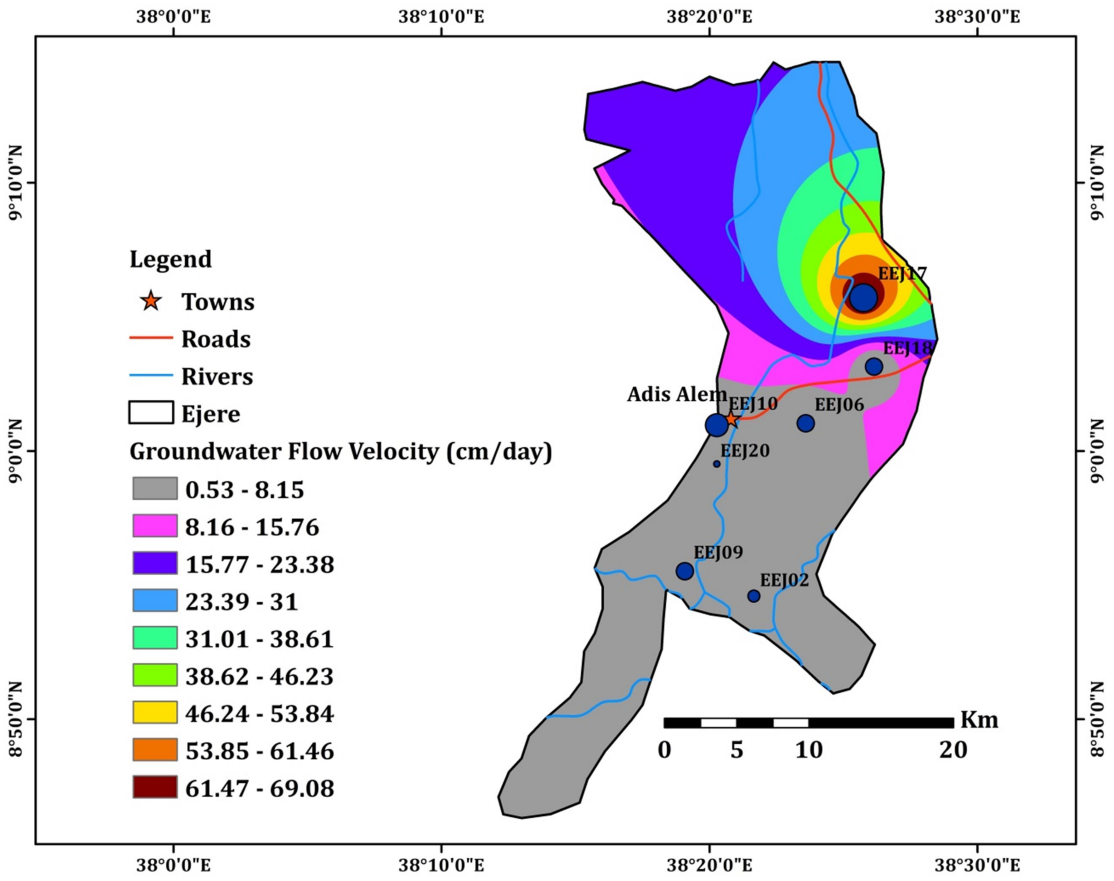

Figure 4.11: Groundwater flow velocity map of Ejere site

Groundwater flow velocity in the Sodo show the range between 0.48 and 11.5 cm/day, where the highest value is observed in the ESD17 and lowest value is in the ESD04 and the average groundwater flow velocity is 3.31 cm/day (Fig.12). In the Sodo site groundwater flow velocity is controlled by the heterogeneous distribution of hydrostratigrphy widely distributed from pyroclastic deposits comprising intermixed various lithologic units and lacustrine deposits with varying response to the flow velocity. In addition, the geomorphological control of Guraghe Mountain has significant role on groundwater flow velocity that is exhibited by high flow velocity reported at Fule Amanuel area (ESD17). Except in ESD17, other hand pump wells show less than 5cm/day. Therefore, as compared to other sites, due to the complex nature of geologic units and geomorphological structures, slight range of average groundwater flow velocity was observed in the Sodo site.

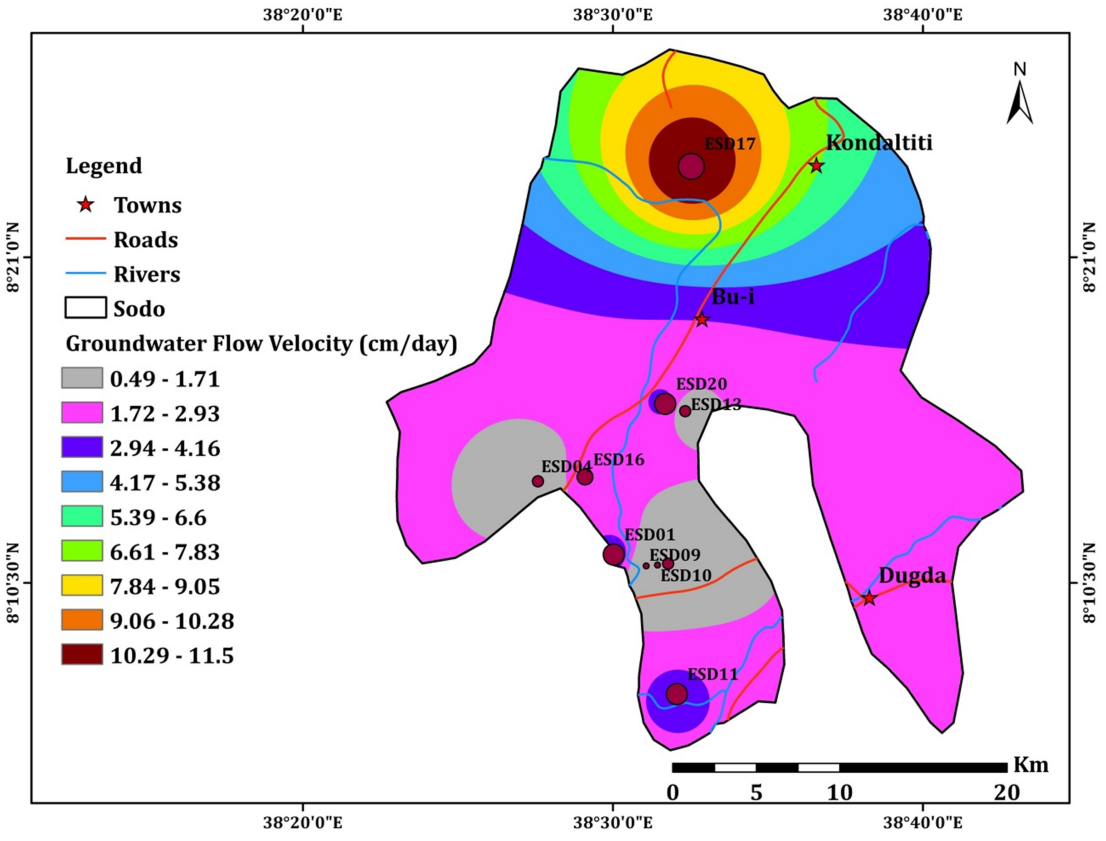

Figure 4.12: Groundwater flow velocity map of Sodo site

Groundwater flow velocity in the Abeshege District was ranged from 0.49 to 69.1cm/day, where the highest value was measured in the EAE02 and lowest value is in the EAE11 and

the average groundwater flow velocity is 14.74 cm/day (Figure 4.13). This site is characterized by heterogeneous distribution of groundwater flow velocity, depths ranged between 44 to 84m and most of hand pump bore wells have served for more than 30 years of long life span. The highest groundwater flow velocity recorded in this site (EAE02) is situated in an area where rivers like Kulit and Darge and spring manifestations were observed in the nearest site. This hand pump well is the longest serving (more than 37 years) among all other wells with no seasonal effect on the level of groundwater. However, some hand pump wells situated in the nearest site were not showing similar range of groundwater velocity that indicates the difference in hydraulic gradient and hydrostartigraphic distributions. The lowest groundwater flow velocity observed in this site is associated to the depressed area where hydraulic gradient and geological structures effect are less manifested.

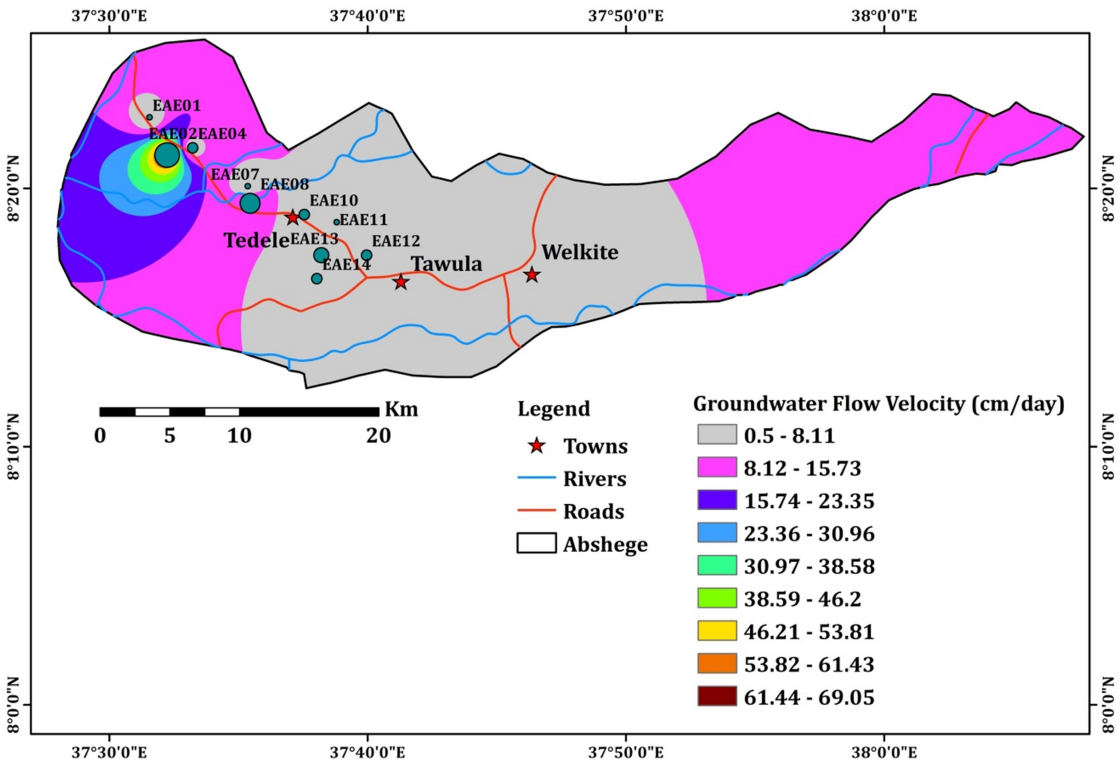

Figure 4.13: Groundwater flow velocity map of Abeshge site

Groundwater flow velocity in all four study sites shows the minimum 0.35 cm/day, maximum 69.1 cm/day (Fig.14). The highest groundwater flow velocity was observed in Abeshge site (EAE02), whereas, the lowest was observed in EME13 in the Mecha site. Comparing the average groundwater flow velocities in each study sites, the highest average value was recorded in the Abeshege site, while the lowest average was in the Sodo site.

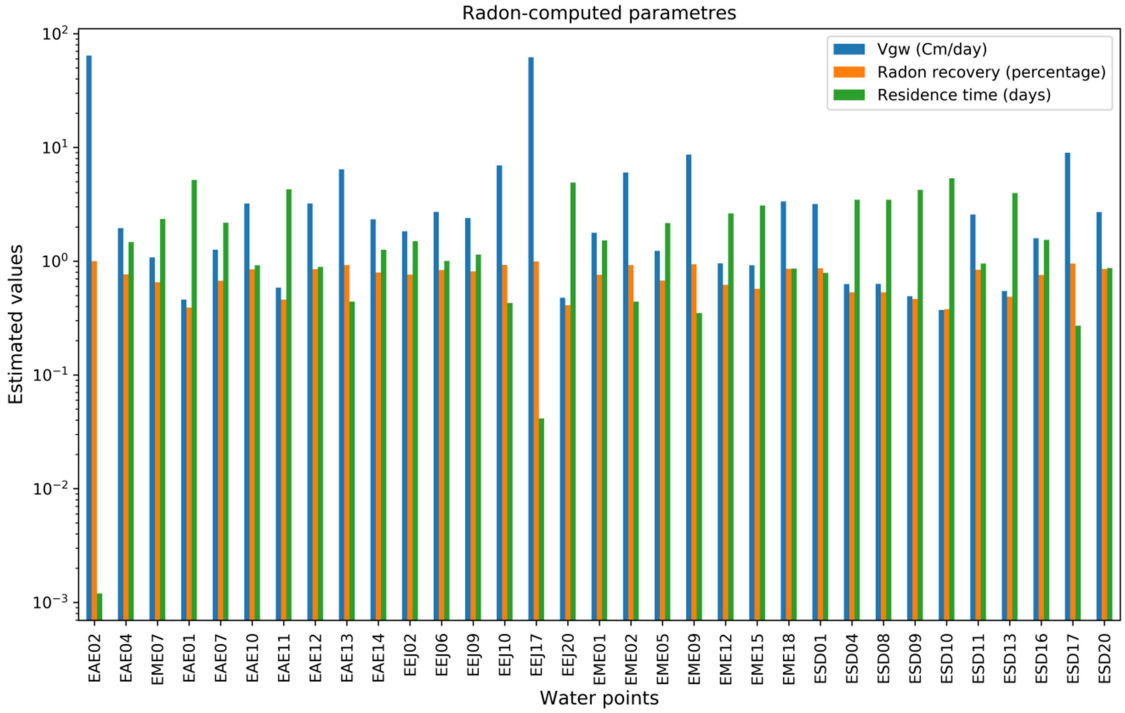

Figure 4.14: Groundwater flow velocity in all four districts

4.4.3. Water residence Time in a Well

The residence time in a well is obtained using equation 1. The results obtained from water residence time shows that there is an inverse relationship between residence time and ^{222}Rn recovery. Hand pump wells with high residence time have low percentage of ^{222}Rn-recovery and low groundwater flow velocity. However, water wells with low water residence time show high percentage of ^{222}Rn recovery and groundwater flow velocity (Figure 4.15).

In the Mecha site, the water residence time in the well ranged between 8.5 hrs and one week in EME09 and EME13 respectively. Whereas, the average residence time in the Mecha site is 2.235 days. In the Ejere site, the water residence time in a well ranged between 1 hr

and 4.9 days in EEJ17 and EEJ20 respectively with an average of 1.47days across the site. The lowest residence time in a well (EEJ17) shows high ^{222}Rn recovery and groundwater flow velocity, while the highest residence time in a well (EEJ20) shows low ^{222}Rn recovery and low groundwater flow velocity. In the Sodo site, water residence time in a well ranged between 7hrs and 5.36days in ESD17 and ESD10 respectively. The average residence time in this site is 2.49 days. This shows the highest water residence time is associated to low groundwater flow velocity and ^{222}Rn recovery. However, low water residence time in a well is also associated to high groundwater flow velocity and high ^{222}Rn recovery. In the Abeshge site, water residence time in a well ranged between 1.73 minutes and 5.18 days in EAE02 and EAE01 respectively and the average water residence time in this site is 1.68 days. The results show similar trends with other study sites that show highest water residence time was observed in low groundwater flow velocity and high percentage of ^{222}Rn recovery and vice versa.

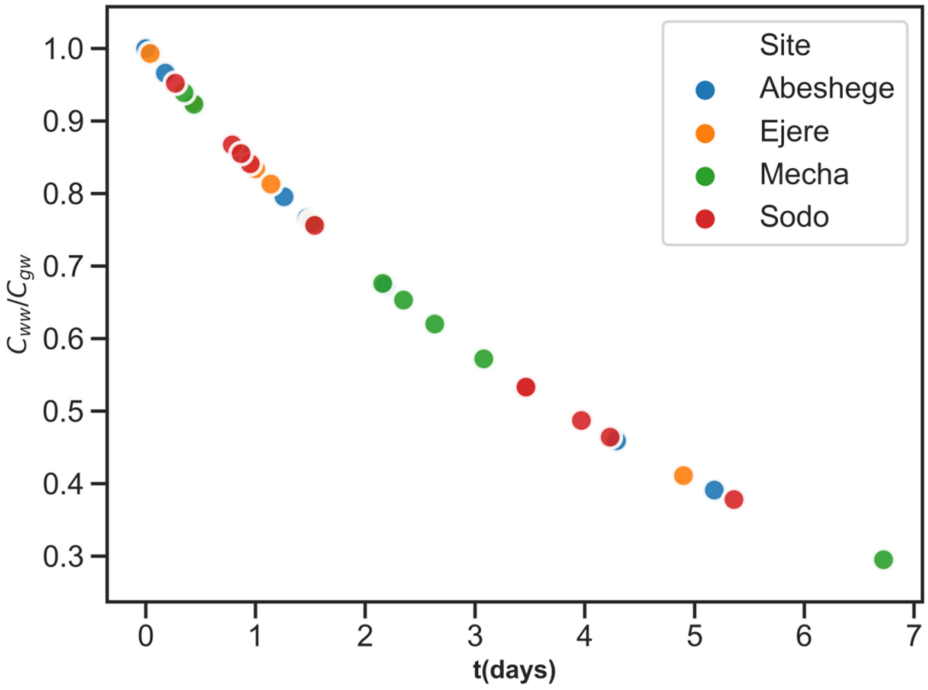

Figure 4.15 Residence time Vs Radon deficit of water wells

4.5. Discussion

4.5.1. ^{222}Rn concentration in shallow groundwaters

The ^{222}Rn technique in shallow hand pump wells has been used as a tracer to estimate groundwater flow velocity. In this study, the ^{222}Rn concentration in the water well (C_{ww}) and aquifer (C_{gw}) were measured in all sampling sites situated in four different basins (Abay, Awash, Ghibe and Ziway Lakes basin) of Ethiopian highland volcanic aquifers. The possible causes of high ^{222}Rn concentration in groundwater is associated with geological, hydrogeological factors such as rock types, host rock mineralogy, shear zones, degree of weathering, frequency of fractures, permeability of host rock, secondary porosity, emanation coefficient of the rock, location of lineaments and climatic factors (Cook et al., 2006; Lindsey & Ator, 1992; Przylibski & Zebrowski, 1999; Sukanya et al., 2021).

Based on the results obtained from the measured samples, in the Mecha site, the highest value of ^{222}Rn concentration in the Mecha Tebelo (EME15) hand pump well is associated to high stress of pumping for the Marawi Town water supply, mixing process and infiltration components of shallow circulation of groundwater system, rising water level (11.38m) that shows significant saturated thickness and high influence of infiltration capacity surrounding the well.

In the Ejere site, the maximum ^{222}Rn concentration in the Sede (EEJ02) hand pump well situated in the Bolango Kebele in the Becho plain of the Awash River basin. The possible cause of high ^{222}Rn concentration in this well is due to the thick alluvial deposits and weathering material, shallow circulation of groundwater and fast surface water infiltration from the alluvial fan of Awash River. In the Sodo site, the highest ^{222}Rn concentration was measured in the Gurambar (ESD01) situated in the Gogeti Kebele. The possible cause of the highest ^{222}Rn concentration in this area is due to the shallow static water level (10m) and variation of water level and shallow groundwater circulation in the top layer of the aquifer. In the Abeshge site, the maximum value of ^{222}Rn concentration was measured in the Hudad 04, Gote 08 (EAE02), longest serving (37 years) pumping well for the larger village community, situated in a topographically depressed area near the Kulit River and spring waters. The possible causes of high ^{222}Rn concentration are due to shallow static water

level (12m), thick weathered materials of saturated zone and high influence of infiltration capacity.

4.5.2. ^{222}Rn recovery and Groundwater Flow velocity in shallow groundwaters

Results obtained from Mecha site hand pump wells shows that the maximum ^{222}Rn recovery and groundwater velocity is in Mecha Chihona (EME09) public well which is associated with a high permeability aquifer surrounding the well and shallow water level (6.67m) circulation with high surface water infiltration from overlying layer facilitated groundwater flow rate. The lowest ^{222}Rn recovery and groundwater flow velocity in EME13 is associated with low permeability aquifer in the vicinity of the HPWs and high residence time of water.

In the Ejere site the highest ^{222}Rn recovery and groundwater velocity among the sampled wells was obtained in the Qarbo (EEJ17) in Damotu area, showing that the highest velocity value is associated with the hydraulic gradient and rugged topography of and the high permeability of the aquifer material in the vicinity of the well. The lowest ^{222}Rn recovery and groundwater flow velocity in EEJ20 is associated with the low permeability of the aquifer material such as massive volcanic formation of the basaltic formation and trachytic units.

In Sodo site, the maximum ^{222}Rn recovery and groundwater velocity is observed in Fule Amanuel (ESD17) hand pump well situated in the hilly mountainous area and the hilly terrain, is associated with the surface topography, hydraulic gradient of the well, surface water hydraulic networks, fractured aquifer formations and geological structures. The lowest ^{222}Rn recovery and groundwater flow velocity in ESD10 is due to low permeability of the welded ash and pyroclastic materials that formed the aquifer in the vicinity of the well.

In the Abeshge site, the highest ^{222}Rn recovery and groundwater velocity observed in the Hudad 4, Gote 8 (EAE02) is associated with the surface hydraulic network interconnection with groundwater and the geomorphologic features, geological structures manifestation, spring manifestation and shallow groundwater level and the hydraulic properties of the aquifer. The lowest ^{222}Rn recovery and groundwater flow velocity in EAE01 is associated

with low permeability of aquifer formation with high residence time in slightly weathered and less fractured volcanic layers.

4.6. Concluding Remark

Groundwater flow velocity in the shallow groundwater of four sites situated in four different basins Abay, Awash, Ziway Lake basin and Ghibe Basin was estimated using ^{222}Rn techniques. The ^{222}Rn was measured to obtain ^{222}Rn concentration in water well and aquifer which is used to estimate ^{222}Rn recovery. Based on the obtained result, the ^{222}Rn concentration ranged between 437 and 12,063 Bq/m^3 and 1480 to 22,184 Bq/m^3 in a well and an aquifer respectively. The highest ^{222}Rn concentration is in the Mecha Tebelo (EME15), while the lowest is in the Mecha Amarit (EME13). The highest ^{222}Rn concentration indicates that groundwater in this area is affected by shallow circulation, surface water infiltration, water level rising and the hydrostratigraphic effect of the basaltic aquifer and alluvial deposits. Groundwater flow velocity ranges from 3.52 to 69.1cm/day, where the highest value was recorded in the EAE02 and EEJ17 in the Awash and Ghibe basin. The possible reason for the highest groundwater velocity is associated to the hydraulic gradient, geological structures, lithostratigraphic formation and hydraulic conductivity of the aquifer. Whereas, the lowest groundwater flow velocity is due the low permeability and high residence time in a less fractured and weathered aquifer formation in the vicinity of the well. This study reported that the ^{222}Rn technique is applicable and can be an alternative method to investigate groundwater flow system, groundwater flow velocity in shallow volcanic aquifers.

Chapter Five

5. ^{222}Rn isotope as a tool for monitoring functionality of water wells

5.1. Introduction

Hand Pump Wells (HPWs) are used as the primary scheme of access to groundwater by rural communities in sub-Saharan Africa (JPM, 2019). More than 25% of rural water supply hand-pump wells in sub-Saharan Africa are non-functional within a few years or at any time after construction (Foster et al., 2020; RWSN, 2009). For instance over 33.3% of rural water services in Ethiopia are not functioning at any point in time (Gurmessa & Mekuriaw, 2019). The sustainability of water supply is a major challenge in the in rural areas of low and middle income countries where the infrastructures, operation and maintenance of HPWs remain problematic (Foster et al., 2018, 2020; Truslove et al., 2019). The premature failures of rural water supply services cause the major challenge to attain the sustainable development goal of save drinking water for all communities. Failures of HPWs may be associated with declining borehole yields, unreliability of pump performance due to poor borehole configurations and degradation of water quality (Banks et al., 2021; Cuthbert et al., 2019; MacAllister et al., 2020, 2022; Mkandawire et al., 2020; Truslove et al., 2019). Thus, the water point functionality analysis has a vital importance in the rural water supply management.

The reduction in functionality of HPWs is often caused by mechanical failures, reduced yield of the aquifer, degradation in groundwater quality and seasonality that controls groundwater level (Carter & Ross, 2016). Poorly functioning HPWs can act as the persistent reservoir of microbial contamination (Ferguson et al., 2011) and rapid transit of contaminated surface water (i.e. likely associated with damaged HPWs head works and poor construction) into the boreholes (Banks et al., 2021). The causes of poor functionality are classified into primary causes (e.g. mechanical failures, reduced yield, poor water quality); secondary causes (e.g. geology, poor siting, lack of spare parts, basic maintenance, local governance arrangements); the underlying conditions (e.g. the institutional, financial and social factors) and long term trends (e.g. changes in demand for water, evolution of

governance arrangements, reduction in regional groundwater availability, climate change, deterioration of water quality) (Bonsor et al., 2015).

Information on the periodic decline in functionality of HPWs can be used to plan preventive maintenance. However, the regular post-construction inspections of HPWs functionality are challenging due to the lack of skilled professionals and financial constraints (inspection, maintenance and construction costs). A few innovative methods have been designed to monitor water production in HPWs. One such example is the use of installed accelerometers (Manandhar et al., 2020) to measure water production in HPWs (Loukatos et al., 2023; Swan et al., 2018; Thomson et al., 2012) With such devices periodic change in water production can be measured. However such methods do not provide information about the casual mechanism behind the decline in water production. Pumping test is the other method to monitor the changes in yields of HPWs (Kruseman & De Ridder, 1983; Rorabaugh, 1953; Theis, 1935). Pumping test methods are logistically intensive as it requires dismantling of the HPW fittings and a number of other logistics (pumps, water level recorder, skilled technicians etc). Dismantling HPWs can be susceptible to the sudden breaking up of the pump components which can be either repaired or replaced by other new components.

Methods that systematically test the post-construction HPWs functionality over time are lacking. Thus, there is a clear need to develop technique to monitor of the post construction changes in HPWs performance. This work aims to demonstrate the capability of the ^{222}Rn isotopic tracer as a tool to monitor the post construction performance of HPWs. The isotope has been previously employed to determine groundwater flow velocity around water wells and to estimate water residence in water wells (Cook et al., 1999; Andreas Englert, 2003; Hamada, 2000; Schubert et al., 2011). Theoretically a well performing HPW is characterized by readily flowing water into and out of the well. A poorly performing well is one in which water flow through the well is slowed because of stagnation within the well or because of low permeability of the aquifer hosing the well. The difference in flow velocities within the well must be reflected in the water residence time in HPWs. ^{222}Rn is an ideal tracer of water residence time. We aim primarily to demonstrate the capability of the ^{222}Rn method by investigating the correlation between ^{222}Rn recovery and performance of

HPWs. We further aim to demonstrate the relation between ^{222}Rn recovery and corresponding groundwater flow velocity and pumping test derived hydraulic properties (hydraulic conductivity, transmissivity, and specific capacity). The advantage of the ^{222}Rn method is that ^{222}Rn is naturally occurring (gaseous isotope with a half-life of 3.824 days existing in all types of groundwaters at variable concentration. It is easy to measure using a hand held device). Therefore, the objective of the current work is to investigate the correlation between ^{222}Rn recovery and pumping test derived borehole performance. A high correlation between the two means one can use the easy-to-measure ^{222}Rn as a proxy for monitoring HPWs performance over a period of time.

5.2. Description of Study area

The study was conducted in the shallow volcanic aquifers of Ethiopian highlands in four selected sites (Mecha, Ejere, Sodo and Abeshege) (Figure 1). The geology of these study sites are characterized by volcanic formations comprising basaltic, trachytic, rhyolitic, welded and unwelded pyroclastic deposits (Abbate et al., 2015; Abebe et al., 1998; Ayalew et al., 2002; Beccaluva et al., 2009; Berhe et al., 1987; Kieffer et al., 2004; Lebas & Mohr, 1970; Macdougall, 1988; Mohr, 1967; Mohr & Zanettin, 1988; Mohr, 1983; Peccerillo et al., 2007; Pik et al., 1998; Woldegabriel et al., 1990). These volcanic formations are characterized by a series of various eruption phases, varying degrees of fracturing and weathering intensity, the effects of local and regional geological structures and geomorphological controls. The unconsolidated materials like alluvial and lacustrine deposits covered the flat plains and along the rivers Banks. The hydrogeology of study sites shows good productivity in fractured and weathered basaltic aquifers and inter-granular alluvial aquifers (Kebede et al., 2005, 2017; Mamo, 2015; Nigate et al., 2020; Walker et al., 2019a). Whereas, the ignimbrite, trachyte and welded pyroclastic flows show low productivity localized aquifers (Ayenew et al., 2008b; Azagegn et al., 2015; Berehanu et al., 2017; Demlie et al., 2008; Kebede et al., 2008; Yitbarek et al., 2012).

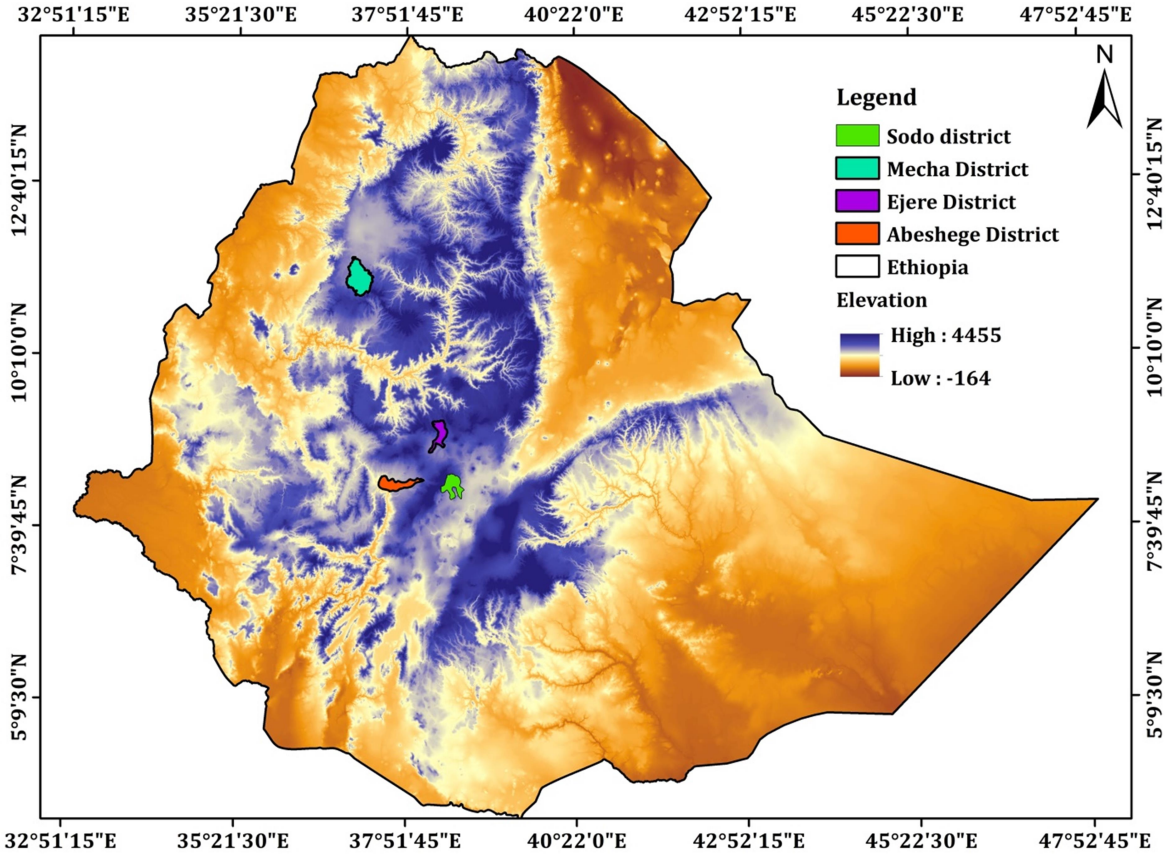

Figure 5.1: Location maps of the four study sites and elevation map of Ethiopia

5.3. Methods

5.3.1. ^{222}Rn recovery and groundwater flow velocity in and around wells

The source of ^{222}Rn in groundwater is the decay of ^{226}Ra that occurs in the aquifer matrix. ^{222}Rn has a half-life of 3.82 days with the decay constant (λ) = 2.43x$\mathbf{10^{-11}}$ $\boldsymbol{day^{-1}}$. When groundwater enters into water well, the ^{222}Rn production stops due to the decay is no longer balanced by ^{222}Rn production because of a lack of contact with the aquifer matrix and degassing which results in a fast decrease in ^{222}Rn concentration. The method assumes that if the flow rate through the well is very low, then the residence time of water in the well will be longer and most of its ^{222}Rn will have decayed leading to a decreased ^{222}Rn recovery. Significant ^{222}Rn concentration in the water well can only present if there is fast flow into and out of the well to replenish the ^{222}Rn faster than it decays leading to quick radon recovery.

The mathematical approach assumes the flow of groundwater takes place in the form of convergence streamline towards the well from the immediate surroundings (fig.2a). The decrease of initial ^{222}Rn equilibrium concentration in the groundwater (natural Rn background $\mathbf{C_{gw}^{\infty}}$) is because of the absence of ^{222}Rn production as quantified in equation (1).

$$\mathbf{C_{ww}^{t} = C_{gw}^{\infty} e^{(\lambda t)}} \qquad (\mathbf{1})$$

Where $\mathbf{C_{ww}^{t}}$ is ^{222}Rn concentration measured before purging the stagnant water from the water well and $\mathbf{C_{gw}^{\infty}}$ is ^{222}Rn concentration representative of the aquifer background, t is water residence time in a well and λ =2.43x$\mathbf{10^{-11}}$ $\boldsymbol{day^{-1}}$. The residence time of water depends on the radius (r) of the well and radon recovery ($\boldsymbol{C_{ww}/C_{gw}}$) in the cross-sectional area A of the well sub-divided into sub-areas (dA), with u being a circumference of the well and du infinitesimally small segment of it (Hamada, 2000) (fig.2b). The mathematical assumption considers the different hydraulic conditions in the aquifer and the water well (filter screen and filter pack) as observed in fig.2c, an empirical relationship between inflow width and well radius, applying horizontal convergence factors (α) based on hydraulic conductivity and radius ($\boldsymbol{k_1, k_2, k_3, r_1, r_2}$ ***and*** $\boldsymbol{r_3}$), flow velocity in the aquifer ($\boldsymbol{V_{gw}}$) and flow velocity in the well ($\mathbf{V_{ww}}$) (Drost et al., 1968).

The horizontal cross-section of water wells in the current study area is considered as all HPWs contain filter screens and filter packs. The radius of the filter screen (r_1), filter pack (r_2) and aquifer (r_3) are measured as 2.5cm, 3.0cm and 7.62cm respectively. Moreover, the horizontal hydraulic conductivities of the filter screen ($\boldsymbol{k_1}$) and filter pack ($\boldsymbol{k_2}$) are in the order magnitude of 10^{-5} and 10^{-4}m/s respectively. However, the hydraulic conductivity of the aquifers ($\boldsymbol{k_3}$) is considered as constant from based on the standard of geologic materials for fractured volcanic aquifers including unconsolidated materials (Heath, 1983). The horizontal convergence factor (α) is determined by using equation (2). An empirical value ($\mathscr{E}$) was computed by non-linear integral equation (3) solved by numerical solution in genetic algorithm computed by MATLAB software. The radon recovery ($\frac{\mathbf{C_{ww}^{t}}}{\mathbf{C_{gw}^{\infty}}}$) in equation (3) is a measured value obtained from ^{222}Rn sampling. Then the flow velocity in the well ($\boldsymbol{V_{ww}}$) was computed from r, λ and $\mathscr{E}$ using equation (4). The $\boldsymbol{V_{ww}}$ and α were used based

on equation (5) to compute groundwater flow velocity (V_{gw}) around wells (Cook et al., 1999, 2003; Hamada, 2000; Schubert et al., 2011).

$$\alpha = \frac{8}{\left(1+\frac{k_3}{k_2}\right)+\left\{1+\left(\frac{r_1}{r_2}\right)^2+\left[\frac{k_2}{k_1}\left(1-\frac{r_1}{r_2}\right)^2\right]\right\}+\left(1-\frac{k_3}{k_2}\right)\left\{\left(\frac{r_1}{r_3}\right)^2+\left(\frac{r_2}{r_3}\right)^2+\frac{k_2}{k_1}\left[\left(\frac{r_1}{r_3}\right)^2-\left(\frac{r_2}{r_3}\right)^2\right]\right\}} \quad (2)$$

$$\frac{C_{ww}^{t}}{C_{gw}^{\infty}} = \frac{1}{\pi}\int_{-\pi/2}^{\pi/2}\frac{1}{\epsilon}\left(1-e^{-2\varepsilon cos\theta}\right)cos\theta d\theta \quad (3)$$

$$\varepsilon = \lambda r / V_{ww} \quad (4)$$

$$V_{gw} = \frac{V_{ww}}{\alpha} \quad (5)$$

Where, V_{gw} is groundwater flow velocity in the vicinity of the well and aquifer obtained from flow velocity in the water well (V_{ww}) and the horizontal convergence factor (α).

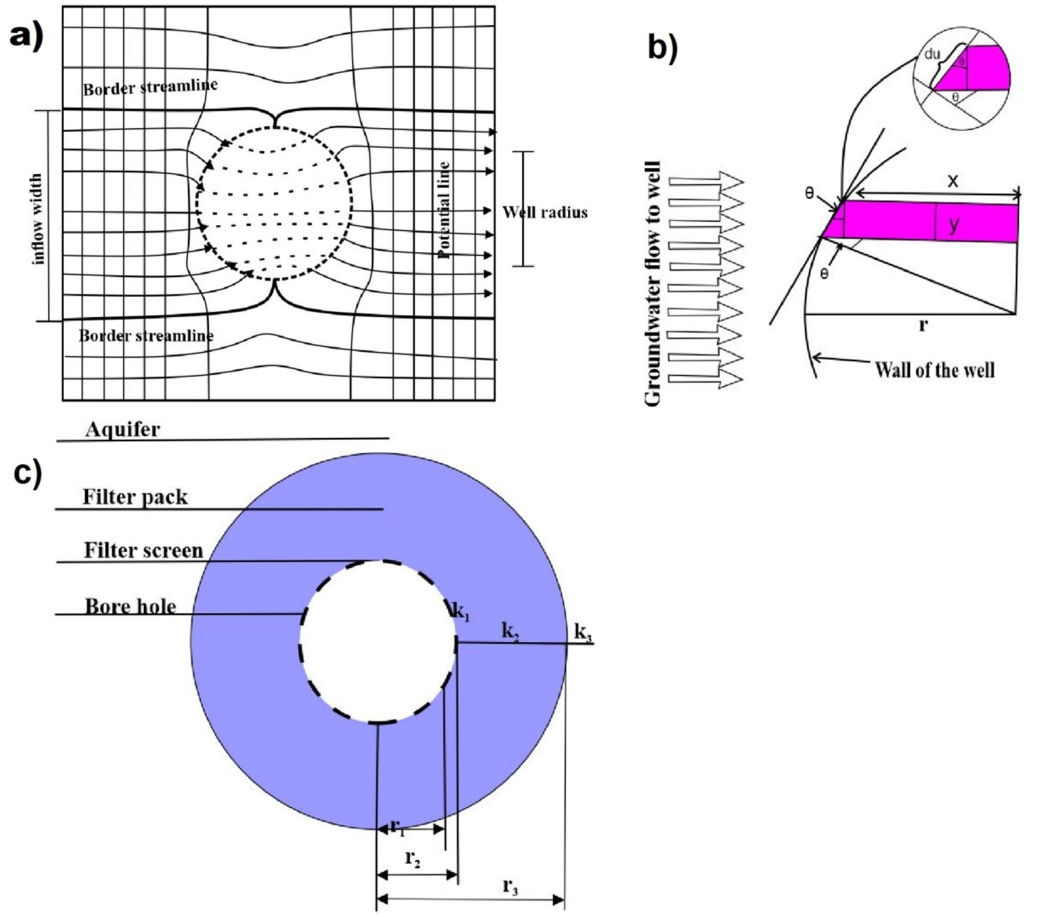

Figure 5.2: a) schematic diagram of the horizontal flow pattern showing the top view within and around a well central dotted line (modified after (Andreas Englert, 2003)). b) Schematic sketch of sub-area (dashed red) of the sectional area of the well with length $2x = 2rcos\theta$ and with $y = rcos\theta d$ (Modified after Hamada (2000)). c) schematic diagram of the horizontal cross-section of a screened well with filter pack (modified after (Drost et al., 1968)).

5.3.2. Defining HPWs functionality Classes

The physical factors contributing to the borehole functionality have been previously reported by (MacAllister, et al., 2022) in the current ^{222}Rn surveyed HPWs. The HPWs functionality categorization was conducted based on three main criteria: a) visual observation of whether the water points are physically working or not, b) yield estimation through a thirty minutes steady stroke test, c) reliability determination estimated from a survey of the frequency breakdowns and length of downtimes of the HPWs over the period of one year (Bonsor et al., 2018; Carter & Ross, 2016). Therefore, based on such criteria HPWs were classified into six functionality categories a) fully functioning (FF), b) unreliable (UR), c) low-yielding (LY) and d) unreliable and low-yielding (UR&LY) e) non-functional (NF) and f) abandoned (AB) HPWs. However, the last two categories (non-functional and abandoned HPWs) are excluded from the current work as they were not amenable for ^{222}Rn sampling. We then investigated the correlation between the ^{222}Rn recovery and the four functionality classes identified by (MacAllister, et al., 2022). These four functionality categories are: a) FF HPWs are defined as physically working, providing sufficient water (10 L/minute) and < 30 days downtime in the year of the survey, b) UR HPWs are defined as physically working, providing sufficient water (10 L/minute) and >30 days downtime in the year of the survey, c) LY HPWs are defined as physically working, providing insufficient water (10 L/minute) and < 30 days downtime in the year of the survey and d) UR&LY HPWs are defined as physically working, providing insufficient water (10 L/minute) and >30 days downtime in the year of the survey.

5.3.4. ^{222}Rn measurement

The ^{222}Rn sampling was conducted on the same boreholes on which pumping test data had been collected. The ^{222}Rn measurement was conducted in 33 of the HPWs. In situ ^{222}Rn was measured for the concentration of ^{222}Rn in a well ($\boldsymbol{C_{ww}}$) and aquifer ($\boldsymbol{C_{gw}}$) in April/2021.

The ^{222}Rn concentration from the water in the well was measured after at least 24 hours of stoppage of pumping. This first water that comes out of the water well at the start of pumping following 24 hours stoppage is considered to represent ^{222}Rn in the water well ($\boldsymbol{C_{ww}}$). Subsequently, the aquifer representative ^{222}Rn concentration representing the groundwater (Cgw) was sampled after running the pumps for at least two hours. A RAD7 (Durrige Company Inc., 2020) radon detector was fitted to a big bottle system to measure the ^{222}Rn. Counting is based on the principle of liquid-gas-membrane extraction (Schmidt et al., 2008). The temperature-adjusted counting was recorded using the sniff technique which was conducted for a period of 2hrs in four cycles for each water point. Four readings were recorded and an average of the last two or three measurements was taken to represent the concentration of a specific grab sample. The ^{222}Rn data was then used to estimate ^{222}Rn recovery, groundwater flow velocity and water residence time in HPWs.

5.3.5. Pumping Test Data analysis

The pumping test data analysis was conducted on the 33 shallow HPWs to compute hydraulic parameters like transmissivity (T), hydraulic conductivity (K) and specific capacity (Sc). The minimum and maximum depths of the boreholes are 18.6 and 84.3m respectively. The pumping test data analysis was carried out using AquiferTest Pro 10 software using a constant discharge rate and recovery test methods. The time against drawdown data was plotted on the log-log scale in the Neuman's type curve superimposed on the type curve until the data points matched. The corrected Theis method replaces (r, t) with s'(r, t) where s' is equal to $\boldsymbol{s} - (\boldsymbol{s^2}/\boldsymbol{2D_0})$ and D_0 is the initial saturated thickness of the unconfined aquifer (Neuman, 1975). The Theis Model (Theis, 1935) considers the radial flow presented in the following equations (6).

$$\mathbf{S(r,t)} = \frac{\mathbf{Q}}{\mathbf{4\pi T}}\mathbf{W(u)} \qquad (\mathbf{6})$$

$$\mathbf{u} = \frac{\mathbf{r^2 S}}{\mathbf{4Tt}} \qquad (\mathbf{7})$$

Where, s(r, t) is the drawdown at the radial distance r from the well at time t after pumping commenced, $\boldsymbol{u} = \frac{\boldsymbol{r^2 S}}{\boldsymbol{4Tt}}$ is the dimensionless quantity that varies with the r distance from an

observation well at time t, T is the transmissivity (m^2/day) and Q denotes the discharge rate (m^3/day), and S is the storativity (dimensionless) and W(u) is the dimensionless exponential integral known as well function which can be approximated as equation (8):

$$\boldsymbol{W(u) = \int_{u}^{\infty} \frac{e^{-y}}{y} dy = -\gamma - ln^{u} + u - \frac{u^2}{2.2!} + \frac{u^3}{3.3!} - \frac{u^4}{4.4!} + \cdots} \quad (\mathbf{8})$$

The Theis curve matching technique determines well function W (u) and 1/u. The T, S and k were obtained from the time-drawdown curve fitting for both linear and log-log plots to obtain the hydraulic parameters using the following equations (9 and 10).

$$\mathbf{T = \frac{2.3Q}{2\pi\Delta s}} \quad (\mathbf{9})$$

$$\mathbf{S = \frac{2.25Tt_0}{r^2}} \quad (\mathbf{10})$$

The behaviour and productivity of the water well were determined using the specific capacity as the discharge ratio per unit drawdown expressed as (L/min)/m (Fitts, 2013) in equation (11).

$$\mathbf{Sc = \frac{Q}{S_w}} \quad (\mathbf{11})$$

5.4. Results

5.4.1. The ^{222}Rn recovery, residence time and groundwater flow velocity of HPWs

The ^{222}Rn concentrations (C_{ww} and C_{gw}), resident time, flow velocity in a well (V_{ww}) and groundwater flow velocity (V_{gw}) of HPWs were presented in Table 1. The C_{ww} ranged between 1,400 and 14,964 Bq/m^3, while the C_{gw} varied between 1,760 and 21,296 Bq/m^3. The ^{222}Rn recovery of HPWs ranged between 38% and 99%. The ^{222}Rn recovery showed a strong correlation with the water well performance classes. A higher ^{222}Rn recovery (>67%) has been obtained in the FF HPWs as compared to UR, LY and UR&LY HPWs (Figure 3a) which showed a recovery of less than 67%. The ^{222}Rn recovery showed distinct features in the five FF HPWs ranging above 90%. The UR HPWs showed both higher and lower ranges of ^{222}Rn recovery as compared to all other functionality classes. The LY HPWs ranged between 62% and 65% ^{222}Rn recovery. The UR&LY HPWs showed low ^{222}Rn

varying between 38% and 49% in five HPWs. The UR&LY showed the lowest value of ^{222}Rn recovery among all other HPWs (Figure 3a).

The V_{ww} showed values ranging between 0.95 and 138 cm/day. The V_{gw} varied between 0.37 and 64.19 cm/day. A good relation between V_{gw} and functionality classes has also been observed (Figure 3b). The FF HPWs showed the higher values of V_{gw}, while low values of V_{gw} were observed in UR&LY HPWs. The V_{gw} showed distinct features of higher outliers in FF HPWs ranging above 64 cm/day. The UR HPWs also showed higher range of V_{gw} as compared to LY and UR&LY HPWs. While the lowest value of V_{gw} was observed in UR HPWs ranging below 1cm/day. The LY HPWs showed low values of V_{gw} ranging between 0.96 and 1.1 cm/day. In UR&LY HPWs, all values of V_{gw} were observed below 1cm/day ranging below 0.37 cm/day.

The water residence time in the well ranged from 8.5 hours to one week. Similar relations have also been observed in the functionality categories where the FF HPWs showed the lowest residence time as compared to all functionality classes. The highest residence time was observed in the UR&LY HPWs. The UR HPWs also showed the highest value of residence time ranging above 3 days. The water residence time shows an inverse relationship with ^{222}Rn recovery and V_{gw}. The highest ^{222}Rn recovery and V_{gw} were correlated to the lowest residence time. An increasing residence time in a well exhibits a decreasing ^{222}Rn production.

Table 5.1: Radon concentrations (C_{ww} and C_{gw}), Radon Deficit and groundwater velocities in water wells and aquifers, the water residence time in the well and functionality of HPWs.

Sample ID	Functionality	BH Depth(m)	C_{ww} (Bq/m^3)	C_{gw} (Bq/m^3)	C_{ww}/ C_{gw}	V_{ww} (Cm/day)	V_{gw} (cm/day)	t(days)
EAE01	LY&UR	70.3	5470±522	13027±835	0.39	9.88E-01	0.4595349	5.181
EAE02	FF	44.9	14964±953	14968±961	0.99	1.38E+02	64.186047	0.0012
EAE04	UR	60.8	8430±650	11573±751	0.76	4.19E+00	1.9488372	1.47
EME07	LY	61.3	2800±368	4160±461	0.65	2.47E+00	1.0786026	2.35
EAE10	FF	84.3	2970±391	3510±421	0.84	6.91E+00	3.2139535	0.921
EAE11	LY&UR	51.5	3920±446	8540±674	0.46	1.26E+00	0.5860465	4.29
EAE12	FF	76.7	7940±627	9330±679	0.85	6.91E+00	3.2139535	0.89

EAE13	UR	73.7	1920±322	2080±332	0.92	1.38E+01	6.4186047	0.44
EAE14	FF	76.9	1400±277	1760±308	0.79	5.02E+00	2.3348837	1.261
EEJ02	FF	49.5	13992±902	21007±102	0.76	4.07E+00	1.8333333	1.5
EEJ06	FF	62.7	13514±874	14954±943	0.83	6.01E+00	2.7072072	1.0033
EEJ09	UR	35.6	12549±825	13988±898	0.81	5.32E+00	2.3963964	1.142
EEJ10	FF	46.9	2860±384	3090±397	0.93	1.54E+01	6.9369369	0.43
EEJ17	FF	47.4	9930±700	11093±720	0.99	1.38E+02	62.162162	0.0415
EEJ20	LY&UR	53.4	4940±497	12064±792	0.41	1.06E+00	0.4774775	4.9
EME01	FF	21.8	8320±644	11573±739	0.76	4.07E+00	1.7772926	1.52
EME02	FF	26	12062±783	12543±807	0.92	1.38E+01	6.0262009	0.44
EME05	UR	49	4110±458	6080±552	0.68	2.82E+00	1.231441	2.16
EAE07	FF	43.5	3010±301	4610±481	0.67	2.71E+00	1.2604651	2.182
EME09	FF	51.4	4310±474	4590±483	0.94	1.98E+01	8.6462882	0.35
EME12	LY	42.5	4570±480	7370±603	0.62	2.19E+00	0.9563319	2.634
EME15	UR	50.3	12063±86	21296±101	0.57	1.84E+00	0.922	3.081
EME18	FF	55.4	6420±568	7500±610	0.86	7.68E+00	3.3537118	0.86
ESD01	FF	25.3	12541±797	13509±856	0.87	8.13E+00	3.1757813	0.79
ESD04	LY&UR	68.6	1520±285	2850±381	0.53	1.61E+00	0.6289063	3.465
ESD08	UR	62	2750±377	5160±508	0.53	1.61	6.30E-01	3.47
ESD09	LY&UR	35.7	3220±405	6940±586	0.46	1.26E+00	0.4921875	4.232
ESD10	LY&UR	51.5	3150±212	8330±640	0.38	9.53E-01	0.3722656	5.36
ESD11	UR	42.9	2330±352	2770±381	0.84	6.58E+00	2.5703125	0.953
ESD13	LY&UR	18.6	1850±313	3800±483	0.49	1.40E+00	0.546875	3.97
ESD16	UR	43.5	7900±625	6000±546	0.76	4.07E+00	1.5898438	1.54
ESD17	FF	47	6750±598	7090±613	0.95	2.30E+01	8.984375	0.271
ESD20	UR	75	2350±350	2750±379	0.86	6.91E+00	2.6992188	0.87

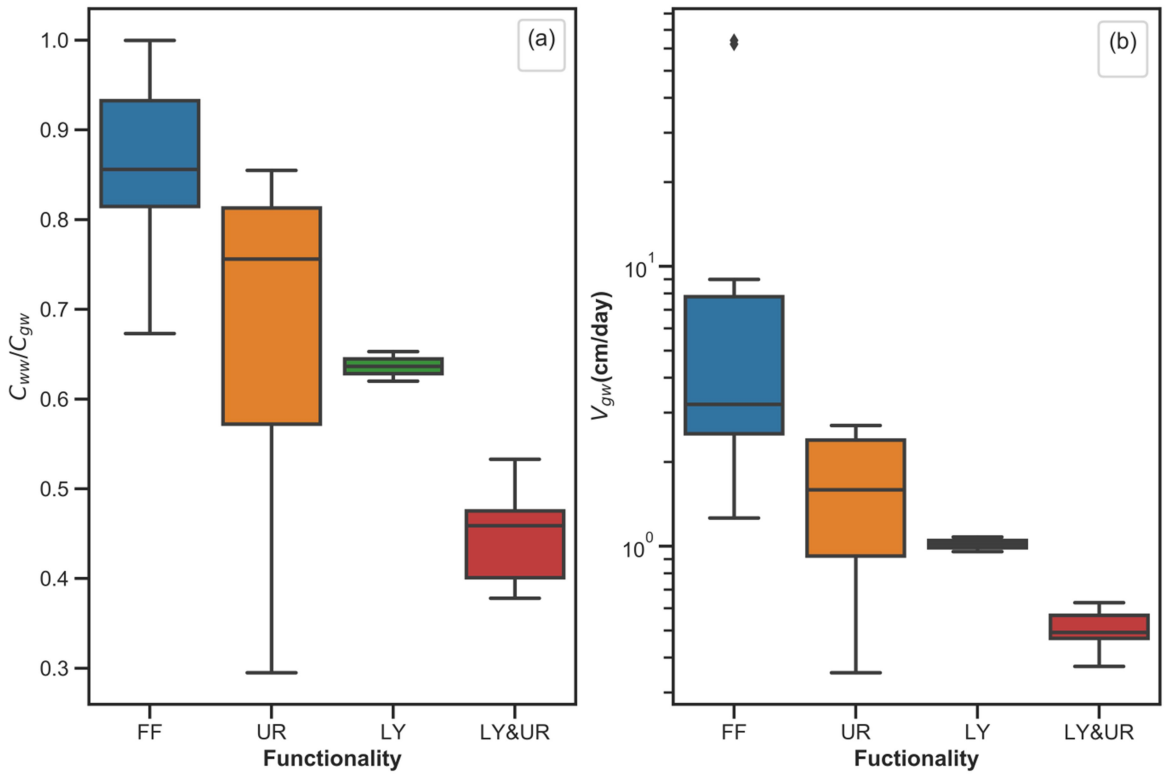

Figure 5.3: Box and Whisker plot of ^{222}Rn recovery and V_{gw} show low range in low yield (LY) and unreliable and low yield (LY&UR) and a higher range in fully functional wells (FF) and unreliable (UR) functionality categories: a) Functionality against radon recovery plot b) Functionality against V_{gw} plot.

5.4.2. Hydraulic parameters

The pumping test data analysis showed the T, K and Sc ranged from 9.50E-02 to 5.33E+03 m^2/day, 0.007 to 283.39 m/day and 0.099 to 1,190.48 (L/min)/m respectively (table 2). The aquifer properties also showed a similar trend with ^{222}Rn recovery and V_{gw} in all functionality categories. The aquifer hydraulic properties are related to the functionality of HPWs. The FF HPWs showed higher ranges of T, K and Sc as compared to other functionality categories (Figure 4). FF HPWs exhibit good performance, reliability and higher aquifer yield in the vicinity of the borehole. Some FF HPWs exceptionally showed higher outliers indicating distinct features of high aquifer permeability and full functionality.

The UR HPWs showed higher ranges of T and K values as compared to Sc. The low values of S_c in UR HPWs show distinct features exhibiting the problems associated with water wells properties than the aquifer property. Whereas, the high values of T and K reveal the properties of the aquifer. The LY HPWs showed lower values of T and K than S_c exhibiting the properties associated with the aquifer setting than water well property. The UR&LY HPWs showed a low range of all aquifer parameters (T, K and Sc) which are associated with the properties of the aquifer and water well, showing all effects of declining yield, unreliability and poor water well performance.

Table 5.2: Water wells hydraulic parameters

Sample ID	Functionality	BH Depth(m)	k(m/day)	T(m2/day)	Sc (L/minute)/m))
EAE01	LY&UR	70.3	4.99E-01	2.45E+01	0.87
EAE02	FF	44.86	9.94E-01	3.21E+01	1.896
EAE04	UR	60.78	6.07E-01	7.05E+00	6.59
EME07	LY	61.34	2.06E-01	7.35E+00	26.66
EAE10	FF	84.3	5.08E+00	1.12E+02	42.6
EAE11	LY&UR	51.45	1.55E-02	6.24E-01	0.94
EAE12	FF	76.7	1.75E-02	9.33E-01	1.41
EAE13	UR	73.66	7.00E-03	9.50E-02	0.325
EAE14	FF	76.88	283.392	5.33E+03	845.547
EEJ02	FF	49.5	1.74E+00	7.18E+01	38.59
EEJ06	FF	62.66	6.60E-02	3.84E+00	5.43
EEJ09	UR	35.6	4.51E-01	1.34E+01	11.48
EEJ10	FF	46.88	1.21E+01	4.81E+02	265.49
EEJ17	FF	47.35	1.01E+00	1.81E+01	21.57
EEJ20	LY&UR	53.39	4.39E-02	1.17E+00	1.72
EME01	FF	21.75	2.14E-02	8.35E-01	777
EME02	FF	26	4.42E+01	1.19E+03	1190.48
EME05	UR	49	1.41E+02	1.61E+03	8.4
EAE07	FF	43.5	2.01E+01	3.88E+02	534.19
EME09	FF	51.4	3.35E+00	1.50E+02	71.35
EME12	LY	42.5	1.63E-01	6.37E+00	25.58
EME15	UR	50.3	4.67E+01	2.67E+02	1.96

EME18	FF	55.4	5.07E-01	2.35E+01	25.21
ESD01	FF	25.3	9.33E+00	1.39E+02	55.83
ESD04	LY&UR	68.6	4.46E-02	9.07E-01	1.52
ESD08	UR	62	1.90E-01	4.04E+00	2.19
ESD09	LY&UR	35.71	1.59E+00	3.60E+01	20.24
ESD10	LY&UR	51.5	4.41E-02	1.22E+00	1.68
ESD11	UR	42.94	2.76E+00	6.23E+01	30.91
ESD13	LY&UR	18.6	1.02E+00	3.65E+00	17.36
ESD16	UR	43.5	1.22E-01	2.58E+00	2.46
ESD17	FF	47	6.71E+00	5.98E+01	45.02
ESD20	UR	75	5.05E-02	1.72E+00	2.49

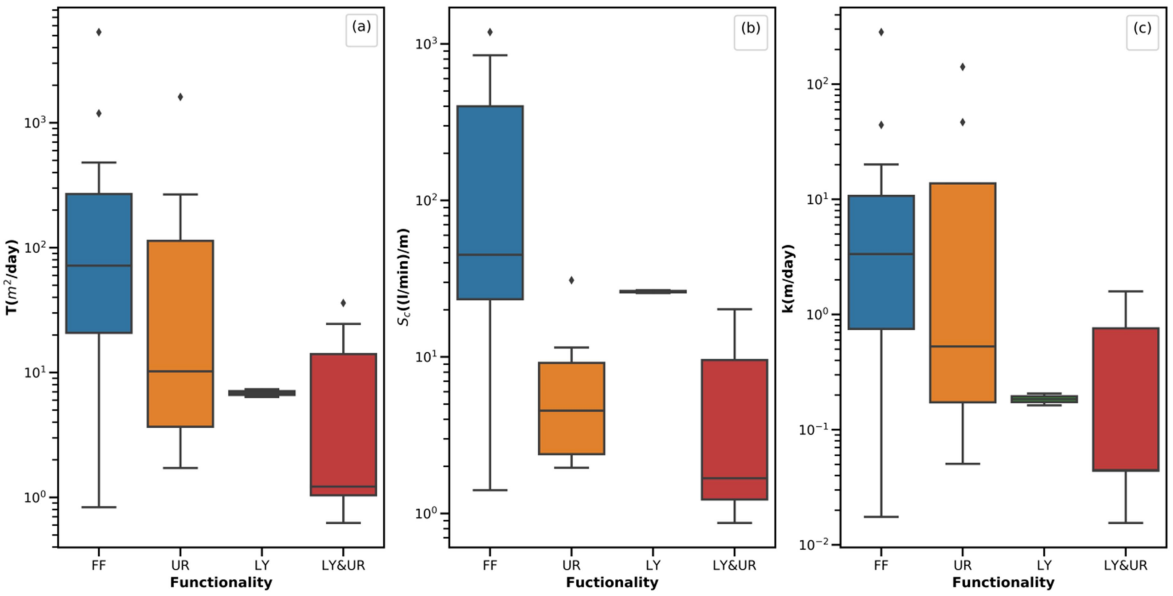

Figure 5.4: Box and Whisker plot of hydraulic parameters of fully functional (FF), unreliable (UR), low-yielding (LY) and unreliable and low yielding (LY&UR) HPWs: a) Functionality against transmissivity, b) Functionality against specific capacity plot and c) Functionality against hydraulic conductivity plot.

5.5. Discussion

5.5.1. The ^{222}Rn isotope as a tool for HPWs functionality monitoring

Understanding the causes for the failures and poor performance of HPWs during post-construction are the key factors to be understood by the water managers. The ^{222}Rn isotope

was efficiently applied as a tool in HPWs' functionality monitoring. The ^{222}Rn recovery and V_{gw} showed distinct trends in different functionality categories. Using this technique helps to provide supplementary information to monitor HPWs' functionality. Previously investigated HPWs functionality monitoring was conducted by the Hidden Crises project and assessment of physical factors contributed to HPWs functionality (MacAllister, 2022) by dismantling the pumps from water wells.

The FF HPWs show high ^{222}Rn recovery, indicating a quick through flow of ^{222}Rn from the aquifer into the borehole and high groundwater flow conditions in the vicinity of the borehole. The inflow and outflow of ^{222}Rn leave the water well quickly. The higher ^{222}Rn recovery shows there is not enough time for stagnation due to too high velocity to capture it. The high values of ^{222}Rn recovery in FF also show the healthy functioning and good performance (high reliability and yield) of HPWs. The low ^{222}Rn recovery in partially functional (UR, LY, UR&LY) HPWs is due to either a high stagnation, declining yield, clogging of the water well screen, poor initial design and construction and problems of pump components. Thus, the ^{222}Rn recovery can be used to monitor the HPWs yield performance and identify functionality categories during post-water well construction. Furthermore, this can be further applied to develop the ^{222}Rn technique as a proxy in HPWs functionality monitoring.

5.5.2. The ^{222}Rn technique for ground water flow velocity estimation in volcanic aquifers

The use of the ^{222}Rn technique to estimate V_{gw} has a vital importance due to its natural occurrence in groundwater, applicable in a single well method, less costly, easy to measure and quick on-site availability of the result. The ^{222}Rn technique was used to estimate V_{gw} in a single well screened for the entire length that reported low V_{gw} ranged from 10^{-5} to 10^{-6}cm/s (Hamada, 2000). The V_{gw} estimation in volcanic aquifers of the current study is similar to the high V_{gw} estimated by Schubert et al. (2011) assuming the horizontal convergence factor (α) streamlines towards the well. The ^{222}Rn method was not previously applied in this volcanic terrain for the purpose of V_{gw} estimation and functionality monitoring.

In the current work, the ^{222}Rn technique has been successfully applied to estimate V_{gw} in the Ethiopian volcanic terrain. The estimation of V_{gw} in volcanic terrain has significant importance in monitoring the HPWs functionality. The results of V_{gw} obtained from ^{222}Rn technique in rural water supply HPWs showed good agreement with the previous functionality assessment conducted by MacAllister et al. (2022). It indicated that high values of V_{gw} are correlated with FF HPWs showing good performance and reliability of healthy functioning and high permeability of the aquifer in the vicinity of the well. Whereas, the low V_{gw} in the UR&LY HPWs are related to the screen clogging effects, poor initial design and construction and problems of pump components and low yielding and permeability associated with the aquifers conditions. Some uncertainty might arise in the ^{222}Rn technique due to the effect of poor sampling and water well purging during sample collection that causes the mixing of ^{222}Rn concentration of water well and an aquifer. The proper sampling, quantification of ^{222}Rn recovery and estimating the horizontal convergence factor (α) are the major pre-conditions to be fulfilled for high V_{gw} estimation in volcanic terrains. Furthermore, the estimation of V_{gw} from quantified ^{222}Rn measurements needs detailed mathematical analysis as this can be difficult for inexperienced professionals.

5.5.3. Correlation between ^{222}Rn recovery and groundwater flow velocity with hydraulic properties

The ^{222}Rn-derived data were correlated with hydraulic properties obtained from pumping test data analysis (Figure 5) to validate the applicability of the ^{222}Rn technique. The ^{222}Rn recovery shows a positive correlation with T, K and Sc. However, the S_c shows a good correlation with ^{222}Rn recovery as compared to T and K, indicating that the S_c is characterized by the function of aquifer setting, properties of the water wells (well radius, degree of penetration and well loss) and pumping durations. The V_{gw} showed a weak negative correlation with T, K and S_c. The residence time showed a strong negative correlation with ^{222}Rn recovery, V_{gw} and S_c, while the residence time showed a weak negative correlation with K and T. The correlation between ^{222}Rn recovery and V_{gw} with hydraulic properties obtained from pumping test data analysis indicates that the ^{222}Rn

technique can be successfully applied as a supplementary or independently used in the HPWs functionality monitoring.

In the FF HPWs, both ^{222}Rn recovery and V_{gw} show a weak correlation with T and S_c due to the fast flow system with insufficient time to capture the difference between the ^{222}Rn recovery in an aquifer and water well (Figure 6a to d). In the UR, LY and UR&LY HPWs, the ^{222}Rn recovery is slightly correlated with T, while it shows a good correlation with Sc (Figure 6a and b). Similarly, the V_{gw} shows a weak correlation with T as compared to with Sc in such HPWs (Figure 6c and d). This reveals that there are problems associated with HPWs' performance and unreliability (poor initial design, clogging effects and increased drawdown created due to pumping) than the aquifer properties in UR, LY, and UR&LY HPWs.

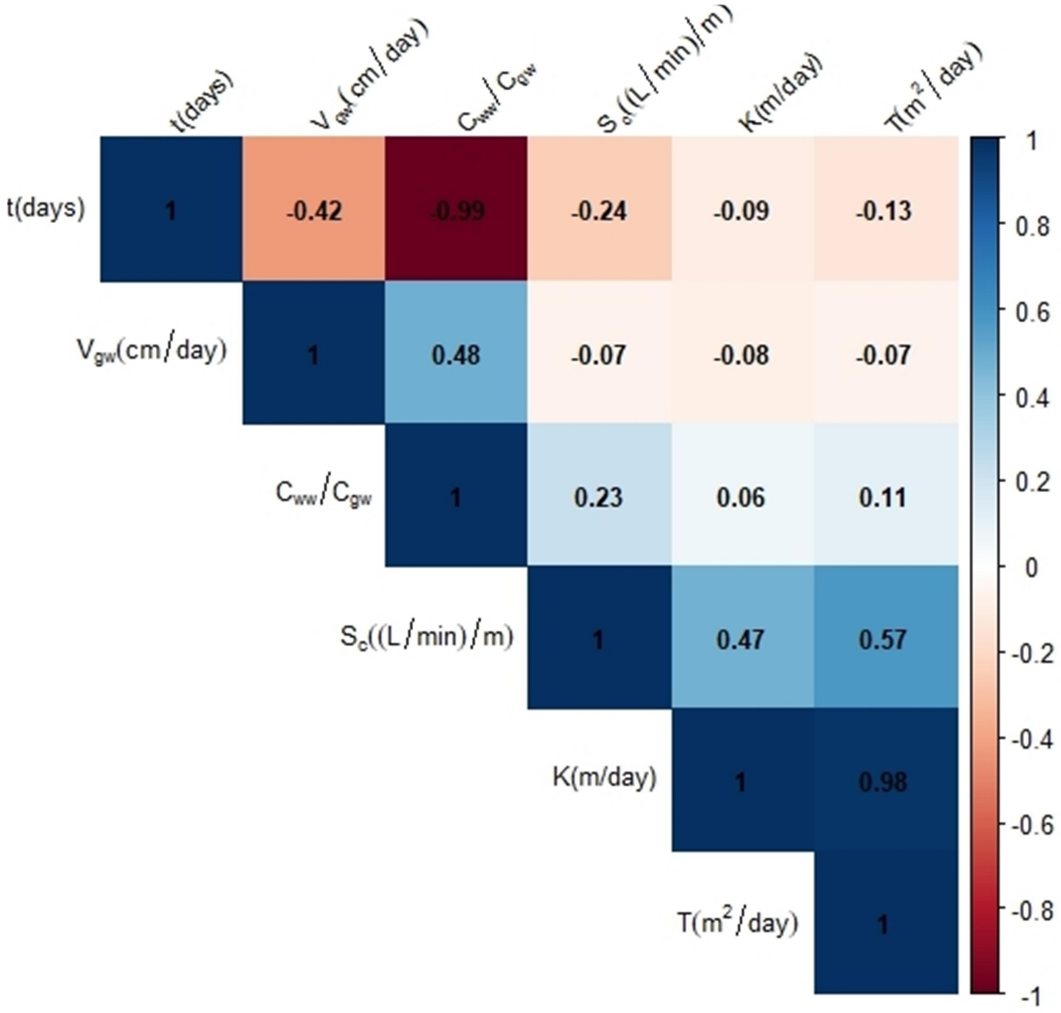

Figure 5.5: The correlation matrix between hydraulic parameters and ^{222}Rn recovery, residence time and groundwater flow velocity

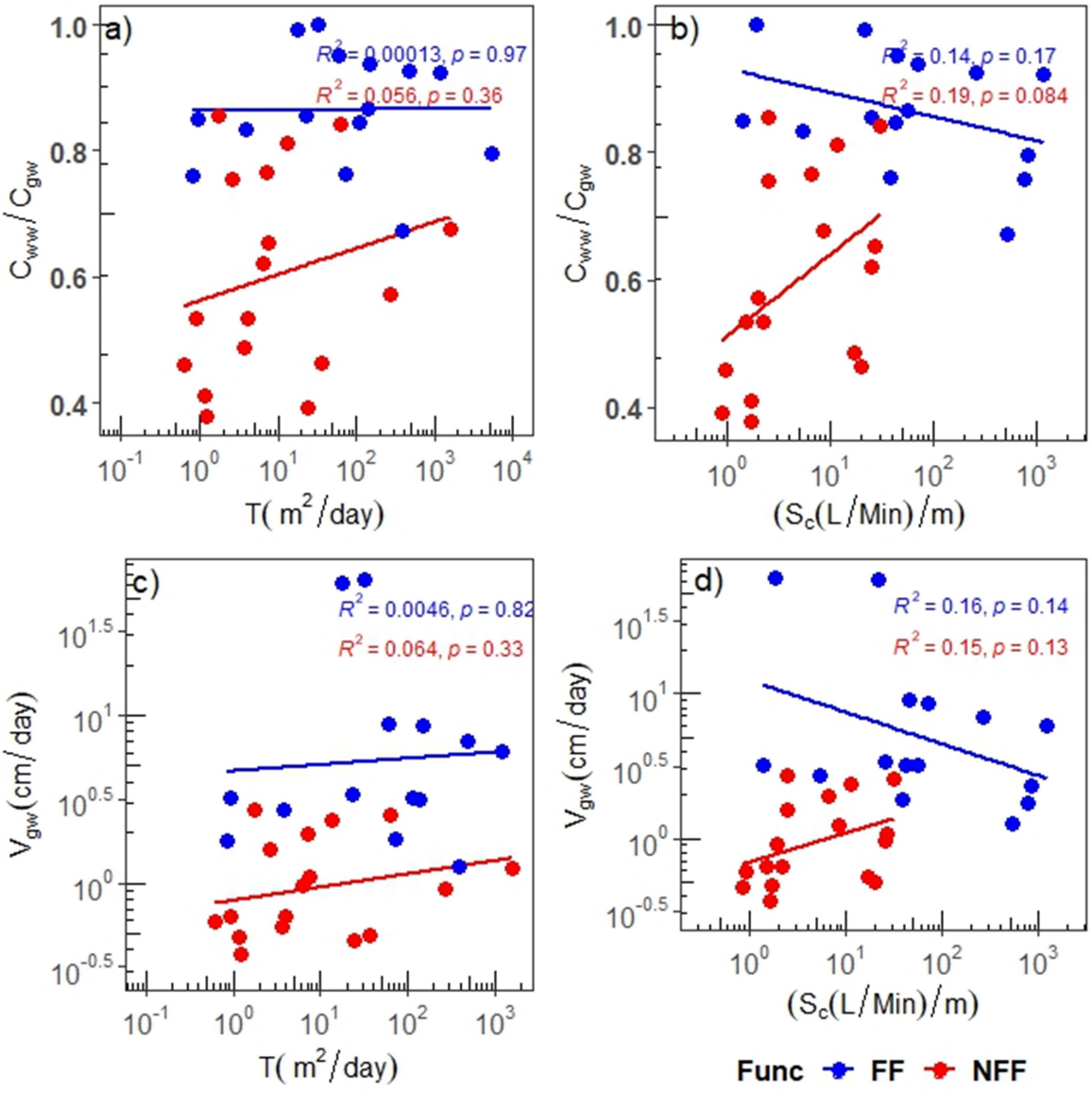

Figure 5.6: The T and Sc plotted against 222Rn recovery and Vgw for FF and NFF (UR, LY and UR&LY). a) T against C_{ww}/C_{gw} , b) S_c against C_{ww}/C_{gw} plots, c) T against V_{gw} and d) S_c against V_{gw} plots

5.5.4. The ^{222}Rn measurement in practice for rural water supply

The ^{222}Rn isotope has been proven as an applicable technique for the HPWs functionality monitoring by providing important information on HPWs performance conditions, groundwater flow velocity and residence time in the well. The HPWs functionality

monitoring has multiple importances for providing complementary information in rural water supply management to minimize the challenges of significant numbers of HPWs early failures after construction in sub-Saharan Africa. The ^{222}Rn measurement practices have been known in the aquifer characterization, surface water-groundwater interaction, fracture zone location, groundwater flow velocity estimation and residence time (Cook et al., 1999; Hamada, 2000; Kebede et al., 2023; Kebede & Zewdu, 2019; Schubert et al., 2011). However, in rural water supply management, the functionality of HPWs has been surveyed by the physical assessment which needs substantial running costs. There was no previous practice of the ^{222}Rn method conducted in Ethiopia to estimate groundwater flow velocity and HPWs functionality during post-construction. This study demonstrated that measurement of ^{222}Rn (^{222}Rn recovery, residence time and V_{gw}) in HPWs can provide important information on the performance of HPWs. High ^{222}Rn recovery and V_{gw} show good performance of HPWs revealing the information about the functionality status of HPWs and the aquifer conditions in the vicinity of the well.

Therefore, the ^{222}Rn technique can be practically applied in the monitoring of rural water supply settings. The cost of operation during data collection and for instrumentation is very cheap as compared to other methods to monitor the functionality of HPWs. The measurability of this technique during field campaigns to collect water samples makes it easy to use in all terrains and can be conducted by all trained professionals. The ^{222}Rn sampling in a single well takes less time (< 3hrs) as compared to other methods that need more than two days for monitoring a single HPWs. The on-site availability of ^{222}Rn recovery data makes the ^{222}Rn technique very useful for rural water supply management to quickly identify the conditions of HPWs and an aquifer in the vicinity of the well. Furthermore, the ^{222}Rn technique can be applicable in all countries and rural communities to monitor HPWs functionality as it needs low investment costs of instrumentation and operations. Thus, this study successfully tested the ^{222}Rn technique as a proxy to examine the HPWs' functionality over a period of time during the post-construction of hand pump boreholes.

5.6. Concluding Remark

The ^{222}Rn technique was employed to estimate ^{222}Rn recovery, flow velocity in a water well, residence time in a well and groundwater flow velocity complemented with determining the pumping test data analysis of the aquifer hydraulic properties (T, K and S_c) to test the applicability of ^{222}Rn technique as an independent tool to inspect post-water well construction in rural water supply HPWs functionality monitoring in shallow volcanic aquifers of Ethiopian highlands. The FF HPWs show above 67% ^{222}Rn recovery, while UR, LY and UR&LY HPWs show between 37% and 67% ^{222}Rn recovery. The ^{222}Rn recovery and V_{gw} are high, while water residence time is low in FF HPWs. This reveals that there is a quick through flow, healthy functioning of boreholes without screen clogging effects and high permeability of the aquifer material in the vicinity of the well. The UR, LY and UR&LY HPWs show low ^{222}Rn recovery, V_{gw} and high water residence time. This is due to the low permeability of the aquifer material surrounding the borehole, declining yield, stagnation of the water in the well due to insufficient flow into the well, screen clogging effect, poor initial design and construction problems. The HPWs with low V_{gw} and ^{222}Rn recovery show a stronger correlation with the aquifer hydraulic properties (T and Sc) than the HPWs with high V_{gw}. Furthermore, the V_{gw} and ^{222}Rn recovery show a good correlation with Sc than with aquifer T in UR, LY and UR&LY HPWs than in FF HPWs. This reveals that there is a problem associated with water wells' conditions than the aquifer properties in the vicinity of the HPWs. Some limitations of the ^{222}Rn technique can occur from poor sampling and purging of stagnant water that might cause mixing of ^{222}Rn concentration (between C_{ww} and C_{gw}). Therefore, this study suggests that the ^{222}Rn technique can be used as an independent tool for HPWs functionality monitoring during post-construction over a period of time.

Chapter Six

6. Conclusion and Recommendation

6.1. Conclusion

The volcanic aquifers of Ethiopian highlands covered a wider spatial extent with a thick volume of heterogeneous and complex inter-fingering of hydrostratigraphic formations. This dissertation work integrated the systematic analysis of integrated aquifer structures hydraulic properties, geospatial methods to estimate the groundwater flow velocity, isotopic method (^{222}Rn technique) and testing the applicability of ^{222}Rn method as a tracer to monitor HPWs functionality. These methods were integrated to investigate the conceptual hydrogeological framework of volcanic aquifer productivity, water wells functionality and hydraulic structures in the Ethiopian volcanic aquifers.

This work analyzed the hydraulic properties of volcanic formations based on the age of the rock emplacement and depth to the aquifer to characterize aquifer productivity in the complex hydrogeology of Ethiopian highland volcanic aquifers and the result was compared with the global volcanic aquifers. The findings reveal that

- The pattern in depth-wise variation may be similar (i.e., weak correlation between depth and hydraulic properties) across various age groups globally; however, each age group has a statistically distant hydraulic property from the other age group.
- The productivity of Ethiopian volcanic aquifers aged from Eocene LB to Quaternary showed that the productivity of major aquifer classes shows the unclear trend of either decreasing or increasing aquifer productivity with increased drilling depth. The depth-wise variations of aquifer productivity have no clear correlation pattern, where deep wells in QV and RMV showed increased productivity, LB showed decreasing productivity and UB showed unclear patterns of aquifer productivity with increased drilling depth.
- The Eocene LB aquifer system shows the lowest productivity as compared to all other aquifer systems. The Oligocene to Miocene UB aquifer shows a weak correlation of aquifer productivity with the aquifer depth. The Miocene RMV (controlled by the major regional fault systems of YTVL and MER) is the second

most productive deep aquifer system although it has no clear trend associated with aquifer depth. The youngest QV is the most productive aquifer system serving as a source of water supply for shallow and deep wells. The results reveal that deep drilling into QV and RMV, although there is complexity in hydro-stratigraphy, encountered a more productive aquifer system than LB and UB aquifer classes.

- Furthermore, this work helps to understand the general flow model and merit-based groundwater wells' effective drilling depth in the broad volcanic aquifers of the Ethiopian highlands.

The volcanic aquifers productivity, storage capacity and flow systems in the aquifer hydraulic structures have paramount importance for sustainable groundwater resources management. Hence, groundwater flow velocity estimation has an important role in understanding groundwater resource management, the sustainability of groundwater resources, groundwater flow dynamics and contaminant transport. Shallow volcanic aquifers of Ethiopian highlands (Mecha, Ejere, Sodo and Abeshege sites) were systematically selected to estimate groundwater flow velocity by using the geospatial technique. The four input raster maps (groundwater elevation head, effective porosity, aquifer saturated thickness and transmissivity maps) were compiled to estimate output resultant maps of groundwater flow velocity magnitude and direction. The results reveal that:

- The groundwater flow velocity in the selected sites varied between 0 to 47.31, 0 to 7.47, 0 to 22.36 and 0 to 195.35 m/day in Mecha, Ejere, Sodo and Abeshege respectively.
- The Abeshege site showed the highest transmissivity and groundwater flow velocity as compared to all other three sites. This is associated with a thick fractured and weathered basaltic aquifer. In the Mecha site, the groundwater flow velocity of the aquifer shows slightly higher values next to the Abeshege site. This is also associated with Quaternary basaltic formation and alluvial deposits in the Lake Tana Graben. In the Sodo site, a medium range of groundwater flow velocity distribution was observed in the pyroclastic and lacustrine deposits as compared to other sites, except in a few pocket areas of higher velocity that are controlled by rugged

topography and geological structures. In the Ejere site, groundwater flow velocity shows the lowest value as compared to all other sites in less fractured and weathered basaltic and trachytic aquifers, while slight increments of groundwater flow velocity magnitude are observed in the thick alluvial deposits of the Becho plain.

- This work has significant importance in supporting other methods of groundwater flow velocity estimation. Thus, we recommend employing this method for understanding the groundwater resources of shallow volcanic aquifers of the Ethiopian highlands, which serve as a major source of rural water supply.

Groundwater flow velocity was estimated in systematically selected sites (Mecha, Ejere, Sodo and Abeshege). The ^{222}Rn technique was used to estimate ^{222}Rn recovery, water flow velocity in a well, residence time in a well and groundwater flow velocity in shallow volcanic aquifers of Ethiopian highlands.

The following results were obtained:

- The ^{222}Rn method applied to this study was measured to obtain ^{222}Rn concentration in a water well (C_{ww}) and aquifer (C_{gw}) that are used to determine ^{222}Rn recovery, water residence time, flow velocity in a well and groundwater flow velocity.
- Based on the obtained result, the ^{222}Rn concentration ranged between 437 and 12,063 Bq/m^3 in a water well and 1,480 and 22,184 Bq/m^3 in an aquifer. The maximum ^{222}Rn concentration is in the EME15, while the lowest is observed in the EME13. The highest ^{222}Rn concentration indicates that groundwater is affected by the composition of host rock, shallow circulation, surface water infiltration, water level rising and the hydrostratigraphic effect of the basaltic aquifer and alluvial deposits.
- Groundwater flow velocity ranged between 0.37 to 69.1cm/day. The highest ^{222}Rn recovery and groundwater flow velocity was observed in the EAE02 situated in the Ghibe basin. The possible reason for the highest groundwater velocity is associated with the hydraulic gradient, geological structures, lithostratigraphic formation and hydraulic conductivity of the aquifer. The lowest ^{222}Rn recovery and groundwater flow velocity was observed in ESD10 situated in the Ziway Lake basin which is

associated with high residence time due to low permeability of the aquifer formation of welded pyroclastic materials.

- The estimated ^{222}Rn recovery and groundwater flow velocity reveal the nature of the aquifer in the vicinity of the well.

The ^{222}Rn technique in complementing the pumping test data analysis of the aquifer hydraulic properties (T, K and S_c), was employed to test its applicability as an independent tool to monitor the functionality of HPWs during post-water well construction in rural water supply in shallow volcanic aquifers of Ethiopian highlands. The results reveal that:

- The FF HPWs show above 67% ^{222}Rn recovery, while UR, LY and UR&LY HPWs show between 37% and 67% ^{222}Rn recovery.
- The ^{222}Rn recovery and V_{gw} are high, while water residence time is low in FF HPWs. This reveals that there is a quick through flow, healthy functioning of boreholes without screen clogging effects and high permeability of the aquifer material in the vicinity of the well.
- The UR, LY and UR&LY HPWs show low ^{222}Rn recovery and V_{gw} and high residence time in a well. This is due to the low permeability of the aquifer material surrounding the borehole, declining yield, stagnation of the water in the well due to insufficient flow into the well, screen clogging effect, poor initial design and construction problems.
- The HPWs with low V_{gw} and ^{222}Rn recovery show a stronger correlation with the aquifer hydraulic properties (T and Sc) than the HPWs with high V_{gw}. Furthermore, the V_{gw} and ^{222}Rn recovery show a good correlation with Sc than with aquifer T in UR, LY and UR&LY HPWs than in FF HPWs. This reveals that there is a problem associated with water wells' conditions than the aquifer properties in the vicinity of the HPWs.
- Some limitations of the ^{222}Rn technique can occur from poor sampling and purging of stagnant water that might cause mixing of ^{222}Rn concentration (between C_{ww} and C_{gw}). Therefore, this study suggests that the ^{222}Rn technique can be used as an independent tool for HPWs functionality monitoring during post-construction over a period of time.

6.2. Recommendation

Volcanic aquifers of Ethiopian highlands covered the wider areal extent (north and south western and southeastern Ethiopian plateaus and MER). This study mainly focused on the north and southwestern Ethiopian plateaus. Volcanic aquifers play a vital role as a source of water supply for domestic, industrial and irrigation purposes. In addition to this dissertation, further improvements are important on the volcanic aquifer productivity, groundwater flow mechanism and water wells functionality to understand all volcanic aquifer classes.

- Geophysical methods to identify the subsurface layer type, thickness, depth to the aquifer, subsurface structures, fracture discontinuities and fracture density analysis are recommended to develop full insights into the depth of the aquifer and age of emplacement to complement the aquifer productivity analysis presented in this work.
- Tracer methods such as salt tracer and direct velocity estimation tools are important to estimate groundwater flow velocity estimation and can be complemented with the current techniques used for groundwater flow velocity estimation. Thus, we give a remark to employ these methods in estimating groundwater flow velocity that helps in understanding groundwater resources management, sustainability of groundwater resources, rural water supply, groundwater flow dynamics and contaminant transport in shallow volcanic aquifers of Ethiopian highlands.
- Detail groundwater geochemical and isotope hydrogeological studies help understand the regional and local groundwater flow mechanism in broader volcanic aquifers.
- Detail study on the volcanic aquifer productivity analysis in the Main Ethiopian Rift system and southeastern Ethiopian Plateau to set up the general framework of Ethiopian volcanic aquifers.

References

Abbate, E., Bruni, P., & Sagri, M. (2015). Geology of Ethiopia: A Review and Geomorphological Perspectives. In World Geomorphological Landscapes. https://doi.org/10.1007/978-94-017-8026-1_2

Abdullah, T., Ali, S. S., Al-Ansari, N., & Knutsson, S. (2021). Seepage Velocity of Different Groundwater Aquifers in Halabja Saidsadiq Basin—NE of Iraq. Environmental Science and Engineering. https://doi.org/10.1007/978-3-030-51210-1_267

Abdullah, T. O., Ali, S. S., Al-ansari, N. A., Knutsson, S., & Laue, J. (2020). Magnitude and Direction of Groundwater Seepage Velocity in Different Soil and Rock Materials. 1–12.

Abebe, T., Mazzarini, F., Innocenti, F., & Manetti, P. (1998). The Yerer-Tullu Wellel volcanotectonic lineament: A transtensional structure in central Ethiopia and the associated magmatic activity. Journal of African Earth Sciences. https://doi.org/10.1016/S0899-5362(97)00141-3

Adyalkar, P. G., & Mani, V. V. S. (1974). Application of groundwater hydraulics to a basaltic water-table aquifer. Journal of Hydrology, 21(3), 211–218. https://doi.org/10.1016/0022-1694(74)90067-5

Agostini, A., Bonini, M., Corti, G., Sani, F., & Manetti, P. (2011). Distribution of Quaternary deformation in the central Main Ethiopian Rift, East Africa. Tectonics, 30(4), 1–21. https://doi.org/10.1029/2010TC002833

Ahmad, M., Tariq, J. A., Rafique, M., Iqbal, N., Choudhry, M. A., & Qureshi, R. M. (2008). Measurement of Groundwater Flow Velocity At.

Ahuja, R., Cassel, K., Bruce, R., & Barnes, B. (1989). Evaluation of spatial distribution of hydraulic conductivity using effective porosity data.

Al-Madhlom, Q., Al-Ansari, N., Abid, B., Laue, J., & Musa, H. (2020). Seepage velocity: Large scale mapping and the evaluation of two different aquifer conditions (silty clayey and sandy). Hydrology, 7(3), 1–30. https://doi.org/10.3390/HYDROLOGY7030060

Alemu, M. (2017). Comparative analysis of the effects of Land Use / Land Cover Changes on Hydrology and Sedimentation : The Case of Wabeand Meki Catchments , Central Ethiopia.

Aley, T. (2002). Groundwater Tracing Handbook. Ozark Underground Laboratory, 1572 Aley Lane, Protem, Missouri, 65733, 35.

Allocca, V., Colantuono, P., Colella, A., Piacentini, S. M., & Piscopo, V. (2022). Hydraulic properties of ignimbrites: matrix and fracture permeabilities in two pyroclastic flow deposits from Cimino-Vico volcanoes (Italy). Bulletin of Engineering Geology and the Environment, 81(6). https://doi.org/10.1007/s10064-022-02712-0

Arriaga, M. A., & Leap, D. I. (2006). Using solver to determine vertical groundwater velocities by temperature variations, Purdue University, Indiana, USA. Hydrogeology Journal, 14(1–2), 253–263. https://doi.org/10.1007/s10040-004-0381-x

Ayalew, D., Barbey, P., Marty, B., Reisberg, L., Yirgu, G., & Pik, R. (2002). Source, genesis, and timing of giant ignimbrite deposits associated with Ethiopian continental flood basalts. Geochimica et Cosmochimica Acta. https://doi.org/10.1016/S0016-7037(01)00834-1

Ayalew, D., Yirgu, G., & Raphaël, P. (1999). Geochemical and isotopic (Sr, Nd and Pb) characteristics of volcanic rocks from southwestern Ethiopia. Journal of African Earth Sciences, 29(2), 381–391. https://doi.org/10.1016/S0899-5362(99)00104-9

Ayenew, T., Demlie, M., & Wohnlich, S. (2008a). Hydrogeological framework and occurrence of groundwater in the Ethiopian aquifers. Journal of African Earth Sciences, 52(3), 97–113. https://doi.org/10.1016/j.jafrearsci.2008.06.006

Ayenew, T., Demlie, M., & Wohnlich, S. (2008b). Journal of African Earth Sciences Hydrogeological framework and occurrence of groundwater in the Ethiopian aquifers. 52, 97–113. https://doi.org/10.1016/j.jafrearsci.2008.06.006

Azagegn, T., Asrat, A., Ayenew, T., & Kebede, S. (2015). Litho-structural control on

interbasin groundwater transfer in central Ethiopia. Journal of African Earth Sciences. https://doi.org/10.1016/j.jafrearsci.2014.10.008

Bakx, W., Bense, V. F., Karaoulis, M., Oude Essink, G. H. P., & Bierkens, M. F. P. (2023). Measuring groundwater flow velocities near drinking water extraction wells in unconsolidated sediments. Water (Switzerland), 15(12). https://doi.org/https://doi.org/10.3390/w15122167

Banks, E. W., Cook, P. G., Owor, M., Okullo, J., Kebede, S., Nedaw, D., Mleta, P., Fallas, H., Gooddy, D., John MacAllister, D., Mkandawire, T., Makuluni, P., Shaba, C. E., & MacDonald, A. M. (2021). Environmental tracers to evaluate groundwater residence times and water quality risk in shallow unconfined aquifers in sub Saharan Africa. Journal of Hydrology, 598(June), 125753. https://doi.org/10.1016/j.jhydrol.2020.125753

Beccaluva, L., Bianchini, G., Natali, C., & Siena, F. (2009). Continental flood basalts and mantle plumes: A case study of the Northern Ethiopian Plateau. Journal of Petrology. https://doi.org/10.1093/petrology/egp024

Berehanu, B., Azagegn, T., Ayenew, T., & Masetti, M. (2017). Inter-Basin Groundwater Transfer and Multiple Approach Recharge Estimation of the Upper Awash Aquifer System. Journal of Geoscience and Environment Protection. https://doi.org/10.4236/gep.2017.53007

Berg, S. J., & Gillham, R. W. (2010). Studies of water velocity in the capillary fringe: The point velocity probe. Ground Water, 48(1), 59–67. https://doi.org/10.1111/j.1745-6584.2009.00606.x

Berhe, S. M., Desta, B., Nicoletti, M., & Teferra, M. (1987). Geology, geochronology and geodynamic implications of the Cenozoic magmatic province in W and SE Ethiopia. Journal - Geological Society (London), 144(2), 213–226. https://doi.org/10.1144/gsjgs.144.2.0213

Bianchi, M., MacDonald, A. M., Macdonald, D. M. J., & Asare, E. B. (2020). Investigating the Productivity and Sustainability of Weathered Basement Aquifers in Tropical Africa Using Numerical Simulation and Global Sensitivity Analysis. Water

Resources Research, 56(9). https://doi.org/10.1029/2020WR027746

Boccaletti, M., Bonini, M., Mazzuoli, R., Abebe, B., Piccardi, L., & Tortorici, L. (1998). Quaternary oblique extensional tectonics in the Ethiopian Rift (Horn of Africa). Tectonophysics. https://doi.org/10.1016/S0040-1951(98)80063-2

Bonsor, H., MacDonald, A., Casey, V., Carter, R., & Wilson, P. (2018). La nécessité d'une approche normalisée pour évaluer la fonctionnalité des approvisionnements en eau des communautés rurales. Hydrogeology Journal, 26(2), 367–370. https://doi.org/10.1007/s10040-017-1711-0

Bonsor, H., Oates, N., Chilton, P. J., Carter, R. C., Casey, V., MacDonald, A. M., Calow, R., Alowo, R., Wilson, P., Tumutungire, M., & Bennie, M. (2015). A hidden crisis: strengthening the evidence base on the sustainability of rural groundwater supplies: results from a pilot study in Uganda. 85 pp. http://nora.nerc.ac.uk/511071/1/Hidden Crisis Final Report v7_bgsreview2%5Bces%5D.pdf

Brace, W. F. (1980). Permeability of crystalline and argillaceous rocks. International Journal of Rock Mechanics and Mining Sciences and Geomechanics, 17(5), 241–251. https://doi.org/10.1016/0148-9062(80)90807-4

Brace, W. F. (1984). Permeability of Crystalline Rocks: New in Situ Measurements. Journal of Geophysical Research, 89(B6), 4327–4330. https://doi.org/10.1029/jb089ib06p04327

Bresciani, E., Cranswick, R. H., Banks, E. W., Batlle-Aguilar, J., Cook, P. G., & Batelaan, O. (2018). Using hydraulic head, chloride and electrical conductivity data to distinguish between mountain-front and mountain-block recharge to basin aquifers. Hydrology and Earth System Sciences, 22(2), 1629–1648. https://doi.org/10.5194/hess-22-1629-2018

Brouye, S. (2003). Modeling tracer injection and well-aquifer interactions : A new mathematical and numerical approach. 39(3), 1–5. https://doi.org/10.1029/2002WR001813

Cant, J. L., Siratovich, P. A., Cole, J. W., Villeneuve, M. C., & Kennedy, B. M. (2018).

Matrix permeability of reservoir rocks, Ngatamariki geothermal field, Taupo Volcanic Zone, New Zealand. Geothermal Energy, 6(1). https://doi.org/10.1186/s40517-017-0088-6

Carter, R. C., & Ross, I. (2016). Beyond "functionality" of handpumpsupplied rural water services in developing countries. Waterlines, 35(1), 94–110. https://doi.org/10.3362/1756-3488.2016.008

Chae, H., Nagano, K., Sakata, Y., Katsura, T., & Kondo, T. (2020). Estimation of fast groundwater flow velocity from thermal response test results. Energy and Buildings, 206, 109571. https://doi.org/10.1016/j.enbuild.2019.109571

Cherry, J. (1990). Groundwater monitoring: some deficiencies and opportunities. Hazardous Waste Site Investigations: Towards Better …. http://www.gfredlee.com/Groundwater/cherry_gw.pdf

Cook 1999.pdf. (n.d.).

Cook, A.J.Love, & J.C.Dighton. (1999). Inferring Ground Water flow In Fractured Rock From Dissolved Radon. Ground Water, 37(4).

Cook, P. G., Favreau, G., Dighton, J. C., & Tickell, S. (2003). Determining natural groundwater influx to a tropical river using radon, chlorofluorocarbons and ionic environmental tracers. Journal of Hydrology, 277(1–2), 74–88. https://doi.org/10.1016/S0022-1694(03)00087-8

Cook, P. G., Lamontagne, S., Berhane, D., & Clark, J. F. (2006). Quantifying groundwater discharge to Cockburn River, southeastern Australia, using dissolved gas tracers 222Rn and SF6. Water Resources Research, 42(10), 1–12. https://doi.org/10.1029/2006WR004921

Cooper, J., & Jacob, C. (1946). A generalized Graphical Method For Evaluating Formation Constants and Summarizing Well-field History. 27(Iv).

Corti, G., Cioni, R., Franceschini, Z., Sani, F., Scaillet, S., Molin, P., Isola, I., Mazzarini, F., Brune, S., Keir, D., Erbello, A., Muluneh, A., Illsley-Kemp, F., & Glerum, A. (2019). Aborted propagation of the Ethiopian rift caused by linkage with the Kenyan rift. Nature Communications, 10(1), 1–11. https://doi.org/10.1038/s41467-

019-09335-2

Corti, G., Sani, F., Philippon, M., Sokoutis, D., Willingshofer, E., & Molin, P. (2013). Quaternary volcano-tectonic activity in the Soddo region, western margin of the Southern Main Ethiopian Rift. Tectonics, 32(4), 861–879. https://doi.org/10.1002/tect.20052

Cox, K. G. (2000). The Karoo Province. c(1984), 239–240.

Custodio, E. (1985). Low permeability volcanics in the Canary Islands (Spain). https://inis.iaea.org/search/search.aspx?orig_q=RN:19056105

Cuthbert, M. O., Taylor, R. G., Favreau, G., Todd, M. C., Shamsudduha, M., Villholth, K. G., MacDonald, A. M., Scanlon, B. R., Kotchoni, D. O. V., Vouillamoz, J. M., Lawson, F. M. A., Adjomayi, P. A., Kashaigili, J., Seddon, D., Sorensen, J. P. R., Ebrahim, G. Y., Owor, M., Nyenje, P. M., Nazoumou, Y., … Kukuric, N. (2019). Observed controls on resilience of groundwater to climate variability in sub-Saharan Africa. Nature, 572(7768), 230–234. https://doi.org/10.1038/s41586-019-1441-7

Davidson, A., & Rex, D. C. (1980). Age of volcanism and rifting in Southwestern Ethiopia.

de Graaf, I. E. M., van Beek, R. L. P. H., Gleeson, T., Moosdorf, N., Schmitz, O., Sutanudjaja, E. H., & Bierkens, M. F. P. (2017). A global-scale two-layer transient groundwater model: Development and application to groundwater depletion. Advances in Water Resources, 102, 53–67. https://doi.org/10.1016/j.advwatres.2017.01.011

Demlie, M., Wohnlich, S., & Ayenew, T. (2008). Major ion hydrochemistry and environmental isotope signatures as a tool in assessing groundwater occurrence and its dynamics in a fractured volcanic aquifer system located within a heavily urbanized catchment, central Ethiopia. Journal of Hydrology. https://doi.org/10.1016/j.jhydrol.2008.02.009

Demlie, M., Wohnlich, S., Wisotzky, F., & Gizaw, B. (2007). Groundwater recharge, flow and hydrogeochemical evolution in a complex volcanic aquifer system,

central Ethiopia. Hydrogeology Journal, 15(6), 1169–1181. https://doi.org/10.1007/s10040-007-0163-3

Deolankar, S. B. (1980). The Deccan Basalts of Maharashtra, India —Their Potential as Aquifers. Groundwater, 18(5), 437–437.

Devlin, J. F. (2020). Groundwater Velocity. https://doi.org/10.1111/j.1745-6584.1970.tb01311.x

Devlin, J. F., Tsoflias, G., McGlashan, M., & Schillig, P. (2009). An inexpensive multilevel array of sensors for direct ground water velocity measurement. Ground Water Monitoring and Remediation, 29(2), 73–77. https://doi.org/10.1111/j.1745-6592.2009.01233.x

Dewandel, B., Lachassagne, P., Wyns, R., Maréchal, J. C., & Krishnamurthy, N. S. (2006). A generalized 3-D geological and hydrogeological conceptual model of granite aquifers controlled by single or multiphase weathering. Journal of Hydrology, 330(1–2), 260–284. https://doi.org/10.1016/j.jhydrol.2006.03.026

Deyassa, G., Kebede, S., Ayenew, T., & Kidane, T. (2014). Crystalline basement aquifers of Ethiopia: Their genesis, classification and aquifer properties. Journal of African Earth Sciences, 100, 191–202. https://doi.org/10.1016/j.jafrearsci.2014.06.002

Dickin, A. . (1988). The North Atlantic Tertiary Province. 111–112.

DJ. MacAllister, D. N. S. K. T. M. P. M. C. S. J. O. M. O. R. C. J. C. V. C. H. F. A. M. M. (2022). Contribution of physical factors to handpump borehole functionality in Africa. Science of The Total Environment, 158343. https://doi.org/10.1016/J.SCITOTENV.2022.158343

Doetsch, J., Linde, N., Vogt, T., Binley, A., & Green, A. G. (2012). Imaging and quantifying salt-tracer transport in a riparian groundwater system by means of 3D ERT monitoring. Geophysics, 77(5). https://doi.org/10.1190/geo2012-0046.1

Drost, W., Klotz, D., Koch, A., Moser, H., Neumaier, F., & Rauert, W. (1968). Point dilution methods of investigating ground water flow by means of radioisotopes.

Water Resources Research, 4(1), 125–146. https://doi.org/10.1029/WR004i001p00125

Englert, A. (2003). Measurement , Estimation and Modelling of Groundwater Flow Velocity at Krauthausen Test Site.

Englert, Andreas. (2003). Measurement , Estimation and Modelling of Groundwater Flow Velocity at Krauthausen Test Site. 109.

Environmental Systems Research Institute (ESRI). (2015). Darcy Velocity (10.3.1.4959). www.esri.com

Essouayed, E., Annable, M. D., Momtbrun, M., & Atteia, O. (2019a). An innovative tool for groundwater velocity measurement compared with other tools in laboratory and field tests. Journal of Hydrology X, 2, 100008. https://doi.org/10.1016/j.hydroa.2018.100008

Essouayed, E., Annable, M. D., Momtbrun, M., & Atteia, O. (2019b). An innovative tool for groundwater velocity measurement compared with other tools in laboratory and field tests. Journal of Hydrology X, 2, 100008. https://doi.org/10.1016/j.hydroa.2018.100008

Fenta, M. C., Anteneh, Z. L., Szanyi, J., & Walker, D. (2020). Hydrogeological framework of the volcanic aquifers and groundwater quality in Dangila Town and the surrounding area, Northwest Ethiopia. Groundwater for Sustainable Development, 11(January). https://doi.org/10.1016/j.gsd.2020.100408

Ferguson, A. S., Mailloux, B. J., Ahmed, K. M., Van Geen, A., McKay, L. D., & Culligan, P. J. (2011). Hand-pumps as reservoirs for microbial contamination of well water. Journal of Water and Health, 9(4), 708–717. https://doi.org/10.2166/wh.2011.106

Fitts, C. R. (2013). Groundwater Science. In Groundwater Science. https://doi.org/10.1016/C2009-0-62950-0

Flow meter, kerfoot1985.pdf. (n.d.).

Foster, T., Furey, S., Banks, B., & Willetts, J. (2020). Functionality of handpump water supplies: a review of data from sub-Saharan Africa and the Asia-Pacific region.

International Journal of Water Resources Development, 36(5), 855–869. https://doi.org/10.1080/07900627.2018.1543117

Foster, T., Willetts, J., Lane, M., Thomson, P., Katuva, J., & Hope, R. (2018). Risk factors associated with rural water supply failure: A 30-year retrospective study of handpumps on the south coast of Kenya. Science of the Total Environment, 626, 156–164. https://doi.org/10.1016/j.scitotenv.2017.12.302

Furi, W., Razack, M., Abiye, T. A., Ayenew, T., & Legesse, D. (2011). Fluoride enrichment mechanism and geospatial distribution in the volcanic aquifers of the Middle Awash basin, Northern Main Ethiopian Rift. Journal of African Earth Sciences. https://doi.org/10.1016/j.jafrearsci.2011.03.004

Furi, W., Razack, M., Abiye, T. A., Kebede, S., & Legesse, D. (2012). Hydrochemical characterization of complex volcanic aquifers in a continental rifted zone: The Middle Awash basin, Ethiopia. Hydrogeology Journal. https://doi.org/10.1007/s10040-011-0807-1

Gani, N. D., Abdelsalam, M. G., Gera, S., & Gani, M. R. (2009). Stratigraphic and structural evolution of the Blue Nile Basin, Northwestern Ethiopian Plateau. Geological Journal. https://doi.org/10.1002/gj.1127

GEBRE, A. G. (2010). Assessment on Hydraulic Properties of the Ethiopian Tarmaber Formations. Addis Ababa University.

GebreEgziabher, M., Jasechko, S., & Perrone, D. (2022). Widespread and increased drilling of wells into fossil aquifers in the USA. Nature Communications, 13,2129. https://doi.org/10.1038/s41467-022-29678-7

Gowing, J., Parkin, G., Forsythe, N., Walker, D., Haile, A. T., & Alamirew, D. (2016). Shallow groundwater in sub-Saharan Africa: Neglected opportunity for sustainable intensification of small-scale agriculture? Hydrology and Earth System Sciences Discussions, 2016(January), 1–33. https://doi.org/10.5194/hess-2015-549

Gowing, J., Walker, D., Parkin, G., Forsythe, N., Haile, A. T., & Ayenew, D. A. (2020). Can shallow groundwater sustain small-scale irrigated agriculture in sub-

Saharan Africa? Evidence from N-W Ethiopia. Groundwater for Sustainable Development, 10(November 2018), 100290. https://doi.org/10.1016/j.gsd.2019.100290

Gupta, R. S. (2017). Hydrology & Hydraulic Systems Hydrology & Hydraulic Systems Ram S . Gupta , PhD , PE.

Gupte, P. R. (2010). Review of Aquifer System of Deccan Trap Area ,. Figure 1.

Gurmessa, B., & Mekuriaw, A. (2019). What determines the operational sustainability of rural drinking water points in Ethiopia? The case of woliso woreda. Journal of Water Sanitation and Hygiene for Development, 9(4), 743–753. https://doi.org/10.2166/washdev.2019.067

Hall, S. H. (1993). Single Well Tracer Tests in Aquifer Characterization. Groundwater Monitoring & Remediation, 13(2), 118–124. https://doi.org/10.1111/j.1745-6592.1993.tb00443.x

Hamada, H. (2000). Estimation of groundwater flow rate using the decay of 222Rn in a well. Journal of Environmental Radioactivity, 47(1), 1–13. https://doi.org/10.1016/S0265-931X(99)00012-0

Hatfield, K., Annable, M., Cho, J., Rao, P. S. C., & Klammler, H. (2004). A direct passive method for measuring water and contaminant fluxes in porous media. Journal of Contaminant Hydrology, 75(3–4), 155–181. https://doi.org/10.1016/j.jconhyd.2004.06.005

Heath, B. R. C. (1983). Basic Ground-Water Hydrology.

Hoehn, E., & Von Gunten, H. R. (1989). Radon in groundwater: A tool to assess infiltration from surface waters to aquifers. Water Resources Research, 25(8), 1795–1803. https://doi.org/10.1029/WR025i008p01795

Hooper, P. (1982). The Columbia River Basa ilts. Science, 215(4539).

Howard, K. W. F., Hughes, M., Charlesworth, D. L., & Ngobi, G. (1992). Hydrogeologic Evaluation Of Fracture Permeability In Crystalline Basement Aquifers Of Uganda. In Applied Hydrogeology (Vol. 1, Issue 1, pp. 55–65). https://doi.org/10.1007/s100400050029

Jackson, T. R., & Fenelon, J. M. (2022). Relation of hydraulic conductivity to depth, alteration, and rock type in the volcanic rocks of Pahute Mesa, Nevada, USA. Hydrogeology Journal, 30(8), 2417–2432. https://doi.org/10.1007/s10040-022-02571-9

Jalludin, M., & Razack, M. (1994). Analysis of pumping tests, with regard to tectonics, hydrothermal effects and weathering, for fractured Dalha and stratiform basalts, Republic of Djibouti. Journal of Hydrology, 155(1–2), 237–250. https://doi.org/10.1016/0022-1694(94)90167-8

Jalludin, Mohamed, & Razack, M. (2004). Assessment of hydraulic properties of sedimentary and volcanic aquifer systems under arid conditions in the Republic of Djibouti (Horn of Africa). Hydrogeology Journal, 12(2), 159–170. https://doi.org/10.1007/s10040-003-0312-2

JPM, W. (2019). World Health Organization and United Nations Children's Fund Joint Monitoring Programme for Water Supply and Sanitation (JMP). Progress on Drinking Water and Sanitation. In New York and Geneva: UNICEF and WHO.

Kahle, S. C., Morgan, D. S., Welch, W. B., Ely, D. M., Hinkle, S. R., Vaccaro, J. J., & Orzol, L. L. (2011). Hydrogeologic framework and hydrologic budget components of the Columbia Plateau regional aquifer system, Washington, Oregon, and Idaho. U.S. Geological Survey Scientific Investigations Report 2011–5124, 66.

Kassune, M., T. Tafesse, N., & Hagos, M. (2018). Characteristics and Productivity of Volcanic Rock Aquifers in Kola Diba Well Field, North-central Ethiopia. Universal Journal of Geoscience, 6(4), 103–113. https://doi.org/10.13189/ujg.2018.060401

Kearl, P. M. (1997). Observations of particle movement in a monitoring well using the colloidal borescope. Journal of Hydrology, 200(1–4), 323–344. https://doi.org/10.1016/S0022-1694(97)00026-7

Kearl, P. M., Roemer, K., Rogoff, E. B., & Renn, R. M. (1998). Characterization of a fractured aquifer using the colloidal borescope. Advances in Environmental Research, 3(1).

Kebede, S. (2013a). Functions of Groundwater. In Groundwater in Ethiopia. https://doi.org/10.1007/978-3-642-30391-3_6

Kebede, S. (2013b). Groundwater in Ethiopia: Features, numbers and opportunities. In Groundwater in Ethiopia: Features, Numbers and Opportunities. https://doi.org/10.1007/978-3-642-30391-3

Kebede, S., Abdalla, O., Sefelnasr, A., Tindimugaya, C., & Mustafa, O. (2017). Interaction of surface water and groundwater in the Nile River basin: isotopic and piezometric evidence. Hydrogeology Journal, 25(3), 1–20. https://doi.org/10.1007/s10040-016-1503-y

Kebede, S., Hailu, K., Siraj, A., & Birhanu, B. (2023). Environmental isotopes (δ18O–δ2H, 222Rn) and electrical conductivity in backtracking sources of urban pipe water, monitoring the stability of water quality and estimating pipe water residence time. Frontiers in Water, 5. https://doi.org/10.3389/frwa.2023.1066055

Kebede, S., Travi, Y., Alemayehu, T., & Ayenew, T. (2005). Groundwater recharge, circulation and geochemical evolution in the source region of the Blue Nile River, Ethiopia. Applied Geochemistry. https://doi.org/10.1016/j.apgeochem.2005.04.016

Kebede, S., Travi, Y., Asrat, A., Alemayehu, T., Ayenew, T., & Tessema, Z. (2008). Groundwater origin and flow along selected transects in Ethiopian rift volcanic aquifers. Hydrogeology Journal. https://doi.org/10.1007/s10040-007-0210-0

Kebede, S., & Zewdu, S. (2019). Use of 222Rn and δ18O-δ2H isotopes in detecting the origin of water and in quantifying groundwater inflow rates in an alarmingly growing lake, Ethiopia. Water (Switzerland), 11(12). https://doi.org/10.3390/w11122591

Kempf, A., Divine, C. E., Leone, G., Holland, S., & Mikac, J. (2013). Field Performance of Point Velocity Probes at a Tidally Influenced Site. Remediation. https://doi.org/10.1002/rem.21337

Kieffer, B., Arndt, N., Lapierre, H., Bastien, F., Bosch, D., Pecher, A., Yirgu, G., Ayalew,

D., Weis, D., Jerram, D. A., Keller, F., & Meugniot, C. (2004a). Flood and shield basalts from Ethiopia: Magmas from the African superswell. Journal of Petrology. https://doi.org/10.1093/petrology/egg112

Kieffer, B., Arndt, N., Lapierre, H., Bastien, F., Bosch, D., Pecher, A., Yirgu, G., Ayalew, D., Weis, D., Jerram, D. A., Keller, F., & Meugniot, C. (2004b). Flood and shield basalts from Ethiopia: Magmas from the African superswell. Journal of Petrology, 45(4), 793–834. https://doi.org/10.1093/petrology/egg112

Klammler, H., Hatfield, K., & Annable, M. D. (2007). Concepts for measuring horizontal groundwater flow directions using the passive flux meter. 30, 984–997. https://doi.org/10.1016/j.advwatres.2006.08.007

Kruseman, G. P., & De Ridder, N. A. (1983). Analysis and evaluation of pumping test data (3rd edition). Bulletin - International Institute for Land Reclamation & Improvement (Wageningen), 11.

Labaky, W., Devlin, J. F., & Gillham, R. W. (2007). Probe for measuring groundwater velocity at the centimeter scale. Environmental Science and Technology, 41(24), 8453–8458. https://doi.org/10.1021/es0716047

Labaky, W., Devlin, J. F., & Gillham, R. W. (2009). Field comparison of the point velocity probe with other groundwater velocity measurement methods. 45(April 2008), 1–9. https://doi.org/10.1029/2008WR007066

Lebas, M. J., & Mohr, P. A. (1970). Tholeiite from the Simien alkali basalt centre, Ethiopia. Geological Magazine. https://doi.org/10.1017/S0016756800058611

Li, F., Dai, C., & Lei, H. (2019). Review of groundwater flow velocity measurement method. Transactions - Geothermal Resources Council, 43, 723–734.

Lile, O. B., Morris, M., & Ronning, J. S. (1997). Estimating groundwater flow velocity from changes in contact resistance during a saltwater tracer experiment. 38(97).

Lindsey, B. D., & Ator, S. W. (1992). Radon in Ground Water of the.

Liu, B., Yan, G., Ma, Y., & Scheuermann, A. (2023). Measurement of In-Situ Flow Rate in Borehole by Heat Pulse Flowmeter: Field-Case Study and Reflection.

Geosciences (Switzerland), 13(5). https://doi.org/10.3390/geosciences13050146

Loukatos, D., Kondoyanni, M., Alexopoulos, G., Maraveas, C., & Arvanitis, K. G. (2023). On-Device Intelligence for Malfunction Detection of Water Pump Equipment in Agricultural Premises: Feasibility and Experimentation. Sensors, 23(2). https://doi.org/10.3390/s23020839

Ma, R., Shi, J., Zhang, Y., & Sun, L. (2016a). Variation of hydraulic conductivity with depth in the North China plain. Arabian Journal of Geosciences, 9(10), 1–13. https://doi.org/10.1007/s12517-016-2597-1

Ma, R., Shi, J., Zhang, Y., & Sun, L. (2016b). Variation of hydraulic conductivity with depth in the North China plain. Arabian Journal of Geosciences, 9(10). https://doi.org/10.1007/s12517-016-2597-1

MacAllister, D. J., MacDonald, A. M., Kebede, S., Godfrey, S., & Calow, R. (2020). Comparative performance of rural water supplies during drought. Nature Communications, 11(1), 1–13. https://doi.org/10.1038/s41467-020-14839-3

MacAllister, D. J., Nedaw, D., Kebede, S., Mkandawire, T., Makuluni, P., Shaba, C., Okullo, J., Owor, M., Carter, R., Chilton, J., Casey, V., Fallas, H., & MacDonald, A. M. (2022). Contribution of physical factors to handpump borehole functionality in Africa. Science of the Total Environment, 851(July), 158343. https://doi.org/10.1016/j.scitotenv.2022.158343

Macdonald, A. M., Bell, R. A., Kebede, S., Azagegn, T., Yehualaeshet, T., Pichon, F., Young, M., McKenzie, A. A., Lapworth, D. J., Black, E., & Calow, R. C. (2019). Groundwater and resilience to drought in the Ethiopian highlands. Environmental Research Letters, 14(9). https://doi.org/10.1088/1748-9326/ab282f

Macdougall, J. D. (1988). Continental flood basalts. Continental Flood Basalts.

Mahoney, J. J. (1988). Deccan Traps. 1884, 151–152.

Mamo, S. (2015). Integrated Hydrological and Hydrogeological System Analysis of the Lake Tana Basin, Northwestern Ethiopiaitle. PhD Thesis, 263.

Manandhar, A., Greeff, H., Thomson, P., Hope, R., & Clifton, D. A. (2020). Shallow aquifer monitoring using handpump vibration data. Journal of Hydrology X, 8(May). https://doi.org/10.1016/j.hydroa.2020.100057

Maréchal, J. C., Dewandel, B., & Subrahmanyam, K. (2004). Use of hydraulic tests at different scales to characterize fracture network properties in the weathered-fractured layer of a hard rock aquifer. Water Resources Research, 40(11), 1–17. https://doi.org/10.1029/2004WR003137

Matsumoto, S., Machida, I., Hebig, K. H., Zeilfelder, S., & Ito, N. (2020). Estimation of very slow groundwater movement using a Single-Well Push-Pull test. Journal of Hydrology, 591(June), 125676. https://doi.org/10.1016/j.jhydrol.2020.125676

Maurice, L., Taylor, R. G., Tindimugaya, C., MacDonald, A. M., Johnson, P., Kaponda, A., Owor, M., Sanga, H., Bonsor, H. C., Darling, W. G., & Gooddy, D. (2019). Characteristics of high-intensity groundwater abstractions from weathered crystalline bedrock aquifers in East Africa. Hydrogeology Journal, 27(2), 459–474. https://doi.org/10.1007/s10040-018-1836-9

Mayer, A., Nguyen, B. T., & Banton, O. (2016). Utilisation du radon-222 pour l'étude des interactions côtières eau souterraine/eau de surface dans l'aquifère côtier de La Crau (sud-est de la France). Hydrogeology Journal, 24(7), 1775–1789. https://doi.org/10.1007/s10040-016-1424-9

Mazor, E., & Nativ, R. (1992). Hydraulic calculation of groundwater flow velocity and age : examination of the basic premises. 138, 211–222.

Medici, G., West, L. J., & Banwart, S. A. (2019). Groundwater flow velocities in a fractured carbonate aquifer-type : Implications for contaminant transport. Journal of Contaminant Hydrology, 222(January), 1–16. https://doi.org/10.1016/j.jconhyd.2019.02.001

Mkandawire, T., Mwathunga, E., MacDonald, A. M., Bonsor, H. C., Banda, S., Mleta, P., Jumbo, S., Ward, J., Lapworth, D., Chavula, G., Gwengweya, G., Whaley, L., & Lark, R. M. (2020). An analysis of hand pump boreholes functionality in Malawi. Physics and Chemistry of the Earth, 118–119(July 2019), 102897.

https://doi.org/10.1016/j.pce.2020.102897

Mohr, P. A. (1967). Major volcano-tectonic lineament in the Ethiopian Rift System. Nature. https://doi.org/10.1038/213664a0

Mohr, P., & Zanettin, B. (1988a). The Ethiopian flood basalt province. Continental Flood Basalts.

Mohr, P., & Zanettin, B. (1988b). The Ethiopian flood basalt provinces. Continental Flood Basalts, 63–110. https://doi.org/10.1007/978-94-015-7805-9_3

Mohr, Paul. (1983). Ethiopian flood basalt province. In Nature (Vol. 303, Issue 5918). https://doi.org/10.1038/303577a0

Morris, D.A. and Johnson, A. I. (1967). Summary of Hydrologic and Physical Properties of Rock and Soil Materials, as Analyzed by the Hydrologic Laboratory of the U.S. Geological Survey. U.S. Geological Survey, 1839-D(USGS Water Supply Paper), 1948–1960.

Neuman, S. P. (1975). Analysis of pumping test data from anisotropic unconfined aquifers considering delayed gravity response. Water Resources Research, 11(2), 329–342. https://doi.org/10.1029/WR011i002p00329

Nigate, F., Ayenew, T., Belete, W., & Walraevens, K. (2017). Overview of the Hydrogeology and Groundwater Occurrence in the Lake Tana Basin, Upper Blue Nile River Basin. 77–91. https://doi.org/10.1007/978-3-319-45755-0_7

Nigate, F., Camp, M. Van, Yenehun, A., Belay, A. S., & Walraevens, K. (2020). Recharge-discharge relations of groundwater in volcanic terrain of semi-humid tropical highlands of Ethiopia: The case of infranz springs, in the upper blue nile. Water (Switzerland), 12(3). https://doi.org/10.3390/w12030853

Ollier, C. D. (1988). Deep weathering, groundwater and climate. Geografiska Annaler, Series A, 70 A(4), 285–290. https://doi.org/10.1080/04353676.1988.11880258

Osorno, T. C., & College, S. N. (2016). Development and Testing of an In-well Point Velocity Probe for Preliminary Site Characterization By.

Owor M, MacDonald AM, Bonsor HC, Okullo J, Katusiime F, Alupo G, Berochan G,

Tumusiime C, Lapworth D, Whaley L, L. R. (2017). UPGro Hidden Crisis Research Consortium: Survey 1 Country Report – Malawi. British Geological Survey (BGS) Open Report, 1–19.

Owor, M., Fallas, H., MacAllister, D., Okullo, J., Katusiime, F., Berochan, G., Whaley, L., Banks, E., Casey, V., & MacDonald, A. M. (2019). UPGro Hidden Crisis Research Consortium: Physical Factors Contributing to Rural Water Supply Functionality Performance in Uganda. 25.

Owor, M., MacDonald, A., Bonsor, H., Okullo, J., Katusiime, F., Alupo, G., Berochan, G., Tumusiime, C., Lapworth, D., Whaley, L., & Lark, R. (2017). UPGro Hidden Crisis Research Consortium; Unravelling past failures for future success in Rural Water Supply Survey 1 Country Report – Uganda. Natural Environment Research Council (NERC), 19 pp.

Peccerillo, A., Donati, C., Santo, A. P., Orlando, A., Yirgu, G., & Ayalew, D. (2007). Petrogenesis of silicic peralkaline rocks in the Ethiopian rift: Geochemical evidence and volcanological implications. Journal of African Earth Sciences, 48(2–3), 161–173. https://doi.org/10.1016/j.jafrearsci.2006.06.010

Piccinini, L., Fabbri, P., & Pola, M. (2016a). Point dilution tests to calculate groundwater velocity : an example in a porous aquifer in northeast Italy. Hydrological Sciences Journal, 61(8), 1512–1523. https://doi.org/10.1080/02626667.2015.1036756

Piccinini, L., Fabbri, P., & Pola, M. (2016b). Point dilution tests to calculate groundwater velocity: an example in a porous aquifer in northeast Italy. Hydrological Sciences Journal, 61(8), 1512–1523. https://doi.org/10.1080/02626667.2015.1036756

Piccirillo, E. ., MELFI, A. ., COMIN-CHIARAMONTI, P., BELLIEN, G., ERNEST0, M., MARQUES, L. ., NARDY, A. J. ., PACCA, I. ., RorSENBERG, A., & STOLFA, D. (1988). Continental Flood Volcanism From the Parana Basin (Brazil). 195–196.

Piersol, M. W., & Sprenke, K. F. (2015). A Columbia river basalt group aquifer in sustained drought: Insight from geophysical methods. Resources, 4(3), 577–

596. https://doi.org/10.3390/resources4030577

Pik, R., Deniel, C., Coulon, C., Yirgu, G., Hofmann, C., & Ayalew, D. (1998). The northwestern Ethiopian Plateau flood basalts: classification and spatial distribution of magma types. Journal of Volcanology and Geothermal Research. https://doi.org/10.1016/S0377-0273(97)00073-5

Porcello, J., Tolan, T., & Lindsey, K. (2009). Groundwater Level Declines in the Columbia River Basalt Group and their Relationship to Mechanisms for Groundwater Recharge: A Conceptual Groundwater System Model. 6(1), 1–22. http://www.keepeek.com/Digital-Asset-Management/oecd/development/the-world-economy_9789264022621-en#.WQjA_1Xyu70%23page3%0Ahttp://www.sciencemag.org/cgi/doi/10.1126/science.1191273%0Ahttps://greatergood.berkeley.edu/images/application_uploads/Diener-Subje

Poulsen, D. L., Cook, P. G., Simmons, C. T., McCallum, J. M., Noorduijn, S. L., & Dogramaci, S. (2019). A constant rate salt tracer injection method to quantify pumped flows in long-screened or open borehole wells. Journal of Hydrology, 574(January), 408–420. https://doi.org/10.1016/j.jhydrol.2019.04.051

Przylibski, T. A., & Zebrowski, A. (1999). Origin of radon in medicinal waters of Ladek Zdroj (Sudety Mountains, SW Poland). Journal of Environmental Radioactivity, 46(1), 121–129. https://doi.org/10.1016/S0265-931X(98)00116-7

Razack, M., & Huntley, D. (1991). Assesing Transmissivity from Specific Capacity in a Large and Hetrogeneous Alluvial Aquifer. Ground Water, 29(6), 856–861.

Rorabaugh, M. I. (1953). Graphical and theoretical analysis of step-drawdown test of artesian well. Proceedings American Society of Civil Engineers, Hydraulics Division, 79(Separate No. 362).

RWSN. (2009). Handpump Data, Selected Countries in Sub-Saharan Africa. Notes, 2004(2005), 2005. http://www.rural-water-supply.net/_ressources/documents/default/203.pdf

Saar, M. O., & Manga, M. (2004). Depth dependence of permeability in the Oregon Cascades inferred from hydrogeologic, thermal, seismic, and magmatic modeling constraints. Journal of Geophysical Research: Solid Earth, 109(4), 1–19. https://doi.org/10.1029/2003JB002855

Schmidt, A., Schlueter, M., Melles, M., & Schubert, M. (2008). Continuous and discrete on-site detection of radon-222 in ground- and surface waters by means of an extraction module. Applied Radiation and Isotopes, 66(12), 1939–1944. https://doi.org/10.1016/j.apradiso.2008.05.005

Schmidt, A., & Schubert, M. (2007). Using radon-222 for tracing groundwater discharge into an open-pit lignite mining lake - A case study. Isotopes in Environmental and Health Studies, 43(4), 387–400. https://doi.org/10.1080/10256010701705419

Schubert, M., Brueggemann, L., Knoeller, K., & Schirmer, M. (2011). Using radon as an environmental tracer for estimating groundwater flow velocities in single-well tests. Water Resources Research, 47(3), 1–8. https://doi.org/10.1029/2010WR009572

Sembroni, A., Faccenna, C., Becker, T. W., Molin, P., & Abebe, B. (2016). Long-term, deep-mantle support of the Ethiopia-Yemen Plateau. Tectonics, 35(2), 469–488. https://doi.org/10.1002/2015TC004000

Singhal, B. B. S. (1997). Hydrogeological characteristics of Deccan trap formations of India. IAHS-AISH Publication, 241(241), 75–80.

Somers, L. D., & McKenzie, J. M. (2020). A review of groundwater in high mountain environments. Wiley Interdisciplinary Reviews: Water, 7(6), 1–27. https://doi.org/10.1002/wat2.1475

Sukanya, S., Noble, J., & Joseph, S. (2021). Factors controlling the distribution of radon (222Rn) in groundwater of a tropical mountainous river basin in southwest India. Chemosphere, 263, 128096. https://doi.org/10.1016/j.chemosphere.2020.128096

Swan, A., Skipworth, P., Walker, L., & Thursfield, G. (2018). Field testing a remote

monitoring system for hand water pumps. Water Practice and Technology, 13(4), 821–831. https://doi.org/10.2166/wpt.2018.093

Taylor, R. G., Scanlon, B., Döll, P., Rodell, M., Van Beek, R., Wada, Y., Longuevergne, L., Leblanc, M., Famiglietti, J. S., Edmunds, M., Konikow, L., Green, T. R., Chen, J., Taniguchi, M., Bierkens, M. F. P., Macdonald, A., Fan, Y., Maxwell, R. M., Yechieli, Y., … Treidel, H. (2013). Ground water and climate change. Nature Climate Change, 3(4), 322–329. https://doi.org/10.1038/nclimate1744

Thao, N. B., Mayer, A., Nofal, S., & Mohammed, G. (2017). Estimation of groundwater flow velocity using Radon in single well tests - Xác đị nh v ậ n t ố c dòng ch ả y n ướ c d ướ i đấ t b ằ ng thí nghi ệ m xác đị nh Radon trong l ỗ khoan đơ n. July 2018.

Thaw, M., GebreEgziabher, M., Villafañe-Pagán, J. Y., & Jasechko, S. (2022). Modern groundwater reaches deeper depths in heavily pumped aquifer systems. Nature Communications, 13(1), 5263. https://doi.org/10.1038/s41467-022-32954-1

Theis, C. V. (1935). The relation between the lowering of the Piezometric surface and the rate and duration of discharge of a well using ground-water storage. Eos, Transactions American Geophysical Union, 16(2), 519–524. https://doi.org/10.1029/TR016i002p00519

Thomson, P., Hope, R., & Foster, T. (2012). GSM-enabled remote monitoring of rural handpumps: A proof-of-concept study. Journal of Hydroinformatics, 14(4), 829–839. https://doi.org/10.2166/hydro.2012.183

Truslove, J. P., Miller, A. V. M., Mannix, N., Nhlema, M., Rivett, M. O., Coulson, A. B., Mleta, P., & Kalin, R. M. (2019). Understanding the functionality and burden on decentralised rural water supply: Influence of millennium development goal 7c coverage targets. Water (Switzerland), 11(3), 1–18. https://doi.org/10.3390/w11030494

UNICEF. (2021, December 9). Finding Water in the Driest Places. https://www.unicef.org/innovation/stories/finding-water-driest-places

Vienken, T., Huber, E., Kreck, M., Huggenberger, P., & Dietrich, P. (2017). How to

chase a tracer – combining conventional salt tracer testing and direct push electrical conductivity profiling for enhanced aquifer characterization. Advances in Water Resources, 99, 60–66. https://doi.org/10.1016/j.advwatres.2016.11.010

Vincent, W., & Joshi, V. G. (1986). Results of Pumping tests in the Deccan Trap Basalts of Central India. Hydrology, 86, 147–168.

Walker, D. (2017). Properties of shallow thin regolith aquifers in sub-Saharan Africa : a case study from northwest Ethiopia. July.

Walker, D., Parkin, G., Gowing, J., & Haile, A. T. (2019a). Development of a hydrogeological conceptual model for shallow aquifers in the data scarce upper Blue Nile basin. Hydrology, 6(2). https://doi.org/10.3390/hydrology6020043

Walker, D., Parkin, G., Gowing, J., & Haile, A. T. (2019b). Development of a hydrogeological conceptual model for shallow aquifers in the data scarce upper Blue Nile basin. Hydrology, 6(2). https://doi.org/10.3390/hydrology6020043

Walton, W. C., & Stewart, J. W. (1961). Aquifer Tests in the Snake River Basalt. Transactions of the American Society of Civil Engineers, 126(3). https://doi.org/10.1061/taceat.0008315

Wilkinson, J. M. (2012). The application and revision of a new relationship to calculate effective porosity from specific capacity on a well database in the Pacific Northwest. 103, 98–103. https://doi.org/10.3178/HRL.6.98

Wilson, P., Bonsor, H., MacDonald, A. M., Whaley, L., Carter, R. C., & Casey, V. (2016). Unravelling past failures for future success in Rural Water Supply Initial project approach for assessing rural water supply functionality and levels of performance. 35. www.geologyshop.com

Woldegabriel, G., Aronson, J. L., & Walter, R. C. (1990). Geology, geochronology, and rift basin development in the central sector of the Main Ethiopia Rift. Bulletin of the Geological Society of America. https://doi.org/10.1130/0016-7606(1990)102<0439:GGARBD>2.3.CO;2

Worthington, S. R. H. (2021). Factors affecting the variation of permeability with

depth in carbonate aquifers. Hydrogeology Journal, 29(1), 21–32. https://doi.org/10.1007/s10040-020-02247-2

Yitbarek, A., Razack, M., Ayenew, T., Zemedagegnehu, E., & Azagegn, T. (2012). Hydrogeological and hydrochemical framework of Upper Awash River basin, Ethiopia: With special emphasis on inter-basins groundwater transfer between Blue Nile and Awash Rivers. Journal of African Earth Sciences, 65, 46–60. https://doi.org/10.1016/j.jafrearsci.2012.01.002

Zlotnik, V., & Tartakovsky, D. M. (2018). Interpretation of Heat-Pulse Tracer Tests for Characterization of Three-Dimensional Velocity Fields in Hyporheic Zone. Water Resources Research, 54(6), 4028–4039. https://doi.org/10.1029/2017WR022476

Zolotukhin, V., & Al'mukhamedov, A. . (1988). Traps of the Siberian Platform. 273–274.

Appendices

Appendix 1: Matlab code used to solve non-linear integral equation of the converging streamline to estimate theoretical water well flow velocity, which in turn be used to estimate groundwater flow velocity.

```
%Main script
%=======================================================
clear all;
nvars=1;
lb = [-2];
ub = [2];

fun =@expr;
iterations=50;

clear gaoutfun1;
rng(100) % For reproducibility

options=optimoptions('ga','Generations',iterations,'PopulationSize',10,'CrossoverFraction',
0.8,...
   'MigrationFraction',0.1,'StallGenLimit',inf,'StallTimeLimit',inf,'OutputFcn',@gaoutfun1,...
   'PlotFcn',@plotfun1,'TolFun',1E-8);
t1=tic;

[T,fval] = ga(fun,nvars,[],[],[],[],lb,ub,@constest,[],options)



load history_Best1;

figure();
```

```
plot(1:length(history_Best1),history_Best1,':b','linewidth',1.5);
title('Optimal values ')
xlabel('Number of generations')
ylabel('Optimal values')



%=====================================================

%Function file

function q=expr(T)
f=@(teta) (1/T)*(1-exp(-2*T*cos(teta))).*cos(teta);
r=integral(f,-pi/2,pi/2)/pi;
q=0.6-r;

%=====================================================

%Constraint Function
function q=expr(T)
f=@(teta) (1/T)*(1-exp(-2*T*cos(teta))).*cos(teta);
r=integral(f,-pi/2,pi/2)/pi;
q=0.6-r;
```

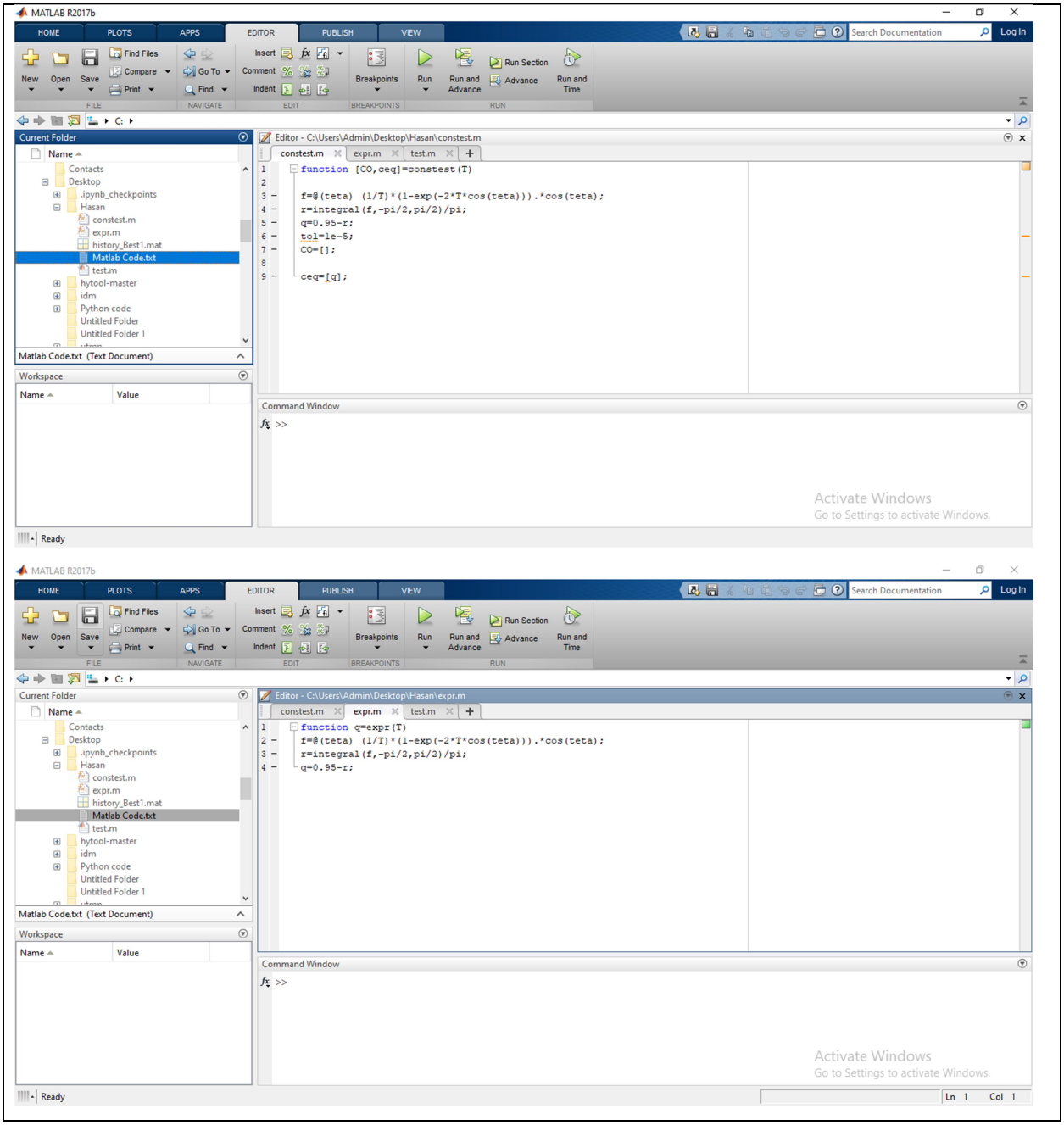
MATLAB R2017b
HOME
PLOTS
APPS
EDITOR
PUBLISH
VIEW
Search Documentation
Log In
New
Open
Save
Find Files
Compare
Print
Go To
Find
Insert
Comment
Indent
Breakpoints
Run
Run and Advance
Run Section
Advance
Run and Time
FILE
NAVIGATE
EDIT
BREAKPOINTS
RUN
C:
Current Folder
Name
Contacts
Desktop
.ipynb_checkpoints
Hasan
constest.m
expr.m
history_Best1.mat
Matlab Code.txt
test.m
hytool-master
idm
Python code
Untitled Folder
Untitled Folder 1
Matlab Code.txt (Text Document)
Editor - C:\Users\Admin\Desktop\Hasan\constest.m
constest.m
expr.m
test.m
function [CO,ceq]=constest(T)
f=@(teta) (1/T)*(1-exp(-2*T*cos(teta))).*cos(teta);
r=integral(f,-pi/2,pi/2)/pi;
q=0.95-r;
tol=1e-5;
CO=[];
ceq=[q];
Workspace
Name
Value
Command Window
>>
Activate Windows
Go to Settings to activate Windows.
Ready
MATLAB R2017b
HOME
PLOTS
APPS
EDITOR
PUBLISH
VIEW
Search Documentation
Log In
New
Open
Save
Find Files
Compare
Print
Go To
Find
Insert
Comment
Indent
Breakpoints
Run
Run and Advance
Run Section
Advance
Run and Time
FILE
NAVIGATE
EDIT
BREAKPOINTS
RUN
C:
Current Folder
Name
Contacts
Desktop
.ipynb_checkpoints
Hasan
constest.m
expr.m
history_Best1.mat
Matlab Code.txt
test.m
hytool-master
idm
Python code
Untitled Folder
Untitled Folder 1
Matlab Code.txt (Text Document)
Editor - C:\Users\Admin\Desktop\Hasan\expr.m
constest.m
expr.m
test.m
function q=expr(T)
f=@(teta) (1/T)*(1-exp(-2*T*cos(teta))).*cos(teta);
r=integral(f,-pi/2,pi/2)/pi;
q=0.95-r;
Workspace
Name
Value
Command Window
>>
Activate Windows
Go to Settings to activate Windows.
Ready
Ln 1
Col 1

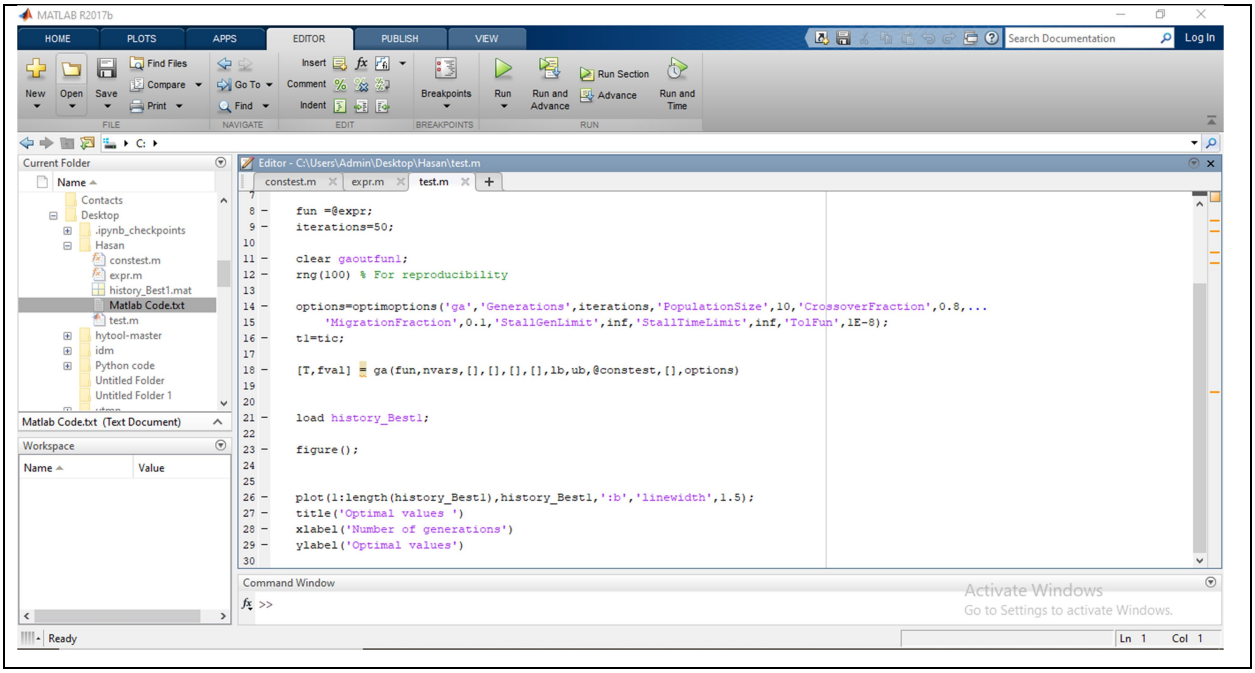

Appendix 2: Supplementary material used geospatial groundwater flow velocity estimation.

Theoretical background for groundwater flow velocity estimation.

The seepage velocity is calculated by dividing the Darcy flux by the effective porosity, as shown in equation 1.

$$\boldsymbol{V_{seep}} = \frac{\boldsymbol{v}}{\boldsymbol{n_{eff}}} \qquad (1)$$

Where V_{seep} is the seepage velocity (m/d), v is the Darcy flux ($m^3/s/m^2$) and n_{eff} is the effective porosity of the aquifer (dimensionless). Darcy velocity is the product of the hydraulic gradient multiplied by the hydraulic conductivity of the aquifer, as in Equation (2):

$$\boldsymbol{v} = -\boldsymbol{k}\frac{\Delta \boldsymbol{h}}{\Delta \boldsymbol{s}} \qquad (2)$$

Where k is the hydraulic conductivity (m/day), Δh is the difference in the hydraulic head (m) and Δs is the distance (m). The hydraulic conductivity can be written in terms of transmissivity and the saturated thickness of the aquifer as in Equation (3):

$$\boldsymbol{k} = \frac{\boldsymbol{T}}{\boldsymbol{b}} \qquad (3)$$

Where T is the transmissivity (m^2/d) and b is the saturated thickness of the aquifer (m). Equation (3) is useful in groundwater hydraulics most of the wells hydraulic calculations and equations are written in terms of transmissivity rather than the hydraulic conductivity. Combining Equations (1)–(3), the seepage velocity can be written as Equation (4):

$$\boldsymbol{V_{seep}} = -\frac{\boldsymbol{T}}{\boldsymbol{bn_{eff}}}\frac{\boldsymbol{\Delta h}}{\boldsymbol{\Delta s}} \qquad (4)$$

Therefore, Equation (4) was used accordingly as model in ArcMap/GIS and as a mapping framework to calculate the seepage velocity of aquifers.

Table S2: Water wells history, hydraulic parameters and calculated effective porosity

Sample ID	SWL	BH Depth	Saturated thickness(b)	T(m2/day)	Specific capacity(Sc)	Initial effective porosity	Effective porosity
EAE01	21.39	70.3	48.91	2.45E+01	0.87	0.03415	0.14935
EAE02	12.59	44.86	32.27	3.21E+01	1.896	0.35604	0.15928
EAE03	53.02	76	22.98	1.37E+03	331.26	0.91148	0.24399
EAE04	49.17	60.78	11.61	7.05E+00	6.59	0.33067	0.17654
EAE07	24.2	43.5	19.3	3.88E+02	534.19	0.94009	0.25381
EAE08	20.52	47.13	26.61	6.13E-01	0.099	0.16406	0.12481
EAE10	62.16	84.3	22.14	1.12E+02	42.6	0.64057	0.20597
EAE11	11.17	51.45	40.28	6.24E-01	0.94	0.32279	0.15031
EAE12	23.41	76.7	53.29	9.33E-01	1.41	0.40014	0.15543
EAE13	60.08	73.66	13.58	9.50E-02	0.325	0.27182	0.13769
EAE14	58.08	76.88	18.8	5.33E+03	845.547	0.99558	0.26363
EAE19	24.45	63.69	39.24	2.66E+00	3.78	0.45598	0.16862
EEJ02	8.17	49.5	41.33	7.18E+01	38.59	0.74581	0.20429
EEJ06	14.92	62.66	47.74	3.84E+00	5.43	0.44992	0.17374
EEJ09	5.94	35.6	29.66	1.34E+01	11.48	0.53468	0.18482
EEJ10	7.23	46.88	39.65	4.81E+02	265.49	0.98967	0.23957
EEJ16	14.92	62.66	47.74	1.65E+00	3.07	0.46527	0.16575
EEJ17	29.49	47.35	17.86	1.81E+01	21.57	0.51993	0.19471
EEJ20	32.82	53.39	20.57	1.17E+00	1.72	0.29018	0.158
EME01	10.32	21.75	11.43	8.35E-01	777	0.88655	0.26179
EME02	11.02	26	14.98	1.19E+03	1190.48	0.99599	0.27118
EME03	17.61	53.26	35.65	2.52E+01	9.59	0.54584	0.1821
EME05	10.05	49	38.95	1.61E+03	8.4	0.54579	0.18012
EME07	2.42	61.34	58.92	7.35E+00	26.66	0.76629	0.19814

EME08	16.37	49.02	32.65	1.61E+03	23.08	0.63647	0.1958
EME09	6.67	51.4	44.73	1.50E+02	71.35	0.8406	0.21493
EME12	4.96	42.5	37.54	6.37E+00	25.58	0.67533	0.19747
EME13	23.06	50	26.94	2.74E+01	1764.71	1.16469	0.28014
EME15	11.38	50.3	38.92	2.67E+02	1.96	0.38614	0.15972
EME18	9.01	55.4	46.39	2.35E+01	25.21	0.71345	0.19723
ESD01	10.35	25.3	14.95	1.39E+02	55.83	0.6017	0.21062
ESD03	19.09	38.05	18.955	3.96E+02	163.04	0.78153	0.23011
ESD04	21.48	68.6	47.12	9.07E-01	1.52	0.38923	0.1564
ESD08	40.7	62	21.3	4.04E+00	2.19	0.31386	0.16119
ESD09	12.99	35.71	22.72	3.60E+01	20.24	0.55486	0.19369
ESD10	23.79	51.5	27.71	1.22E+00	1.68	0.32471	0.15769
ESD11	20.37	42.94	22.57	6.23E+01	30.91	0.60457	0.20058
ESD13	15.01	18.6	3.59	3.65E+00	17.36	0.26838	0.19125
ESD16	22.3	43.5	21.2	2.58E+00	2.46	0.32313	0.16274
ESD17	38.9	47	8.1	5.98E+01	45.02	0.46946	0.20691
ESD19	52	80	28	2.63E+02	158.23	0.85329	0.22955
ESD20	41	75	34	1.72E+00	2.49	0.38988	0.1629

Appendix 3: Water wells functionality classification, Aquifer hydraulic properties and Radon data (Radon recovery, flow velocity in water well, groundwater flow velocity and residence time in a well)

Sample ID	Functionality	BH Depth(m)	k(m/day)	T(m2/day)	Sc (L/minute)/ m))	C_{ww} (Bq/m^3)	C_{gw} (Bq/m^3)	C_{ww}/C_{gw}	V_{ww}(Cm/day)	V_{gw}(cm/day)	t(days)
EAE01	LY&UR	70.3	4.99E-01	2.45E+01	0.87	5470±522	13027±835	0.39	9.88E-01	0.4595349	5.181
EAE02	FF	44.86	9.94E-01	3.21E+01	1.896	14964±953	14968±961	0.99	1.38E+02	64.186047	0.0012
EAE04	UR	60.78	6.07E-01	7.05E+00	6.59	8430±650	11573±751	0.76	4.19E+00	1.9488372	1.47
EME07	LY	61.34	2.06E-01	7.35E+00	26.66	2800±368	4160±461	0.65	2.47E+00	1.0786026	2.35
EAE10	FF	84.3	5.08E+00	1.12E+02	42.6	2970±391	3510±421	0.84	6.91E+00	3.2139535	0.921
EAE11	LY&UR	51.45	1.55E-02	6.24E-01	0.94	3920±446	8540±674	0.46	1.26E+00	0.5860465	4.29
EAE12	FF	76.7	1.75E-02	9.33E-01	1.41	7940±627	9330±679	0.85	6.91E+00	3.2139535	0.89
EAE13	UR	73.66	7.00E-03	9.50E-02	0.325	1920±322	2080±332	0.92	1.38E+01	6.4186047	0.44
EAE14	FF	76.88	283.392	5.33E+03	845.547	1400±277	1760±308	0.79	5.02E+00	2.3348837	1.261
EEJ02	FF	49.5	1.74E+00	7.18E+01	38.59	13992±902	21007±102	0.76	4.07E+00	1.8333333	1.5
EEJ06	FF	62.66	6.60E-02	3.84E+00	5.43	13514±874	14954±943	0.83	6.01E+00	2.7072072	1.0033
EEJ09	UR	35.6	4.51E-01	1.34E+01	11.48	12549±825	13988±898	0.81	5.32E+00	2.3963964	1.142
EEJ10	FF	46.88	1.21E+01	4.81E+02	265.49	2860±384	3090±397	0.93	1.54E+01	6.9369369	0.43
EEJ17	FF	47.35	1.01E+00	1.81E+01	21.57	9930±700	11093±720	0.99	1.38E+02	62.162162	0.0415
EEJ20	LY&UR	53.39	4.39E-02	1.17E+00	1.72	4940±497	12064±792	0.41	1.06E+00	0.4774775	4.9
EME01	FF	21.75	2.14E-02	8.35E-01	777	8320±644	11573±739	0.76	4.07E+00	1.7772926	1.52
EME02	FF	26	4.42E+01	1.19E+03	1190.48	12062±783	12543±807	0.92	1.38E+01	6.0262009	0.44
EME05	UR	49	1.41E+02	1.61E+03	8.4	4110±458	6080±552	0.68	2.82E+00	1.231441	2.16
EAE07	FF	43.5	2.01E+01	3.88E+02	534.19	3010±301	4610±481	0.67	2.71E+00	1.2604651	2.182
EME09	FF	51.4	3.35E+00	1.50E+02	71.35	4310±474	4590±483	0.94	1.98E+01	8.6462882	0.35
EME12	LY	42.5	1.63E-01	6.37E+00	25.58	4570±480	7370±603	0.62	2.19E+00	0.9563319	2.634
EME15	UR	50.3	4.67E+01	2.67E+02	1.96	12063±86	21296±101	0.57	1.84E+00	0.922	3.081

EME18	FF	55.4	5.07E-01	2.35E+01	25.21	6420±568	7500±610	0.86	7.68E+00	3.3537118	0.86
ESD01	FF	25.3	9.33E+00	1.39E+02	55.83	12541±797	13509±856	0.87	8.13E+00	3.1757813	0.79
ESD04	LY&UR	68.6	4.46E-02	9.07E-01	1.52	1520±285	2850±381	0.53	1.61E+00	0.6289063	3.465
ESD08	UR	62	1.90E-01	4.04E+00	2.19	2750±377	5160±508	0.53	1.61	6.30E-01	3.47
ESD09	LY&UR	35.71	1.59E+00	3.60E+01	20.24	3220±405	6940±586	0.46	1.26E+00	0.4921875	4.232
ESD10	LY&UR	51.5	4.41E-02	1.22E+00	1.68	3150±212	8330±640	0.38	9.53E-01	0.3722656	5.36
ESD11	UR	42.94	2.76E+00	6.23E+01	30.91	2330±352	2770±381	0.84	6.58E+00	2.5703125	0.953
ESD13	LY&UR	18.6	1.02E+00	3.65E+00	17.36	1850±313	3800±483	0.49	1.40E+00	0.546875	3.97
ESD16	UR	43.5	1.22E-01	2.58E+00	2.46	7900±625	6000±546	0.76	4.07E+00	1.5898438	1.54
ESD17	FF	47	6.71E+00	5.98E+01	45.02	6750±598	7090±613	0.95	2.30E+01	8.984375	0.271
ESD20	UR	75	5.05E-02	1.72E+00	2.49	2350±350	2750±379	0.86	6.91E+00	2.6992188	0.87

Appendix 4: Hydraulic parameters estimated by analytical methods during pumping test data analysis.

LLPW9: Lege-Tafo-Lege-Dadi Ayat from the RMV aquifer class

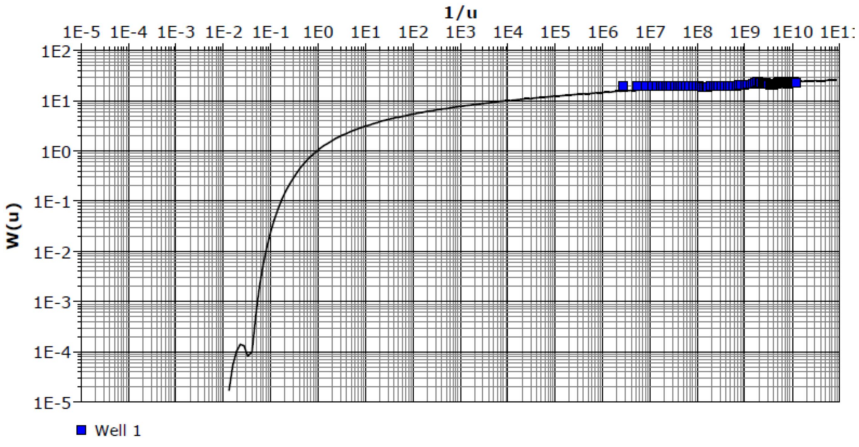

Calculation using Theis

Observation Well	Transmissivity [m²/d]	Hydraulic Conductivity [m/d]	Storage coefficient	Radial Distance to PW [m]	
Well 1	8.77×10^{3}	5.13×10^{3}	1.00×10^{-7}	0.61	

AMW4: Melka Kunture, Rift Margin volcanics

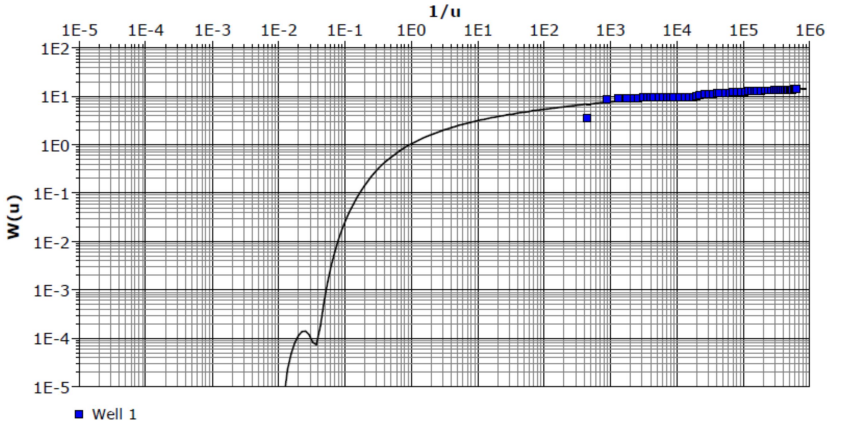

Calculation using Theis

Observation Well	Transmissivity [m²/d]	Hydraulic Conductivity [m/d]	Storage coefficient	Radial Distance to PW [m]	
Well 1	1.30×10^{3}	1.33×10^{1}	9.19×10^{-5}	0.61	

AMW7: Chancho, Upper basalt aquifer class

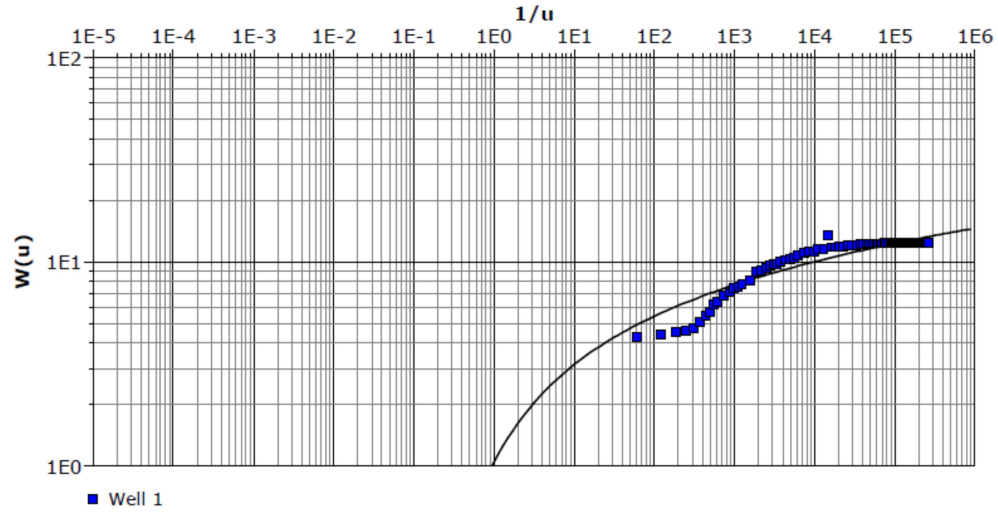

Calculation using Theis					
Observation Well	Transmissivity [m²/d]	Hydraulic Conductivity [m/d]	Storage coefficient	Radial Distance to PW [m]	
Well 1	2.14×10^{0}	1.35×10^{-2}	1.08×10^{-6}	0.61	

MBH001: Sululta deepest well (858m) in the upper basalt aquifer class

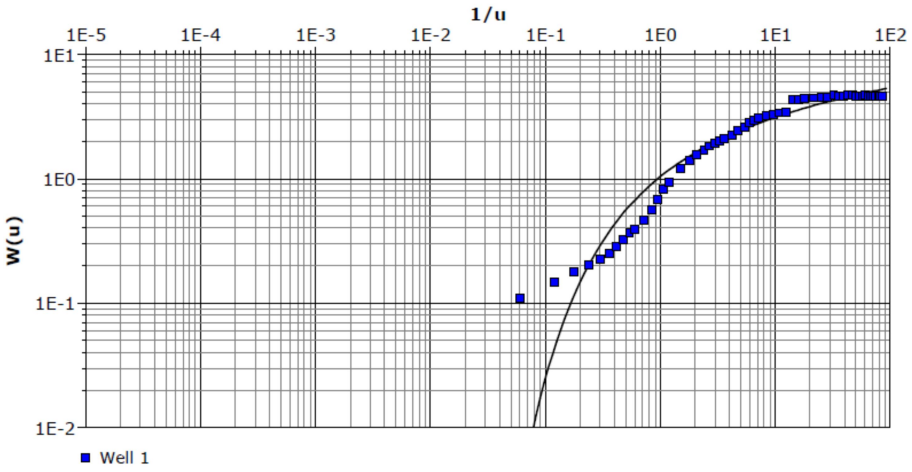

Calculation using Theis					
Observation Well	Transmissivity [m²/d]	Hydraulic Conductivity [m/d]	Storage coefficient	Radial Distance to PW [m]	
Well 1	1.06×10^{0}	1.52×10^{-2}	3.29×10^{-3}	0.25	

Appendix 5: Published article on the Sustainability journal entitled "Estimation groundwater flow velocity in shallow volcanic aquifers of the Ethiopian highlands using geo-spatial technique"

sustainability

MDPI

Article

Estimating Groundwater Flow Velocity in Shallow Volcanic Aquifers of the Ethiopian Highlands Using a Geospatial Technique

Hassen Shube [1,2,*], Seifu Kebede [3], Tilahun Azagegn [1], Dessie Nedaw [1], Muhammed Haji [2] and Shankar Karuppannan [2]

[1] School of Earth Sciences, Addis Ababa University, Addis Ababa P.O. Box 1176, Ethiopia; tilahun.azagegn@aau.edu.et (T.A.); dessie.nedaw@aau.edu.et (D.N.)
[2] Department of Applied Geology, School of Applied Nartural Sciences, Adama Science and Technology University, Adama P.O. Box 1888, Ethiopia; mohehaji@gmail.com (M.H.); geoshankar1984@gmail.com (S.K.)
[3] School of Agricultural, Earth and Environmental Sciences, Center for Water Resources Research, University of KwaZulu Natal, Pietermaritzburg 3209, South Africa; kebedegurmessas@ukzn.ac.za
* Correspondence: hassenshube@gmail.com

Abstract: The shallow volcanic aquifer is the major rural water supply source in the Ethiopian highlands. A significant number of hand pump wells in these aquifers experience a rapid decline in yield and poor performance within a short period of time after construction. Hence, reliable estimation of groundwater flow velocity is important to understand groundwater flow dynamics, aquifer responses to stresses and to optimize the sustainable management of groundwater resources. Here, we propose the geospatial technique using four essential input raster maps (groundwater elevation head, transmissivity, effective porosity and saturated thickness) to investigate groundwater flow velocity magnitude and direction in the shallow volcanic aquifers of the Ethiopian highlands. The results indicated that the high groundwater flow velocity in the Mecha site, ranging up to 47 m/day, was observed in the fractured scoraceous basalts. The Ejere site showed groundwater flow velocity not exceeding 7 m/day in the fractured basaltic aquifer and alluvial deposits. In the Sodo site, the groundwater flow velocity was observed to exceed 22 m/day in the fractured basaltic and rhyolitic aquifers affected by geological structures. The Abeshege site has a higher groundwater flow velocity of up to 195 m/day in the highly weathered and fractured basaltic aquifer. In all study sites, aquifers with less fractured basalt, trachyte, rhyolite, welded pyroclastic, and lacustrine deposits exhibited lower groundwater flow velocity values. The groundwater flow velocity directions in all study sites are similar to the groundwater elevation head, which signifies the local and regional groundwater flow directions. This work can be helpful in shallow groundwater resource development and management for rural water supply.

Keywords: groundwater flow velocity; geospatial technique; groundwater tools; rural water supply; shallow aquifer; Ethiopia

check for updates

Citation: Shube, H.; Kebede, S.; Azagegn, T.; Nedaw, D.; Haji, M.; Karuppannan, S. Estimating Groundwater Flow Velocity in Shallow Volcanic Aquifers of the Ethiopian Highlands Using a Geospatial Technique. *Sustainability* **2023**, *15*, 14490. https://doi.org/10.3390/su151914490

Academic Editor: Dino Musmarra

Received: 2 August 2023
Revised: 11 September 2023
Accepted: 25 September 2023
Published: 5 October 2023

1. Introduction

Groundwater has a crucial role as a source of water supply in several parts of the world's rural and urban centers. The strategic importance of groundwater for water supply is due to its resilience to more frequent and extreme drought and increased variability in precipitation, sustaining climate change adaptation strategies and groundwater-related ecosystems in sub-Saharan Africa, including Ethiopia [1–3]. Shallow groundwater in sub-Saharan Africa represents a neglected opportunity for promoting small-scale irrigation activities [4]. Since rainfall-dependent agricultural activities have been affected by seasonal variations of climate effects, shallow groundwater can be used as an alternative source for small-scale irrigation. Despite its importance for the water supply, the shallow groundwater

Appendix 6: Published article on Hydrogeology journal entitled "variations in hydraulic structures with respect to depth and age of a large igneous province in Ethiopia"

Hydrogeology Journal
https://doi.org/10.1007/s10040-023-02749-9

REPORT

Variation in hydraulic structure with respect to depth and age of a large igneous province in Ethiopia

Hassen Shube[1] · Selfu Kebede[2]

Received: 22 April 2023 / Accepted: 3 November 2023

Abstract

Depth-wise variation in hydraulic structures of volcanic aquifers is rarely investigated when compared to basement and other rocks. A comprehensive dataset is presented here on the hydraulic properties of volcanic aquifers from a large igneous province in Africa. Age- and depth-wise variation in transmissivity (T), yield (Q), hydraulic conductivity (K) and specific capacity (S_c) of volcanic aquifers and water wells were systematically examined for stratigraphic units of various ages (Eocene to Quaternary Period) and well depth (18–882 m). The T ranges from 0.02 to 9,830 m^2/day. There is a good correlation between the age of the emplacement of the rocks and their hydraulic properties. The oldest (Eocene) basalts show lower productivity (T, K and Q) when compared to the youngest (Quaternary) basalts. There is no statistically significant depth-wise variation of T, K and Q when one single formation is investigated. The insights gained from the analysis show that increasing the depth of drilling does not necessarily increase aquifer yields and can inform global-scale groundwater modelling efforts. The data challenge the widely held assumption that K and Q decrease with depth. Unlike basement rocks, volcanic rocks show no statistically significant change in hydraulic properties along its depth profile to the depth of 900 m.

Keywords Volcanic aquifers · Age · Drilling depth · Productivity · Arid regions · Ethiopia

Introduction

Eight percent of the earth's surface (terrestrial and seafloor) is made up of volcanic rocks. Volcanic aquifers serve as an important source of drinking and productive water globally. Large igneous provinces occur in the Deccan Traps of India (Mahoney 1988), Karoo in southern Africa (Cox 1988), Siberia (Zolotukhin and Al'mukhamedov 1988), Columbia River in North America (Hooper 1982), Parana-Etendeka in South America (Piccirillo et al. 1988), East Africa (Mohr and Zanettin 1988; Mohr 1983) and the North Atlantic region (Dickin 1988) (Fig. 1). Unlike basement aquifers, which show distinct decreasing aquifer productivity with increasing aquifer depths (Bianchi et al. 2020; Dewandel et al. 2006; Deyassa et al. 2014; Howard et al. 1992; Maréchal et al. 2004), the depth- and age-wise variations in volcanic aquifers are little understood.

Data on the hydraulic structure of volcanic rocks have several important bearings as inputs to global-scale groundwater models and in the groundwater resources development and management sector. Global-scale groundwater models that account for the lateral flow of groundwater are rare and emerged only recently (de Graaf et al. 2017), but the accuracy of the models is challenged by the lack of a coherent representation of the vertical distribution of hydraulic conductivity (K) of the subsurface in different geological settings across the globe. The vertical variations in K in volcanic rocks of Nevada, USA, were investigated with respect to the influence of depth, rock alteration, rock type and overburden pressure on the heterogeneity of K values, showing that the shallow part of the flow system has higher K values than the deeper flow systems (Jackson and Fenelon 2022); the K variations are dependent on hydraulically interconnected fracture networks (Allocca et al. 2022). However, in carbonate aquifers, the K variation with depth is controlled

This article is part of the special issue "Hydrogeology of arid environments"

✉ Hassen Shube
hassenshube@gmail.com

[1] School of Earth Sciences, Addis Ababa University, POBOX 1176, Addis Ababa, Ethiopia

[2] School of Agricultural, Earth and Environmental Sciences, Centre for Water Resources Research, University of KwaZulu Natal, Pietermaritzburg, South Africa

Published online: 27 November 2023

Appendix 7: Submitted article to Environmental Radioactivity journal currently under review entitled "^{222}Rn isotope as a tool for monitoring functionality of water wells"

Abstract

In Sub-Saharan Africa, hand pump-fitted water wells (HPWs) are characterized by poor functionality marked by rapid post-construction decline in yield. A substantial number of the HPWs show a low degree of reliability and poor water quality. Monitoring changes in performance is prerequisite to inform preventive maintenance of the HPWs. Borehole performance monitoring often requires a logistically demanding pumping test procedure. Here we demonstrate the applicability of a naturally occurring Radon-222 isotope (^{222}Rn) as a complementary tool to monitor post-construction performance of HPWs. We measured ^{222}Rn recovery (the ratio of ^{222}Rn in the HPWs to that of the aquifer) in 32 HPWs and the host aquifers. Pumping and reliability tests have been conducted on the HPWs before taking the ^{222}Rn measurements. The HPWs have been classified into four functionality classes a) high yield and reliable, b) high yield but unreliable, c) low yield and reliable and d) low yield and unreliable. In the first category, there is a high ^{222}Rn recovery revealing a quick through flow of groundwater in the wells. This further demonstrates the healthy functioning of boreholes without screen clogging effects and a high permeability of the aquifer material in the vicinity of the well. The fourth category shows the lowest ^{222}Rn recovery revealing a slow flow of water in the well owing to low permeability, declining water level, screen clogging, poor initial design and high water stagnation in the boreholes. The substantial difference in ^{222}Rn recovery between the four categories reveals the isotopic tracer can be used as a promising independent tool to monitor post-construction changes in the performance of HPWs without the need for dismantling the HPWs for inspection.

Keywords: Rural water supply; ^{222}Radon; aquifer hydraulic properties; functionality; hand pump wells; Ethiopia